

**JANUARY, 2014**

**M.Sc. in Mechanical Engineering**

**ALPEREN TOZLU**

**UNIVERSITY OF GAZIANTEP  
GRADUATE SCHOOL OF  
NATURAL & APPLIED SCIENCES**

**AN ANALYSIS ON FLOW MODES IN PNEUMATIC  
CONVEYING SYSTEMS**

**M. Sc. THESIS  
IN  
MECHANICAL ENGINEERING**

**BY  
ALPEREN TOZLU  
JANUARY 2014**

**An Analysis on Flow Modes in Pneumatic Conveying Systems**

**M.Sc. Thesis**

**in**

**Mechanical Engineering**

**University of Gaziantep**

**Supervisor**

**Prof. Dr. Melda Özdiñ ÇARPINLIOĞLU**

**Assoc. Prof. Dr. A. İhsan KUTLAR**

**Co-Supervisor**

**by**

**Alperen TOZLU**

**JANUARY 2014**

© 2014 [Alperen TOZLU]


REPUBLIC OF TURKEY  
UNIVERSITY OF GAZİANTEP  
GRADUATE SCHOOL OF NATURAL & APPLIED SCIENCES  
NAME OF THE MECHANICAL ENGINEERING DEPARTMENT

Name of the thesis: An Analysis on Flow Modes in Pneumatic Conveying Systems

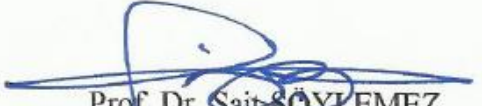
Name of the student: Alperen TOZLU

Exam date: 03.01.2014


Approval of the Graduate School of Natural and Applied Sciences

  
Assoc. Prof. Dr. Metin BEDİR  
Director

I certify that this thesis satisfies all the requirements as a thesis for the degree of Master of Science.

  
Prof. Dr. Sait SÖYLEMEZ  
Head of Department

This is to certify that we have read this thesis and that in our consensus/majority opinion it is fully adequate, in scope and quality, as a thesis for the degree of Master of Science/Doctor of Philosophy.

  
Assoc. Prof. Dr. A. İhsan KUTLAR

  
Prof. Dr. Melda Özdiñ ÇARPINLIOĞLU

Co-Supervisor

Supervisor

Examining Committee Members

Signature

Prof. Dr. Hüseyin YAPICI

Prof. Dr. Melda Özdiñ ÇARPINLIOĞLU

Prof. Dr. Sait SÖYLEMEZ

Assoc. Prof. Dr. Vedat ORUÇ

Assist. Prof. Dr. Emrah ÖZAHİ


**I hereby declare that all information in this document has been obtained and presented in accordance with academic rules and ethical conduct. I also declare that, as required by these rules and conduct, I have fully cited and referenced all material and results that are not original to this work.**

Alperen TOZLU

## ABSTRACT

### AN ANALYSIS ON FLOW MODES IN PNEUMATIC CONVEYING SYSTEMS

**TOZLU, Alperen**

**M.Sc. in Mechanical Engineering**

**Supervisor: Prof. Dr. Melda Özdiñ ÇARPINLIOĞLU**

**Co-Supervisor: Assoc. Prof. Dr. Ahmet İhsan KUTLAR**

**Jan 2014**

**109 pages**

In this study, an experimental investigation on flow mode analysis of pneumatic particle conveying was conducted. An experimental test set-up and coupled measurement system were constructed for the purpose.

The measurements were conducted in three separate test cases consisted of which vertical, horizontal test pipelines and a horizontal continuous conveying with a particle feeder. The covered particles of semolina, wheat, sand, polyethylene, zeolite and tea with the ranges of loose poured bulk density,  $200 \text{ kg/m}^3 < \rho_{blp} < 2400 \text{ kg/m}^3$  and average particle diameter,  $150 \text{ } \mu\text{m} < d_p < 2750 \text{ } \mu\text{m}$  were used in the range of  $21697 < \text{Re} < 156992$ . The measurements of the local static pressures, pressure drops,  $\Delta P$  and pressure gradients  $\Delta P/L$  were performed as a function of minimum fluidization velocity,  $U_{mf}$ . The velocity and pressure measurements which were evaluated through a custom design program FDRIPCS.vi in LabView 2009 SP1® environment were carried out in the error margins of  $\pm 1.16 \%$  and  $\pm 3.31 \%$  respectively.

The visual observation of the flow field through the functional relationships between  $P_1$  vs  $P_2$ ,  $\Delta P$  vs  $U_{air}$  were used to determine  $U_{mf}$ . The transported particles as a ratio of mass flow rate of air;  $\dot{M}_p/\dot{M}_a$ , calculated local permeability factors  $P_f$  and  $P_{f\text{mf}}$  and  $\text{Re}_{mf}$  corresponding to  $U_{mf}$  were used to analyze the flow modes with the covered ranges of  $21697 < \text{Re}_{mf} < 147600$ ,  $3.65 \text{ m/s} < U_{mf} < 24.83 \text{ m/s}$ ,  $0.0052 \text{ m}^2/\text{Pa.s} < P_f$

$\text{mf} < 0.92 \text{ m}^2/\text{Pa.s}$  and  $0.25 \% < \dot{M}_p/\dot{M}_a < 51.99 \%$ . The functional relationship between  $P_{f\text{mf}} = f(\text{Re}_{\text{mf}})$  was used to verify the flow mode analysis.

The observed modes were defined as: unstable zone, transition of fluidized dense phase, fluidized dense phase, slug flow, transition of plug flow, plug flow and dilute phase. The defined flow modes were the severe function of experimental methodology besides particle characteristics. It is seen that the value of loose poured bulk density,  $\rho_{blp}$  is dominant to determine flow modes when it is compared with average particle diameter,  $d_p$  in vertical test case. On contrary to this,  $d_p$  of particles are found to be more significant in comparison with  $\rho_{blp}$  for investigation of flow modes in horizontal test case. It seems that fluidized dense phase is in the range of  $0.0052 \text{ m}^2/\text{Pa.s} < P_f < 0.2 \text{ m}^2/\text{Pa.s}$ , slug flow and plug flow are valid for  $0.2 \text{ m}^2/\text{Pa.s} < P_f < 0.56 \text{ m}^2/\text{Pa.s}$  and dilute phase is inside  $0.56 \text{ m}^2/\text{Pa.s} < P_f$ .

**Key Words:** Loose poured bulk density, minimum fluidization velocity, permeability factor, air particle mass flow rate ratio, Reynolds number, pressure drops and pressure gradients.

## ÖZET

### PNÖMATİK TAŞIMA SİSTEMLERİNDE AKIM MODLARINA YÖNELİK BİR ANALİZ

**TOZLU, Alperen**

**M.Sc. Makine Mühendisliği**

**Tez Yöneticisi: Prof. Dr. Melda Özdiç ÇARPINLIOĞLU**

**Yardımcı Tez Yöneticisi: Doç. Dr. Ahmet İhsan KUTLAR**

**Ocak 2014**

**109 sayfa**

Bu çalışmada, pnömatik parçacık taşınmasındaki akım modlarına yönelik deneysel bir araştırma gerçekleştirildi. Bu amaçla deneysel bir test düzeneği ve buna bağlı ölçüm sistemi inşa edildi.

Ölçümler dikey, yatay boru hatları ve parçacık beslemeli yatay boru hattından oluşan üç ayrı test düzeneği için yapıldı.  $200 \text{ kg/m}^3 < \rho_{blp} < 2400 \text{ kg/m}^3$  ve  $150 \text{ } \mu\text{m} < d_p < 2750 \text{ } \mu\text{m}$  aralıklarındaki irmik, bulgur, polietilen, kum, zeolit ve çay  $21697 < Re < 156992$  değerleri arasında kullanıldı. Noktasal statik basınçlar, basınç düşüşleri  $\Delta P$ , ve basınç gradyanları  $\Delta P/L$  minimum akışkanlaşma hızının  $U_{mf}$ , fonksiyonu olarak alındı. Hız ve basınç ölçümleri LabView ortamında hazırlanan FDRIPCS.vi programı ile  $\pm \% 1.16$  ve  $\pm \% 3.31$  hata oranlarıyla yapıldı.

$P_1 - P_2$  ve  $\Delta P - U_{air}$  arasındaki fonksiyonel bağlantı minimum akışkanlaşma hızının hesaplanması için akım alanı boyunca ölçüldü ve görsel olarak incelendi. Taşınan parçacıkların yükleme oranı  $\dot{M}_p/\dot{M}_a$ , hesaplanan noktasal geçirgenlik faktörü  $P_f$ , ve  $U_{mf}^2$ ye bağlı olan  $P_{f\text{mf}}$  ve  $Re_{mf}$   $21697 < Re_{mf} < 147600$ ,  $3.65 \text{ m/s} < U_{mf} < 24.83 \text{ m/s}$ ,  $0.0052 \text{ m}^2/\text{Pa.s} < P_{f\text{mf}} < 0.92 \text{ m}^2/\text{Pa.s}$  and  $0.25 \% < \dot{M}_p/\dot{M}_a < 51.99 \%$  verilen aralıklarda akım modu analizi için kullanıldı.

Gözlemlenen akım modları: hareketsiz alan, hareketsiz alan ile akışkanlaşmış yoğun faz geçişi, akışkanlaşmış yoğun faz, tıkalı akış, birikintili akışa geçiş, birikintili akış ve seyrek faz oldu. Tanımlanan akım modları deneysel metodolojinin fonksiyonu



olmasının yanı sıra parçacık karakteristiği ile de ilgilidir.  $\rho_{blp}$  dikey test düzeneğinde  $d_p$ 'ye göre daha belirgin bir etkiye sahiptir. Buna tezat olarak,  $d_p$  ise yatay test düzeneğinde  $\rho_{blp}$ 'ye göre daha kayda değer bir etki göstermektedir. Sonuç olarak, akışkanlaşmış yoğun faz aralığı  $0.0052 \text{ m}^2/\text{Pa.s} < P_f < 0.2 \text{ m}^2/\text{Pa.s}$ , tıkalı akış ve birikintili akış aralığı  $0.2 \text{ m}^2/\text{Pa.s} < P_f < 0.56 \text{ m}^2/\text{Pa.s}$  ve seyrek faz  $0.56 \text{ m}^2/\text{Pa.s} < P_f$  olduğunda görülmektedir.

**Anahtar Kelimeler:** Göreceli yoğunluk, minimum akışkanlaşma hızı, geçirgenlik faktörü, minimum akışkanlaşma hızındaki geçirgenlik faktörü, hava ve parçacık kütle akış debi oranları Reynolds sayısı, basınç düşüşleri ve basınç gradyenleri.

## ACKNOWLEDGEMENTS

I am grateful to my supervisor Prof. Dr. Melda Özdiñ ÇARPINLIOĞLU for her advice, valuable comments, help and especially for the facilities that she provided for this study

I am also grateful to the members of thesis committee; Prof. Dr. Hüseyin YAPICI, Prof. Dr. Sait Söylemez and Assoc. Dr. Vedat ORUÇ for their comments and suggestions.

I want to thank Assoc. Prof. Dr. A. İhsan KUTLAR and Assist. Prof. Dr. Emrah ÖZAHİ for their valuable help, encouragement and contributions to this study.

This study would have never been completed without continuous encouragement of my wife Burcu TOZLU and my family. Therefore, I'm indebted for their support and great patience which they had shown during this study.

I wish also to thank the personnel of the Mechanical Engineering Department especially Mr. İbrahim KORKMAZ and workshop of the Mechanical Engineering Department.

I would also like to express my thanks to Research Fund of the University of Gaziantep for the research project supported under the code MF 12-15.

## CONTENTS

ABSTRACT .....	v
ÖZET .....	vii
ACKNOWLEDGEMENTS .....	ix
CONTENTS .....	x
LIST OF FIGURES .....	xii
LIST OF TABLES.....	xvii
LIST OF SYMBOLS .....	xxviii
<i>Greek letters</i> .....	xix
<i>Subscripts</i> .....	xix
CHAPTER 1: INTRODUCTION.....	1
CHAPTER 2: LITERATURE SURVEY.....	3
2.1 Introduction .....	3
2.2 Pneumatic Conveying Systems Terminology.....	4
2.3 Flow Modes in Pneumatic Conveying Systems .....	6
2.4 Conclusion.....	20
CHAPTER 3: EXPERIMENTAL TEST SET-UP AND MEASUREMENTS.....	23
3.1 Introduction .....	23
3.2 Experimental Test Set-up .....	24
3.2.1 Blower Unit.....	25
3.2.2 Settling Tank .....	25
3.2.3 Pipeline System .....	26
3.2.4 Particle Feeder .....	27
3.2.4.1 Modification of Particle Feeder.....	29
3.3 Measurement Devices and Methods .....	29
3.3.1 Pitot Tube and Traverse Mechanism .....	30
3.3.2 Manometers.....	31
3.3.3 Pressure Transmitters.....	32
3.3.4 Data Acquisition and Software Program .....	33
3.4 Properties of the Tested Solid Particles.....	35
3.5 Calibration .....	37
3.5.1 Pressure Transmitter Calibration .....	37
3.5.2 Particle Feeder Calibration.....	38
3.6 Uncertainty Analysis of Measurement Devices .....	39
3.7 Conclusion.....	42
CHAPTER 4: EXPERIMENTS ON THE STATE OF MINIMUM FLUIDIZATION AND FLOW MODE DETERMINATION .....	44
4.1 Introduction .....	44
4.2 Methodology for the Minimum Fluidization State Determination .....	44
4.3 Results in the Vertical Test Case .....	47

4.4 Results in the Horizontal Test Case .....	57
4.5 Results in the Continuous Conveying with Particle Feeder .....	67
4.6 Conclusion .....	78
CHAPTER 5: CORRELATIONS FOR FLOW MODE ANALYSIS .....	79
5.1 Introduction .....	79
5.2 Flow Mode Analysis through Variation of Permeability with $\dot{M}_p/\dot{M}_a$ .....	79
5.2.1 Determination of Plug-Slug Flow Modes through Test Case 2 (Horizontal) ..	79
5.2.2 Determination of Plug Flow and Dilute Phase through Continuous Conveying .....	83
5.2.3 Determination of Unstable Zone and Fluidized Dense Phase through Test Case 1 (Vertical).....	90
5.3 A Correlation Study in terms of Fluidized Dense Phase at Onset of Fluidization ...	96
5.4 Conclusion.....	97
CHAPTER 6: CONCLUSION AND SUGGESTIONS FOR FURTHER INVESTIGATIONS .....	99
LIST OF REFERENCES .....	103
APPENDIX 1 .....	106
TECHNICAL SPECIFICATIONS OF THE DRIVE UNIT OF BLOWER.....	106
APPENDIX 2 .....	107
TECHNICAL SPECIFICATIONS OF THE PARTICLE FEEDER.....	107
APPENDIX 3 .....	108
TECHNICAL SPECIFICATIONS OF THE PRESSURE TRANSMITTER.....	108
APPENDIX 4 .....	109
TECHNICAL SPECIFICATIONS OF THE DATA ACQUISITION BOARD .....	109

## LIST OF FIGURES

Figure 2.1 Geldart fluidization diagram.....	9
Figure 2.2 Molerus fluidization diagram. ....	10
Figure 2.3 Dixon slugging diagram .....	12
Figure 2.4.a-b Mainwaring and Reed pneumatic conveying predictive diagrams .....	13
Figure 2.5. Fargette pneumatic conveying predictive diagram .....	14
Figure 2.6. Chambers pneumatic conveying predictive diagram .....	15
Figure 2.7. Diagram of the mode of flow prediction of Sanchez .....	17
Figure 2.8. Pan pneumatic conveying predictive diagram .....	18
Figure 2.9. Jones and Williams proposed mode of flow predictive diagram .....	19
Figure 3.1 Vertical test set-up .....	23
Figure 3.2 Vertical test chamber.....	24
Figure 3.3 Horizontal test set-up .....	25
Figure 3.4 Flange between PVC pipe and acrylic glass pipe .....	26
Figure 3.5 Metal block (body) of particle feeder.....	28
Figure 3.6 Blade of particle feeder .....	28
Figure 3.7 Modification of particle feeder .....	29
Figure 3.8 Cross sectional velocity distribution .....	30
Figure 3.9 Cross sectional velocity distribution and 1/7 <sup>th</sup> power law.....	31
Figure 3.10 Block diagram of FDRIPCS.vi .....	34
Figure 3.11 Control panel of FDRIPCS.vi.....	34
Figure 3.12 Different mash size sieves .....	36

Figure 3.13 Calibration of pressure transmitters .....	38
Figure 4.1 Local static pressure variation in empty pipe in Test case 1 .....	45
Figure 4.2 Local static pressure variation in empty pipe in Test case 2 .....	46
Figure 4.3 Visual observation of Z1 at L10 a) unstable zone b) just start of fluidization state c) - d) fluidized dense phase .....	50
Figure 4.4 Pressure variation for W, PE and T at L10.....	51
Figure 4.5 Pressure variation for W, PE and T at L30.....	51
Figure 4.6 Pressure variation for W, PE and T at L50.....	52
Figure 4.7 Minimum fluidization state change as a function of bed thickness for W particles .....	53
Figure 4.8 Minimum fluidization state change as a function of bed thickness for Z1 particles .....	54
Figure 4.9 Minimum fluidization state change as a function of bed thickness for Z2 particles .....	54
Figure 4.10 Minimum fluidization state change as a function of bed thickness for PE particles .....	55
Figure 4.11 Minimum fluidization state change as a function of bed thickness for SE particles .....	55
Figure 4.12 Minimum fluidization state change as a function of bed thickness for T particles .....	56
Figure 4.13 Minimum fluidization state change as a function of bed thickness for S particles .....	56
Figure 4.14 Horizontal test case with particles .....	57
Figure 4.15 Visual observation of polyethylene .....	59
Figure 4.16 Pressure variation and minimum fluidization state change in test case 2 ...	60
Figure 4.17 $\Delta P$ as a function of $U_{air}$ for T.....	62
Figure 4.18 $\Delta P$ as a function of $U_{air}$ for S.....	63
Figure 4.19 $\Delta P$ as a function of $U_{air}$ for SE.....	63
Figure 4.20 $\Delta P$ as a function of $U_{air}$ for W .....	64
Figure 4.21 $\Delta P$ as a function of $U_{air}$ for PE.....	64

Figure 4.22 $\Delta P/ L$ as a function of $U_{air}$ for T .....	65
Figure 4.23 $\Delta P/ L$ as a function of $U_{air}$ for S .....	65
Figure 4.24 $\Delta P/ L$ as a function of $U_{air}$ for SE .....	66
Figure 4.25 $\Delta P/ L$ as a function of $U_{air}$ for W .....	66
Figure 4.26 $\Delta P/ L$ as a function of $U_{air}$ for PE .....	67
Figure 4.27 $\Delta P$ as a function of $U_{air}$ for S particles with the range of $0.50 < \dot{M}_p/\dot{M}_a < 14.20$ .....	70
Figure 4.28 $\Delta P$ as a function of $U_{air}$ for S particles with the range of $0.65 < \dot{M}_p/\dot{M}_a < 23.74$ .....	71
Figure 4.29 $\Delta P$ as a function of $U_{air}$ for S particles with the range of $1.08 < \dot{M}_p/\dot{M}_a < 29.14$ .....	71
Figure 4.30 $\Delta P$ as a function of $U_{air}$ for SE particles with the range of $0.25 < \dot{M}_p/\dot{M}_a < 4.18$ .....	72
Figure 4.31 $\Delta P$ as a function of $U_{air}$ for SE particles with the range of $0.37 < \dot{M}_p/\dot{M}_a < 11.70$ .....	72
Figure 4.32 $\Delta P$ as a function of $U_{air}$ for SE particles with the range of $0.43 < \dot{M}_p/\dot{M}_a < 17.56$ .....	73
Figure 4.33 $\Delta P$ as a function of $U_{air}$ for W particles with the range of $0.38 < \dot{M}_p/\dot{M}_a < 9.47$ .....	73
Figure 4.34 $\Delta P$ as a function of $U_{air}$ for W particles with the range of $0.43 < \dot{M}_p/\dot{M}_a < 12.20$ .....	74
Figure 4.35 $\Delta P/ L$ as a function of $U_{air}$ for S particles with the range of $0.50 < \dot{M}_p/\dot{M}_a < 14.20$ .....	74
Figure 4.36 $\Delta P/ L$ as a function of $U_{air}$ for S particles with the range of $0.65 < \dot{M}_p/\dot{M}_a < 23.74$ .....	75
Figure 4.37 $\Delta P/ L$ as a function of $U_{air}$ for S particles with the range of $1.08 < \dot{M}_p/\dot{M}_a < 29.14$ .....	75
Figure 4.38 $\Delta P/ L$ as a function of $U_{air}$ for SE particles with the range of $0.25 < \dot{M}_p/\dot{M}_a < 4.18$ .....	76
Figure 4.39 $\Delta P/ L$ as a function of $U_{air}$ for SE particles with the range of $0.37 < \dot{M}_p/\dot{M}_a < 11.7$ .....	76
Figure 4.40 $\Delta P/ L$ as a function of $U_{air}$ for SE particles with the range of $0.43 < \dot{M}_p/\dot{M}_a < 17.56$ .....	77

Figure 4.41 $\Delta P/ L$ as a function of $U_{air}$ for W particles with the range of $0.38 < \dot{M}_p/\dot{M}_a < 9.47$ .....	77
Figure 4.42 $\Delta P/ L$ as a function of $U_{air}$ for W particles with the range of $0.43 < \dot{M}_p/\dot{M}_a < 12.20$ .....	78
Figure 5. 1 $P_f$ values as a function of $\dot{M}_p/\dot{M}_a$ for SE in test case 1 .....	80
Figure 5.2 $P_f$ values as a function of $\dot{M}_p/\dot{M}_a$ for W in test case 1.....	81
Figure 5.3 $P_f$ values as a function of $\dot{M}_p/\dot{M}_a$ for S in test case 1. ....	81
Figure 5.4 $P_{f2}$ as a function of $\dot{M}_p/\dot{M}_a$ for S, SE and W in test case 1. ....	82
Figure 5.5 $P_{f3}$ as a function of $\dot{M}_p/\dot{M}_a$ for S, SE and W in test case 1 .....	82
Figure 5.6 $P_{f4}$ as a function of $\dot{M}_p/\dot{M}_a$ for S, SE and W in test case 1. ....	83
Figure 5.7 $P_f$ values as a function of $\dot{M}_p/\dot{M}_a$ for SE with 10 mm orifice in continuous conveying .....	83
Figure 5.8 $P_f$ values as a function of $\dot{M}_p/\dot{M}_a$ for SE with 15 mm orifice in continuous conveying.....	85
Figure 5.9 $P_f$ values as a function of $\dot{M}_p/\dot{M}_a$ for SE with 20 mm orifice in continuous conveying.....	85
Figure 5.10 $P_f$ values as a function of $\dot{M}_p/\dot{M}_a$ for W with 15 mm orifice in continuous conveying.....	86
Figure 5.11 $P_f$ values as a function of $\dot{M}_p/\dot{M}_a$ for W with 20 mm orifice in continuous conveying.....	86
Figure 5.12 $P_f$ values as a function of $\dot{M}_p/\dot{M}_a$ for S with 10 mm orifice in continuous conveying.....	87
Figure 5.13 $P_f$ values as a function of $\dot{M}_p/\dot{M}_a$ for S with 15 mm orifice in continuous conveying .....	87
Figure 5.14 $P_f$ values as a function of $\dot{M}_p/\dot{M}_a$ for S with 20 mm orifice in continuous conveying.....	88
Figure 5.15 $P_{f2}$ as a function of $\dot{M}_p/\dot{M}_a$ for SE, W and S in continuous conveying .....	88
Figure 5.16 $P_{f3}$ as a function of $\dot{M}_p/\dot{M}_a$ for SE, W and S in continuous conveying.....	89
Figure 5.17 $P_{f4}$ as a function of $\dot{M}_p/\dot{M}_a$ for SE, W and S in continuous conveying .....	89
Figure 5.18 $P_{f_{mf}}$ values as a function of $U_{mf}$ in test case 1 .....	91
Figure 5.19 $P_{f_{mf}}$ values as a function of $U_{mf}$ for SE in test case 1.....	91



Figure 5.20 $P_{f\text{mf}}$ values as a function of $U_{mf}$ for Z1 in test case 1.....	92
Figure 5.21 $P_{f\text{mf}}$ values as a function of $U_{mf}$ for Z2 in test case 1.....	92
Figure 5.22 $P_{f\text{mf}}$ values as a function of $U_{mf}$ for S in test case 1.....	93
Figure 5.23 $P_{f\text{mf}}$ values as a function of $U_{mf}$ for PE in test case 1.....	93
Figure 5.24 $P_{f\text{mf}}$ values as a function of $U_{mf}$ for W in test case 1. ....	94
Figure 5.25 $P_{f\text{mf}}$ values as a function of $U_{mf}$ for T in test case 1.....	94
Figure 5.26 $P_{f\text{mf}}$ values as a function of $\rho_{blp}$ and $d_p$ for covered particles at L10 in test case 1.....	95
Figure 5.27 $P_{f\text{mf}}$ values as a function of $\rho_{blp}$ and $d_p$ for covered particles at L30 in test case 1.....	95
Figure 5.28 $P_{f\text{mf}}$ values as a function of $\rho_{blp}$ and $d_p$ for covered particles at L50 in test case 1.....	96
Figure 5.29 Figure 5.29 Normalized pressure and velocity values for L10.....	97
Figure 5.30 Figure 5.29 Normalized pressure and velocity values for L30.....	98
Figure 5.31 Figure 5.29 Normalized pressure and velocity values for L50.....	98
Figure 6.1 Proposed flow mode diagram with regarding $P_{f\text{mf}}$ as a function of $Re_{mf}$ ....	100

## LIST OF TABLES

Table 2.1 Summary of proposed criteria in terms of modes of flow in pneumatic conveying system.....	22
Table 3.1 Blower calibration .....	32
Table 3.2 Physical characteristics of solid particles .....	37
Table 3.3 Calibration of particle feeder .....	39
Table 3.4 Statistical parameters used in uncertainty analysis .....	40
Table 3.5 Uncertainty analyze of pressure measurements based on the method in [33-37] .....	41
Table 3.6 Uncertainties of measurements utilized in the study according to the method in [33-37] .....	42
Table 4.1 Minimum fluidization velocities corresponding to the visual observation of the shape.....	49
Table 4.2 $U'_{mf}$ of W, S, SE, PE and T in test case 2 .....	58
Table 4.3 Mass flow rates of particles with respect to air for continuous conveying. ...	68
Table 6.1 Limit of flow modes in test cases.....	100

## LIST OF SYMBOLS

$A_f$	De-aeration parameter, Pa.s/m
$d_p$	Average particle diameter, m
D	Pipe diameter, m
$h$	Alcohol height in manometer, m
$F_H$	Adhesion force, N
Fr	Froude number
$F_t$	Average tensile force, N
$g$	Gravitational acceleration, m/s <sup>2</sup>
Grt	Sanchez parameter based on de-aeration, m
$K_{sp}$	Single plug factor in Eq 2.12
$K_1$	Constant in Eq 2.9
$K_2$	Constant in Eq 2.10
L	Length, m
$\dot{m}_p$	Mass flow rate of particles in modified particle feeder, kg/s
$\dot{M}_p$	Mass flow rate of conveyed particles, kg/s
Nc	Chambers flow mode parameter
P	Total pressure of atmospheric air, Pa
$P_{dyn}$	Dynamic pressure of air, Pa
$P^*$	Sanchez parameter based on permeability
$P_f$	Permeability parameter, m <sup>2</sup> /Pa.s
$P_{f\,mf}$	Permeability parameter at minimum fluidization velocity, m <sup>2</sup> /Pa.s
$\Delta P$	Pressure drop, Pa
Re	Reynolds number
$t$	Time, s
$t_c$	Calculated time, s
$t_{da}$	De-aeration time, s
$U$	Superficial gas velocity, m/s
$U_{air}$	Superficial air velocity, m/s

$U_{mb}$	Minimum bubbling velocity, m/s
$U_{mf}$	Minimum fluidization velocity at vertical test case, m/s
$U'_{mf}$	Minimum fluidization velocity at horizontal test case, m/s
$U''$	Minimum fluidization velocity at continuous conveying, m/s
$U_{sp}$	Gas slug velocity, m/s
$U_t$	Terminal velocity, m/s
$T$	Air temperature, K
$V$	Volume, m <sup>3</sup>

#### *Greek letters*

$\varepsilon$	Voidage
$\rho_g$	Density of fluid, kg/m <sup>3</sup>
$\rho_s$	Density of solid particle, kg/m <sup>3</sup>
$\rho_{blp}$	Loose poured bulk density, kg/m <sup>3</sup>
$\rho_{alc}$	Alcohol density, kg/m <sup>3</sup>
$\theta$	Inclination angle of alcohol manometer, degree
$\mu$	Dynamic viscosity, Pa.s
$\Omega$	Fargette flow mode parameter

#### *Subscripts*

air	Air
av	Average
mf	minimum fluidization

#### *Abbreviates and others*

SE	semolina
W	wheat
PE	polyethylene
S	sand
Z1	zeolite 1
Z2	zeolite 2
T	tea

## **CHAPTER 1**

### **INTRODUCTION**

In this thesis, an experimental study is supported by Research Fund of University of Gaziantep through the project coded MF 12-15 which is carried out in order to investigate flow modes for a variety of solid particles for two main test cases which are conducted at vertical and horizontal pipeline systems. Furthermore, the behavior of the covered particles is investigated in the continuous conveying for control and comparison of flow modes with the previous ones.

In Chapter 2, literature survey on the manner is summarized. Available definitions and methods for the determination of flow modes are presented, analyzed and compared for pneumatic conveying systems.

In Chapter 3, the details of the experimental test set-up which is designed and constructed for determination of flow modes are presented. Measurement instruments and techniques, calibration and experimental procedure are given in that Chapter. Furthermore, uncertainty analyses of the measurement chains are carried out.

In Chapter 4, the methodology of the determination of minimum fluidization velocity is presented for the vertical, horizontal test case and also continuous conveying. Additionally, the flow modes are detected considering the minimum fluidization velocities for the covered particles in reference to visual observations of the flow field. Moreover, the effects of loose poured bulk densities and average diameters of the covered particles are investigated to determine the flow modes in pneumatic conveying systems.

In Chapter 5, the detected flow modes are considered in order to define their limits by means of permeability,  $P_f$  and  $\dot{M}_p/\dot{M}_a$ . On the other hand, a correlation study is carried out by using trial and error procedure and the variation of the normalized pressure  $\Delta P/P_{\text{dyn}}$  with respect to the normalized velocity  $U_{\text{air}} / U_{\text{mf}}$  is considered for the vertical test case.

In Chapter 6, the general concluding remarks as a result of the experimental study are given. Some apparent deductions and further recommendations are highlighted.

## **CHAPTER 2**

### **LITERATURE SURVEY**

#### **2.1 Introduction**

In this study, pneumatic conveying systems are analyzed due to their importance in industrial area. However, the flow modes in pneumatic conveying systems are not clearly understood.

Pneumatic conveying systems are widely used in various industrial settings due to the spectrum of materials to be conveyed. Basically, it becomes important phenomenon in decision stage of the effective flow modes to reduce the required energy for conveying of any particles in well-designed conveying pipeline systems in industry. There are some classifications of flow modes for conveyed both powders and bulk solid particles based on mean particle size and density difference, and also by taking into account inter particle cohesion forces. The material properties and flow parameters are defined with different symbols by each scientist in the literature. The available literature based on the flow modes and classifications are tabulated with their proposed critical equations in order to collect all for ease usage and well understanding.

## 2.2 Pneumatic Conveying Systems Terminology

Pneumatic conveying systems are used in industrial applications for transporting solid particle materials through a pipeline system with the aid of medium gas. These systems are quite simple to setup in a factory. Because of this reason pneumatic conveying systems find widespread applications in the area of chemical, food, textile, pharmaceutical industries etc. Simple pneumatic conveying system requires a blower to provide air supply; feeder for feeding particles to a system; and a pipeline and a receiver for transports and collecting materials respectively. In gas-solid flow structure, the combined flow character plays an important role in terms of transport effectiveness and energy consumption, which are called as modes of flow in two-phase flow jargon. Gas velocity, gas flow rate, minimum fluidization velocity, particle size, particle density, bulk density and particle shape are the most important parameters used to identify a two-phase flow mode.

In practice, non-suspension or dense phase flow is desirable for measure of conveying in terms of the ratio of conveyed material in amount to the amount of air supply whereas the suspension or dilute phase flow is not. However, many products are/have to be conveyed in dilute phase conveying system.

Particle/air interaction parameters such as permeability, air retention and de-aeration are all dependent on physical properties of conveyed materials such as: particle size, size distribution, density of particle, loose-poured bulk density and shape. Loose-poured bulk density,  $\rho_{blp}$ , of bulk materials is the mass per unit volume which is measured when particle is in a loose, non-compacted or poured condition, expressed as follows:

$$\rho_{blp} = (1-\varepsilon)(\rho_s - \rho_g) \quad (2.1)$$



where  $\rho_s$  is density of solid particle conveyed,  $\rho_g$  is fluid density and  $\varepsilon$  is bulk voidage.

Permeability,  $P_f$  is a measure of how the air flows through the material under a motive force and can be expressed as ratio of superficial velocity of gas,  $U$  to pressure drop per unit pipe length,  $\Delta P/L$  occurring in flow line:

$$P_f = U/(\Delta P/L) \quad (2.2)$$

Superficial gas velocity  $U$  is defined as:

$$U = Q/A \quad (2.3)$$

where  $Q$  is volumetric gas flow rate and  $A$  is cross-sectional area of bed/pipe.

Air retention is the ability of a material to retain air in the void spaces of the material after the air supply has been terminated. De-aeration,  $A_f$  is a measure of how the air naturally escapes from the material and can be expressed as;

$$A_f = t(\Delta P/L) \quad (2.4)$$

where  $t$  is the time related to the pressure drop decay plot from fluidization pressure to atmospheric pressure.

Minimum fluidization velocity,  $U_{mf}$  at the onset of fluidization is commonly given as;

$$U_{mf} = P_{f\,mf}(\Delta P/L) \quad (2.5)$$

Fluidization is defined as an aerated state of material. Saltation is a process of deposition of particles along horizontal pipeline which occurs when air velocity falls below minimum conveying value. Dense phase (non-suspension) is defined as a state which occurs when gas velocity is under saltation velocity of particle conveyed. Dilute phase (suspension) is another typical state which may occur when gas velocity becomes equal to or gets above the saltation velocity of particle. Slug flow is described by presence of liquid rich slugs that span entire channel or pipe area. This type of flow is proper to implement for conveying friable and/or granular products. When air mass flow rate is reduced, some conveyed particles accumulate at bottom of pipeline and form long plugs. This type of flow just described is known as plug flow. In plug flows, high fluctuations in pressure may take place and that may cause vibration in whole systems resulting from formation of long plug structures. This region is referred as an unstable zone.

### **2.3 Flow Modes in Pneumatic Conveying Systems**

At design stage of a pneumatic conveying system, it would be most desirable to identify flow modes by applying a proper prediction scheme rather than realizing on experimental work in regarding to huge cost saving aspect. It is more convenient to determine modes of flow using some predictive techniques instead of experimentally conveying material in a pipeline at beginning of design stage providing a considerable benefit in terms of cost. In literature, there are two distinct classifications in order to form generalized charts in terms of flow modes; i) based on physical properties of particles conveyed [1-3], and ii) based on particle/air interaction of gas-solid phase [4-9]. Moreover, improvements to the classifications based on physical properties of particles are carried out taking into account a loose-poured bulk density parameter [10-14] and inter particle cohesion forces [15].

The gas-solid flow character was classified into four categories by Geldart [1] in terms of mean particle size and density difference as shown in figure 2.1. This classification is summarized as follows;

1) Powders in Group A in which material has a small mean size and/or a low particle density (less than about  $1.4 \text{ g/cm}^3$ ) behave as dense phase expansion after minimum fluidization. When superficial gas velocity is high enough in order to form slugging conditions, the slugs are axisymmetric, while the superficial gas velocity is increased further, slug flow tends to transition to turbulent. Some cracking catalysts can be given as typical examples.

2) Powders in Group B will bubble at minimum fluidization velocity in contrast to powders in Group A. The materials in this group have mean size and density ranges of  $40\mu\text{m} \leq d_p \leq 500\mu\text{m}$  and  $1.4 \text{ g/cm}^3 \leq \rho_s \leq 4 \text{ g/cm}^3$ , respectively. Sand is a typical example for this group.

3) Powders in Group C are difficult to fluidize at all due to interparticle cohesive forces. The powder lifts as a plug in small diameter tubes, or channels (rat-holes) badly. The interparticle forces are greater than the fluid forces exerted on particle. This behavior generally occurs in the case of materials that have very small particle size, strong electrostatic force and are very wet or sticky. Pulverized powders are examples of this group.

4) The materials in Group D have comparatively large and/or very dense particles. The materials in this group can be spouted if gas is admitted only through a centrally positioned hole. The flow regime among the particles may be turbulent.

Geldart [1] proposed a criterion to determine the boundary between the powders in Groups A and B according to whether the superficial gas velocity at minimum bubbling,  $U_{mb}$  is greater than superficial gas velocity at minimum fluidization,  $U_{mf}$  or not. In Group A,

$$U_{mb}/U_{mf} \geq 1 \quad (2.6)$$

Geldart [1, 16-18] used three different types of low density powder which are diakon, fresh and spent catalyst in his experiment. He proposed a linear representing the relationship between mean particle size,  $d_p$  and minimum bubbling velocity,  $U_{mb}$ , and compared it with the equation which was given by Davies and Richardson [18] for the superficial gas velocity at minimum fluidization, which are given respectively as follows;

$$U_{mb} = 100 d_p \quad (2.7)$$

$$U_{mf} = 0.0008g d_p^2 (\rho_s - \rho_g) \mu \quad (2.8)$$

where  $g$  is gravitational acceleration and  $\mu$  is dynamic viscosity. The equation describing the limit of Group A and B is obtained by inserting Eqs. (2.7) and (2.8) into Eq. (2.6), [1].

The boundary between Group B and D is not so clear as is between Group A and B. However, the proposed criterion by Geldart [1] is given in Table 2.1. There is no criterion proposed or attempt in describing the boundary between Group A-C.

Molerus [4-6] considered interparticle cohesion forces in addition to Geldart's classification as shown in figure 2.2. The limiting conditions between Group A-C; Group A-B and Group B-D were defined using semi-empirical criteria by analyzing the forces exerted by the gas on the particles and the cohesion forces between particles.

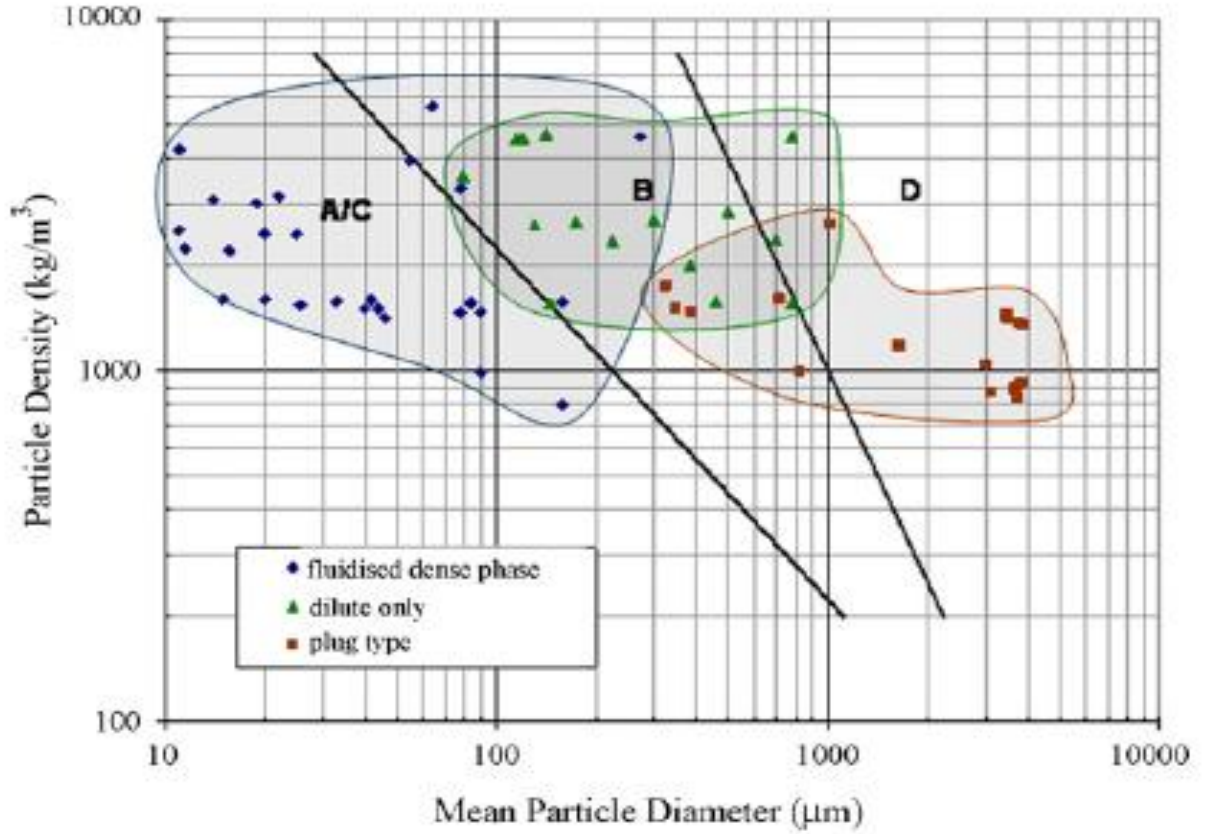


Figure 2.1 Geldart fluidization diagram

There is no boundary between Group A-C in Geldart's diagram. However, Molerus [4-6, 19-21] proposed an equation describing the boundary between Group A-C for hard particles as;

$$D_{1max}/F_T = 10(\rho_s - \rho_g) d_p^3 g/F_H = K_1 = 1/100 \quad (2.9)$$

where  $D_{1max}$  is maximum drag force,  $F_T$  is average tensile force transmitted per particle,  $F_H$  is adhesion force transmitted in a particles contact. Molerus [5] also defined an equation describing Group A-B boundary for hard particles as follows;

$$(\rho_s - \rho_g)\pi d_p^3 g/6F_H = K_2 = 0.16 \quad (2.10)$$

To predict the Group B-D boundary, the following equation is proposed by Molerus [5];

$$(\rho_s - \rho_g)d_p g = 15.3 \quad (2.11)$$

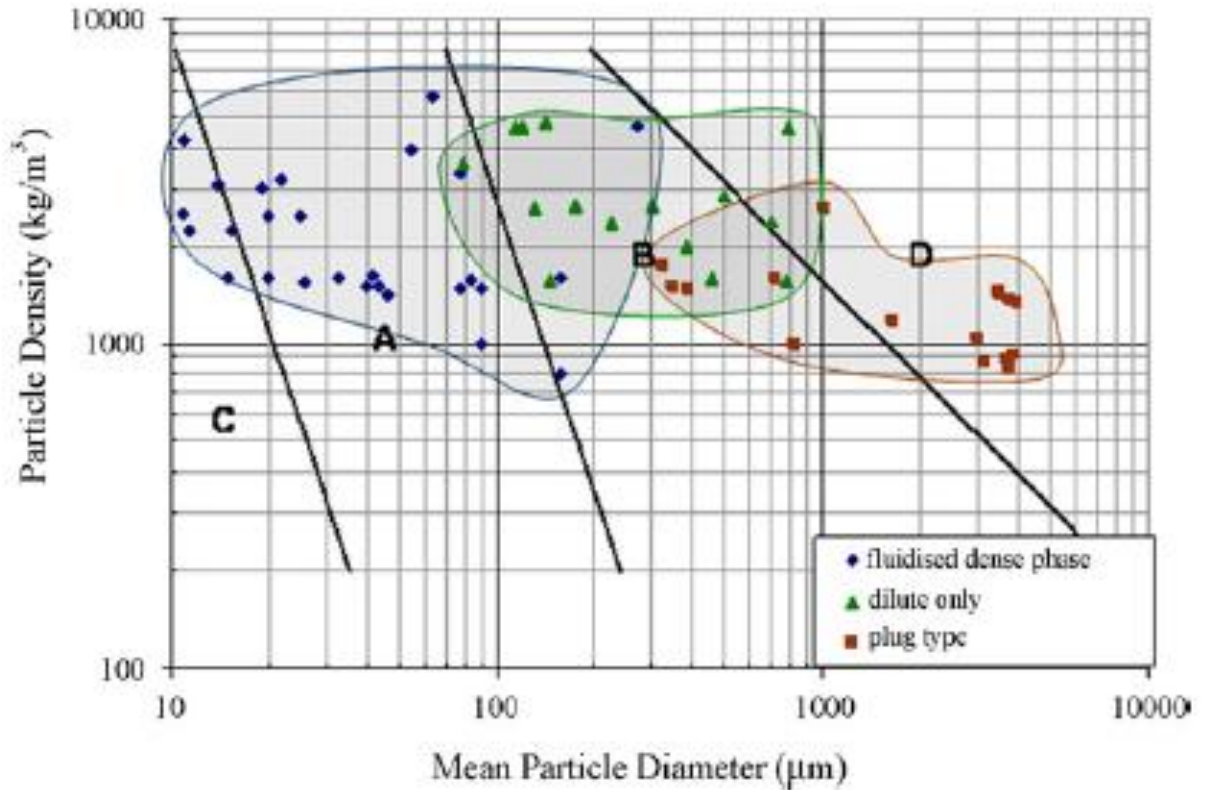


Figure 2.2 Molerus fluidization diagram

Dixon [3] classified gas-solid flows into three groups as i) axisymmetric slugs, ii) weak asymmetric slugs (dunes) and iii) no slugs at all which is given in figure 2.3. He considered the relationship between the gas slug velocity,  $U_{sp}$ , terminal

velocity,  $U_t$ , and minimum fluidization velocity,  $U_{mf}$  using the following equations;

$$U_{sp} = 0.35(K_{sp}gD)^{1/2} \quad (2.12)$$

where  $D$  is pipe diameter and  $K_{sp}=1$  for axisymmetric slugs;  $K_{sp}=2$  for asymmetric slugs.

$$U_t = 0.152(\rho_s - \rho_g)^{0.714} d_p^{1.14} g^{0.714} / \mu^{0.428} \rho_g^{0.258} \quad (2.13)$$

$$\rho_s(1-\varepsilon) = 150(1-\varepsilon)^2(\mu U_{mf})/(\varepsilon^3 g \cdot d_p^2) + 1.75(1-\varepsilon)(\rho_g U_{mf}^2)/(\varepsilon \cdot g \cdot d_p) \quad (2.14)$$

where  $\varepsilon$  is voidage which is ratio of space volume among particles/powders in a bed to total volume of bed.

According to Dixon [3], there is no stable slug formation if  $U_t < U_{sp}$  hence the boundary between no slugging and asymmetric slugs is denoted at  $U_t = U_{sp}$ . No full bore plug flow occurs if  $U_{mf} < U_{sp}$  hence the boundary between axisymmetric slug and weak asymmetric slugs is given by  $U_{mf} = U_{sp}$ .

Mainwaring and Reed [7] presented his experimental work in the form of two diagrams as a function of permeability and de-aeration factors of materials tested with respect to steady state fluidization pressure drop per unit length for dense phase conveying at minimum fluidization as shown in figure 2.4.a and figure 2.4.b. With regarding to permeability factor, two areas were differentiated with respect to the constant minimum fluidization velocity of 50 mm/s. The data above this critical line belong to the conveying in a dense phase plug flow in which the materials have the high permeability factors. On the other hand, the other data below the line has the character of those conveyed in dilute phase or fluidized dense phase. In terms of classification with respect to the specified parameter of the de-aeration factor divided by the particle density, they found that the materials having the high values of the

specified parameter (above the demarcation line) can be conveyed in fluidized dense phase while other materials below the demarcation line can be conveyed in a dilute phase or plug flow.

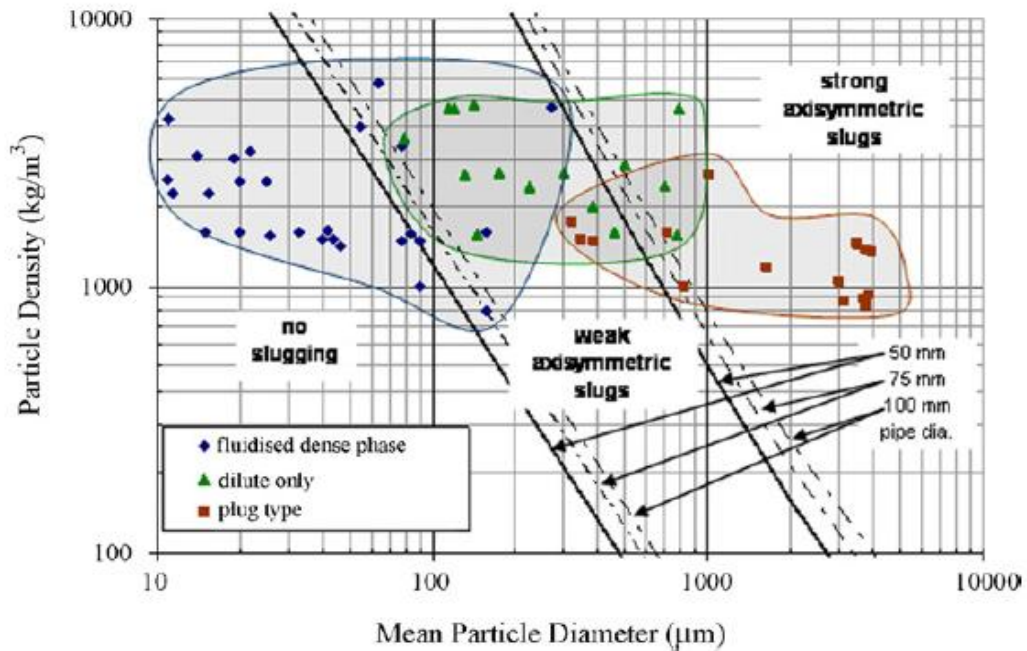


Figure 2.3 Dixon slugging diagram

A conventional pressure vessel system (blow tank) was used in their experiment. A wide range of products were conveyed at low velocity in dense phase. The fine powders conveyed such as cement, pulverized coal etc. and coarse granular materials such as mustard seed, plastic pellets etc. have the characteristics in the range of  $990 \text{ kg/m}^3 \leq \rho_s \leq 4610 \text{ kg/m}^3$ ,  $22 \mu\text{m} \leq d_p \leq 1650 \mu\text{m}$ ,  $400 \text{ kg/m}^3 \leq \rho_{blp} \leq 2600 \text{ kg/m}^3$ , and typical air mass flow rates used during the experimental work are in the ranges of  $5 \text{ g/s} < \dot{m}_{air} < 100 \text{ g/s}$  for conveying of pulverized coal, and  $2 \text{ g/s} < \dot{m}_{air} < 20 \text{ g/s}$  for conveying of  $1000 \mu\text{m}$  sand.



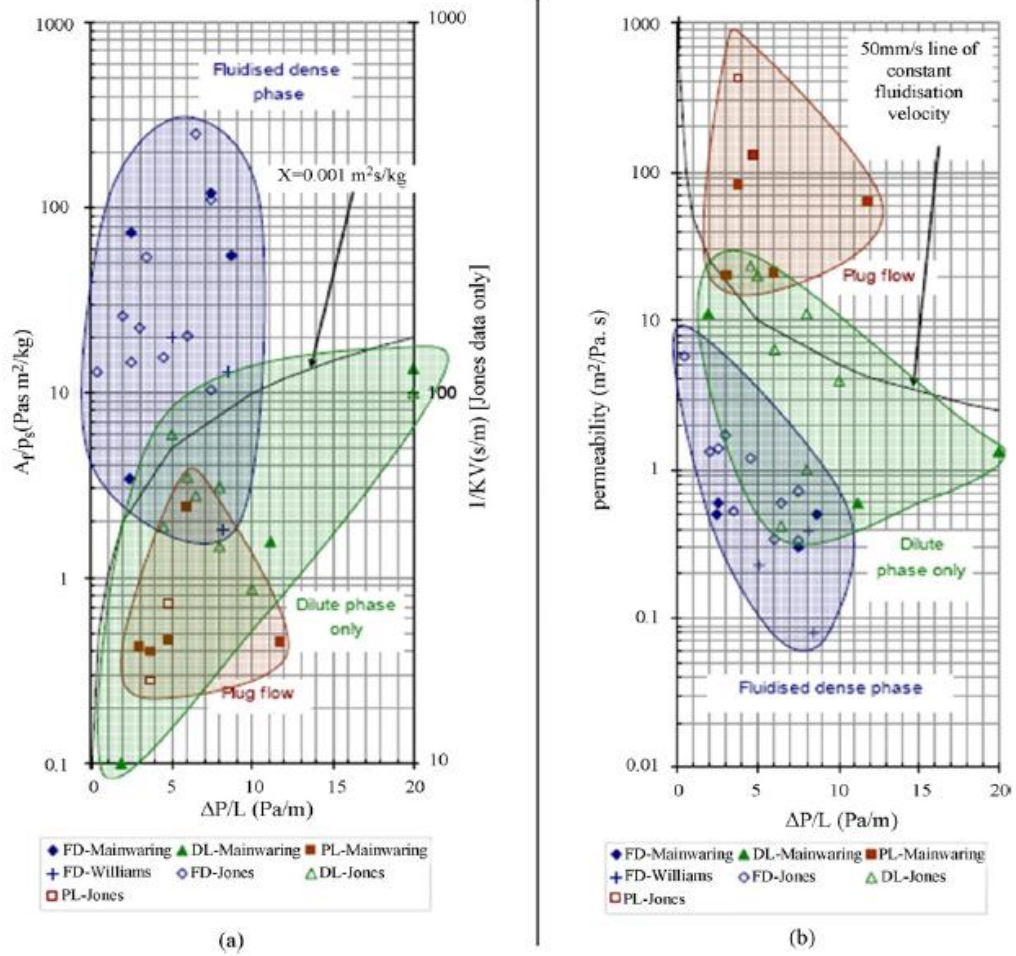


Figure 2.4.a and 2.4.b Mainwaring and Reed pneumatic conveying predictive diagrams

Mainwaring and Reed [7] proposed the limit line separating two modes of fluidized dense phase and plug flow by introducing a new parameter defined as  $X = t/\rho_s = 0.001 \text{ m}^3\text{s/kg}$ .

Fargette et al. [8] classified the powders conveyed in a dense phase, which are particularly used in steel manufacturing process, based on the permeability factor, air retention and cohesion of powders. Their classification is shown in figure 2.5. They defined the pneumatic flow parameter,  $\Omega$  as follows:

$$\Omega = t_{da} / \rho_{bip} P_f \quad (2.15)$$

If  $\Omega > 4000$ , the mode of flow becomes fluidized dense phase; plug flow if  $\Omega < 18$  and flow is dilute only if  $18 < \Omega < 4000$ .

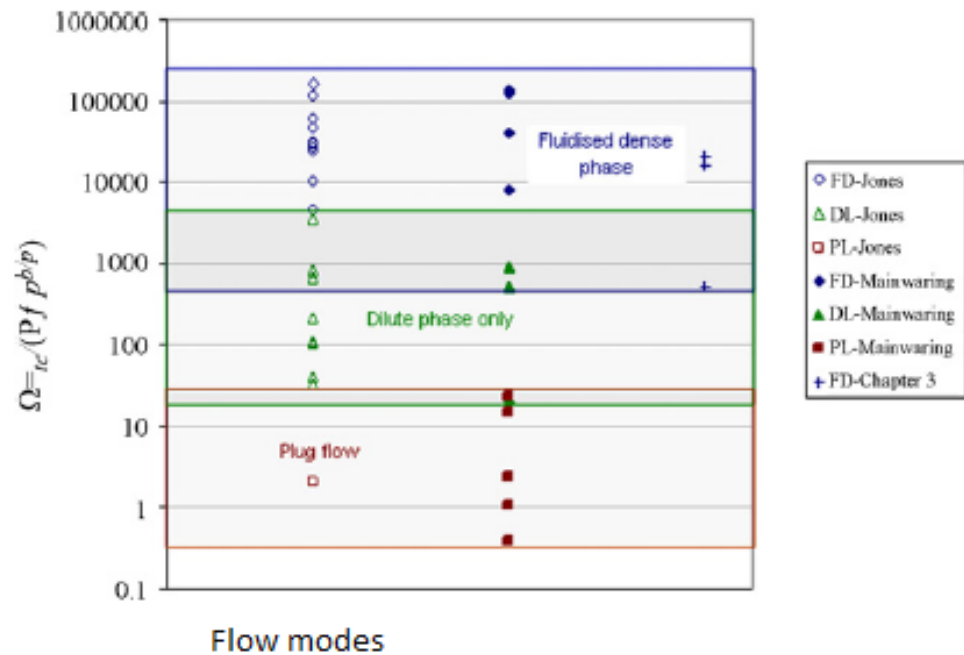


Figure 2.5 Fargette pneumatic conveying predictive diagram

Chambers et al. [22] introduced a parameter similar to that of Fargette et al. [8], in figure 2.6, but now  $N_c$  is based on permeability, de-aeration time and particle density instead of loose-poured bulk density, as;

$$Nc = \rho_s P_f / t_{da} \quad (2.16)$$

They classified the conveying of materials into three flow modes as follows i) dense phase slugging mode, ii) lean phase mode and iii) dense phase moving bed mode. The conveyed material is appropriate for slugging dense phase transportation for  $Nc > 0.01$ ; and for  $Nc < 0.001$ , the material can be conveyed as a dense phase conveying in a moving bed flow. At intermediate range of  $0.001 < Nc < 0.01$ , the material can be conveyed only in a lean phase mode.

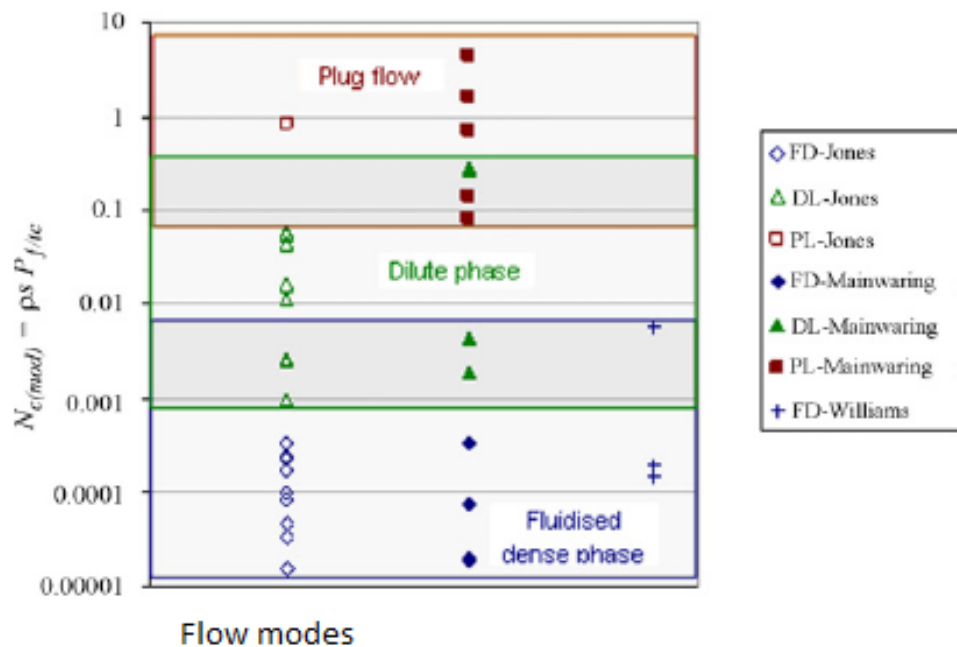


Figure 2.6 Chambers pneumatic conveying predictive diagram

Sanchez et al. [9, 23-28] took into consideration of the measurement of the permeability and de-aeration time of the particles to predict the feasibility of conveying particles in dense phase mode by reviewing and comparing the available methods in literature and they presented the results in a diagram as shown in figure

2.7. The measurements of the permeability factor and the de-aeration parameter were carried out by means of their fluidization equipment. Many types of materials such as alumina, glass bead, sand, polyester etc. were tested having properties in the range of  $912 \text{ kg/m}^3 \leq \rho_s \leq 4350 \text{ kg/m}^3$ ,  $7.67 \mu\text{m} \leq d_p \leq 5412 \mu\text{m}$ ,  $0.006 \text{ m/s} \leq U_{mf} \leq 1.58 \text{ m/s}$ ,  $0.005 \text{ m}^2/\text{bar.s} \leq P_f \leq 1.72 \text{ m}^2/\text{bar.s}$ . They classified the material conveying in dense phase mode into two general groups; the primary parameters such as particle size, shape and bulk density, permeability, de-aeration, cohesiveness etc., and the secondary parameters such as adhesion, moisture, electrostatics, elasticity and temperature sensitivity. As a result of their analyses, they found that some materials do not obey Geldart's classification traced to the secondary parameters. They also defined a group of dimensionless parameters and presented their results in terms of these dimensionless parameters such as de-aeration factor, permeability factor and Froude number based on minimum fluidization velocity as;

$$Grt = \mu t_{da} / d_p (\rho_s + \rho_g / 2) \quad (2.17)$$

$$P^* = P_f \rho_s (g d_p)^{1/2} / d_p \quad (2.18)$$

$$Fr_{mf} = U_{mf} / (g d_p)^{1/2} \quad (2.19)$$

Pan [13] modified Geldart's classification using loose-poured bulk density instead of difference between particle and gas densities as shown in figure 2.8. He classified the flow in conveying of bulk solid materials into three modes: i) PC1: smooth transition from dilute to fluidized dense-phase, ii) PC2: dilute-phase, unstable-zone and slug-flow, and iii) PC3: dilute phase only considering pressure drop and air mass flow rate.

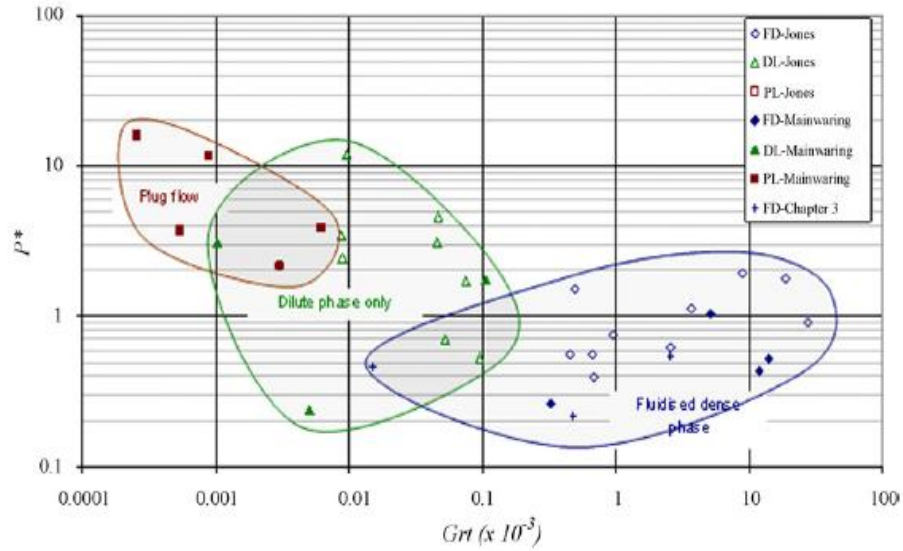


Figure 2.7 Diagram of the mode of flow prediction of Sanchez

i) In flow regime PC1, the air mass flow rate is decreased for a constant particle mass flow rate, the pressure drop also decreases and transition to dense phase from dilute phase occurs. Many types of fine powders as fly ash, pulverized coal etc. were used in the range of  $1415 \text{ kg/m}^3 \leq \rho_s \leq 2217 \text{ kg/m}^3$ ,  $11.5 \text{ }\mu\text{m} \leq d_p \leq 46.3 \text{ }\mu\text{m}$ ,  $368 \text{ kg/m}^3 \leq \rho_{blp} \leq 957 \text{ kg/m}^3$ .

ii) PC2 is divided into three distinct groups: dilute-phase, unstable-zone, and slug flow. In dilute-phase, the particles are distributed evenly over the entire cross section of the pipe. As the air mass flow rate is decreased, the air velocity is not adequate to transport all particles and some particles falls down to the bottom of the pipeline, forming long plugs and this produces high fluctuations in pressure and vibration. This region is referred to the unstable zone. If the air mass flow rate is decreased even further, the particles are conveyed in the form of slugs. Many types of materials such as narasin, barley, wheat etc. were used in the range of  $834 \text{ kg/m}^3 \leq \rho_s \leq 1745 \text{ kg/m}^3$ ,  $325 \text{ }\mu\text{m} \leq d_p \leq 3910 \text{ }\mu\text{m}$ ,  $458 \text{ kg/m}^3 \leq \rho_{blp} \leq 880 \text{ kg/m}^3$ .

iii) Heavy granular and/or crushed particles can only be conveyed in dilute-phase, PC3. Otherwise the particles interlock forming a packed bed. Many types of materials in this group such as high silica flux and primary concentrate were used in the range of  $2664 \text{ kg/m}^3 \leq \rho_s \leq 4742 \text{ kg/m}^3$ ,  $142 \text{ }\mu\text{m} \leq d_p \leq 300 \text{ }\mu\text{m}$ ,  $1519 \text{ kg/m}^3 \leq \rho_{bp} \leq 2778 \text{ kg/m}^3$ .

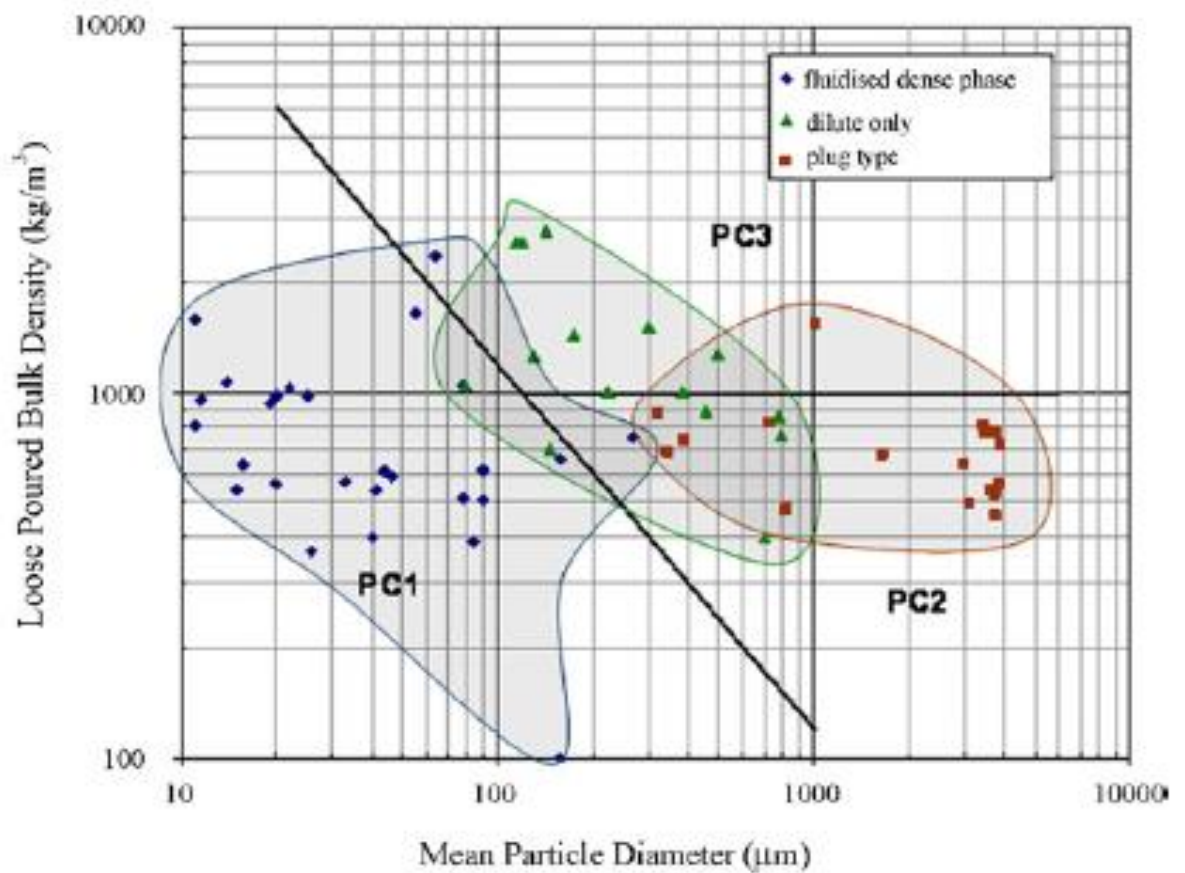


Figure 2.8 Pan pneumatic conveying predictive diagram

Williams and Jones [14] analyzed Geldart, Molerus and Dixon's classification diagrams and replaced the particle density parameter used there with

that of loose-poured bulk density in their charts. Jones and Williams [15,29] also established two types of predictive charts based on basic particle parameter and air-particle parameter as shown in figure 2.9. The improvements were tried to be made by first replacing the particle density with loose-poured bulk density used in the prediction parameter techniques. An air-particle based technique was improved such that in the new scheme there is no necessary of use of any de-aeration parameter. The equations which describe these boundaries between the fluidized dense phase and dilute only (Eq. 2.20), and dilute only and plug flow (Eq. 2.21) were introduced in Table 1 as follows;

$$P_f \rho_{bfp}^{3/4} \approx 300 \quad (2.20)$$

$$P_f \approx 20 \times 10^{-6} \quad (2.21)$$

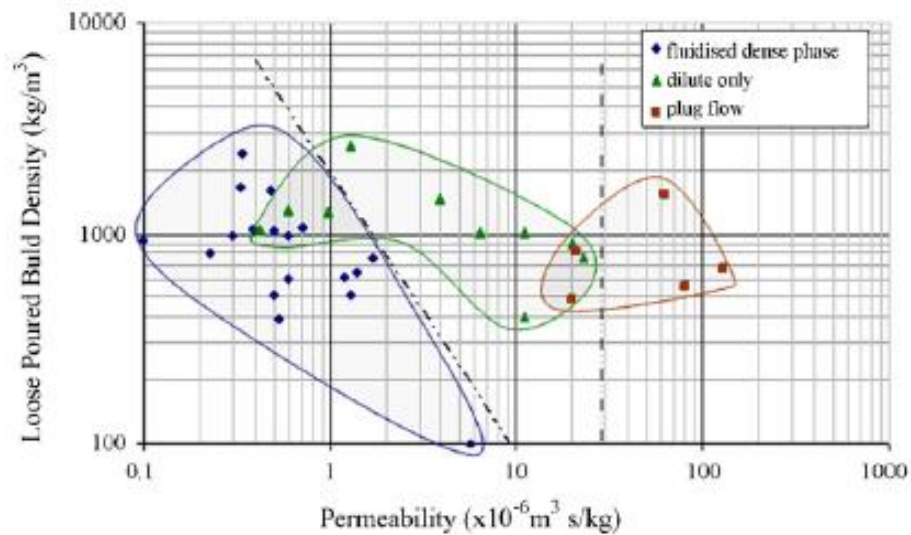


Figure 2.9 Jones and Williams proposed mode of flow predictive diagram

They also modified Chambers et al.'s parameter as follows;

$$P_f \rho_s / t_c = Nc(\text{mod}) \quad (2.22)$$

where  $t_c$  is de-aeration time as defined by Jones [15] and Sanchez [9].

If  $Nc(mod) < 8 \times 10^{-4}$ , flow is fluidized dense-phase. It is dilute only when  $8 \times 10^{-4} < Nc(mod) < 0.07$  and plug flow if  $Nc(mod) > 0.07$ .

## 2.4 Conclusion

Geldart's [1] classification is practical in estimating of flow modes for pneumatic conveying systems. However, it is unsuitable alone for prediction of flow mode in dense phase. Moreover, Dixon's [3] approach is convenient at the design stage, but provisional for an accurate prediction of flow modes. Mainwaring and Reed's [7] approach is more reliable predictive method than the Geldart's [1] and Dixon's [3] approaches due to the introduction of permeability and de-aeration factors instead of relying only on physical properties of particles. Fargette et al. [8] the air/particle interaction into consideration by introducing a non-dimensional parameter composed of de-aeration time, permeability and loose-poured bulk density. Chambers [22] also introduced another dimensionless parameter similar to that proposed by using Fargette et al. [8] using particle density instead of loose poured bulk density. According to Sanchez [9], some materials do not obey Geldart's[1] classification due to the secondary parameter properties of materials. Molerus [5] modified the Geldart's [1] classification and also described the criterion between Geldart's [1] Group A-C by considering cohesion forces. Pan [13] sorted the flow mode as a function of loose poured bulk density and median particle diameter showing agreement with those of Geldart[1], Dixon[3] and Mainwaring and Reed [7]. Jones and Williams [15] reviewed all available works in their study and also proposed new criteria for Geldart's [1] Group A-B and B-D by taking into account loose poured bulk density and permeability.

Hence, there are many flow mode diagrams and proposed criteria to use in determination of flow modes for pneumatic conveying of powders/granular particles from Geldart's approach [1] to the study of Jones and Williams [15]. As it can be seen, some of the scientists considered only physical properties of particles/powders



while others took into account both physical properties of particles and air/particle interaction. There are some agreements and conflicting results among the proposed approaches. Thus, all proposed criteria are reviewed and sorted out by Tozlu et. al. [30] for further studies and also the available classifications of modes of flow for pneumatic conveying of powders and granular particles are summarized as shown in Table 2.1.

Table 2.1 Summary of Proposed Criteria in Terms of Modes of Flow in Pneumatic Conveying System

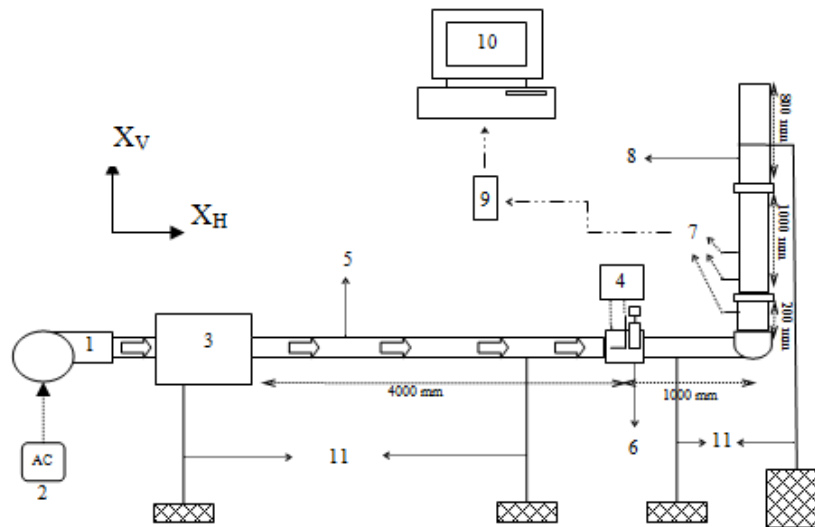
Authors	Modes of flow	Predictive diagrams	Limitations	Boundaries and formulations	
Geldart [1]	A-Fluidized dense-phase	Particle density difference - mean particle diameter (kg/m <sup>3</sup> ) - (m)	$\rho_s < 1.4 \text{ gr/cm}^3$	A/C-B $(\rho_s - \rho_g)H_p = 22.5 \times 10^{-3}$	
	B- Dilute phase		$\rho_s > 1.4 \text{ gr/cm}^3$ $50Q_{um} > d_p > 4Q_{um}$	B-D $(\rho_s - \rho_g)H_p^2 = 10^{-3}$	
	C- Difficult to fluidize		Difficult to fluidization		
	D- Plug mode of dense phase		Large or dense particles		
Dixon [3]	Axisymmetric slugs- Plug type	Particle density difference - mean particle diameter (kg/m <sup>3</sup> ) - (m)	-	Axisymmetric/asymmetric $\frac{d_p(\rho_s - \rho_g)}{D^{0.5}} = \frac{1.64 \times 10^{-3}}{d_p} + 2.68D^{0.5} - \frac{\rho_g d_p}{D}$	
	Weak asymmetric slugs- Dilute phase		$V_{mf} < V_{sp}$ (m/s)	No slugging/asymmetric $\frac{d_p^{1.14}(\rho_s - \rho_g)^{0.714}}{D^{0.5}} = 13.6 \times 10^3$	
	No slugging- Fluidized dense-phase		$V_f < V_{sp}$ (m/s)		
Mainwaring and Reed [4]	Plug type	Permeability- ( $\Delta P/L$ )	$V_{mf} > 50 \text{ mm/s}$	$V_{mf} = P_f \left( \frac{\Delta P}{L} \right)_{ss} = 50 \text{ mm/s}$	
	Dilute only or fluidizes dense-phase		$V_{mf} < 50 \text{ mm/s}$		
	Fluidized dense phase	De-aeration/density- ( $\Delta P/L$ )	$X > 0.001 \text{ m}^3/\text{kg}$	$\frac{\Delta P}{L} X = \frac{A_f}{\rho_s}$	
	Dilute only or plug flow		$X < 0.001 \text{ m}^3/\text{kg}$		
Fargette et al. [5]	Fluidized dense phase	Non-dimensional parameter ( $\Omega$ )	$\Omega > 4000$	$\Omega = \frac{t_{da}}{P_f \rho_{bp}}$	
	Dilute only		$18 < \Omega < 4000$		
	Plug flow		$18 < \Omega$		
Chambers et al. [6]	Dense-phase/moving bed	Non-dimensional parameter ( $N_c$ )	$N_c < 0.001$	$N_c = \frac{\rho_s P_f}{t_{da}}$	
	Lean phase mode		$0.001 < N_c < 0.01$		
	Slugging dense-phase		$N_c > 0.01$		
Sanchez et al. [7]	Fluidized dense phase	Non-dimensional parameters: $Grt$ , $P^*$ , $Fr_{mf}$	$Grt > 0.2 \times 10^3$	$Grt = \frac{\mu}{d_p(\rho_s + \rho_g/2)} t_{da}$ $P^* = \frac{P_f \rho_s \sqrt{g d_p}}{d_p}$ $Fr_{mf} = V_{mf} / \sqrt{g d_p}$	
Molerus [8]	Geldart's A-Fluidized dense-phase	Particle density difference - mean particle diameter (kg/m <sup>3</sup> ) - (m)		A-C (for hard particles) $10 \frac{(\rho_s - \rho_g) H_p^3 g}{F_H} = 0.01$	
	Geldart's B- Dilute phase			A-B (for hard particles) $\frac{(\rho_s - \rho_g) (\pi d_p^3 g / 6)}{F_H} = 0.16$	
	Geldart's C-Difficult to fluidized				B-D $(\rho_s - \rho_g) H_p g = 1.53$
	Geldart's D- Plug flow				
Pan [9]	PC1- Fluidized dense-phase	Loose poured bulk density-Mean particle diameter (kg/m <sup>3</sup> ) - ( $\mu\text{m}$ )	-	PC1-PC2/3 $d_p \rho_{bp} = 0.1206$	
	PC2- Unstable zone- slug flow- dilute phase		$d_p > 100 \mu\text{m}$	PC2-PC3 $\rho_{bp} = 1000$	
	PC3 Dilute only		-		
Williams & Jones [10]	Geldart's A-	Loose poured bulk density-Mean particle diameter (kg/m <sup>3</sup> ) - ( $\mu\text{m}$ )		A/C-B $\rho_{bp} d_p = 12 \text{ kl } 10^{-3}$	
	Geldart's B- Dilute phase			B-D $\rho_{bp} d_p^2 = 539 \times 10^{-6}$	
	Geldart's C-				
	Geldart's D- Plug flow			Asymmetric slugs - axisymmetric slugs $\frac{d_p \rho_{bp}}{D^{0.5}} = \frac{0.885 \times 10^{-3}}{d_p} + 1.44D^{0.5}$	
	Dixon's Axisymmetric slugs- Plug type				No slugging- asymmetric slugs $\frac{d_p^{1.14} \rho_{bp}^{0.714}}{D^{0.5}} = 87.4 \times 10^3$
	Dixon's Weak asymmetric slugs- Dilute only				
	Dixon's no slugging- Fluidized dense-phase			A/C-B $\rho_{bp} d_p^2 = 1.27 \times 10^{-9}$	
	Molerus's A-			B-D $\rho_{bp} d_p = 0.841$	
	Molerus's B-				
Molerus's C-					
Molerus's D- Plug flow					
Jones & Williams [11]	Chambers – Fluidized dense-phase	Non-dimensional parameter ( $N_{c(mod)}$ )	$N_{c(mod)} < 8 \times 10^{-4}$	$N_{c(mod)} = \frac{\rho_s P_f}{t_c}$	
	Chambers – Dilute only		$8 \times 10^{-4} < N_{c(mod)} < 0.07$		
	Chambers – Plug flow		$N_{c(mod)} > 0.07$		
	Fluidized dense-phase	Loose poured bulk density-permeability (kg/m <sup>3</sup> ) - (m <sup>3</sup> /kg)		$P_f \rho_{bp}^{3/4} \approx 300$	
	Dilute only			$P_f \approx 20 \times 10^{-6}$	
Plug flow					

## CHAPTER 3

### EXPERIMENTAL TEST SET-UP and MEASUREMENTS

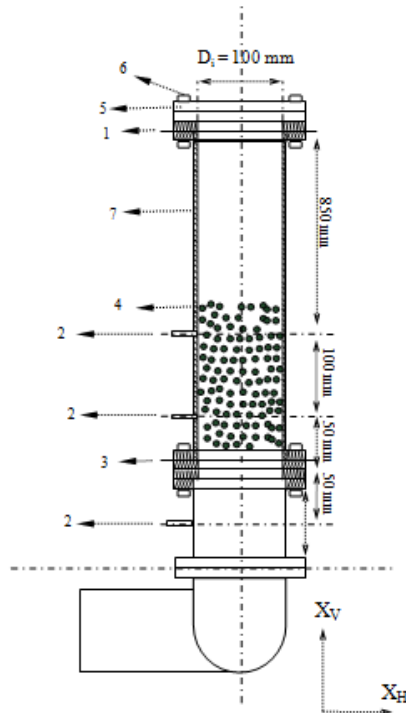
#### 3.1 Introduction

In this chapter, the construction of the experimental test set-up and the utilized measurement devices are presented. The measurements and the methodology of the experimental study are also given in detail.



- |                         |                       |                  |              |              |                                      |
|-------------------------|-----------------------|------------------|--------------|--------------|--------------------------------------|
| 1. Blower unit          | 2. AC control unit    | 3. Settling tank | 4. Manometer | 5. PVC pipe  | 6. Pitot-tube and traverse mechanism |
| 7. Pressure Transmitter | 8. Acrylic glass pipe | 9. Daq board     | 10. PC       | 11. Supports |                                      |

Figure 3.1 Vertical test set-up



- |                           |                          |                           |                    |
|---------------------------|--------------------------|---------------------------|--------------------|
| 1. Upper perforated plate | 2. Pressure transmitters | 3. Lower perforated plate | 4. Solid particles |
| 5. Flange plate           | 6. Screw                 | 7. Acrylic test chamber   |                    |

Figure 3.2 Vertical test chamber

### 3.2 Experimental Test Set-up

Type of the set-up is an open circuit blower type air flow test system coupled with the measurement devices. The main components consist of a blower, a settling tank, pipeline systems which are PVC pipe and acrylic glass pipe, and a particle feeder unit. In addition to these main components, a pitot tube and a traverse mechanism, a multitube and an inclined alcohol manometer, pressure transmitters and a data acquisition card are used for the measurements. The vertical test set-up (test case 1) and vertical test chamber are given in figures 3.1 and 3.2, respectively. The horizontal test set-up (test case 2) is shown in figure 3.3.

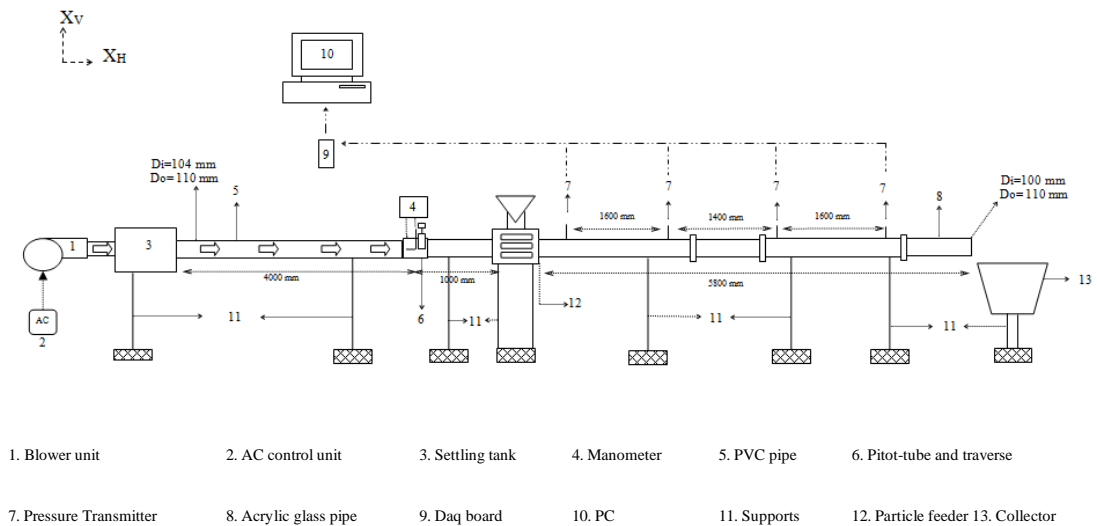


Figure 3.3 Horizontal test set-up

### 3.2.1 Blower Unit

The blower section is located at the exit of a vertical shaft centrifugal fan which is driven by an AC speed control unit. The maximum air flow rate delivered by the fan is measured to be  $0.207 \text{ m}^3/\text{s}$ .

The vertical centrifugal fan which is capable to supply  $0.21 \text{ m}^3/\text{s}$  of air at 2835 rpm is used to feed air. The exit cross sectional area of the fan is in rectangular form with dimensions 250 mm x 300 mm. A 2.95 HP/2.2kW- 2835 rpm electric motor drives the fan. An AC speed control unit has a frequency control. The technical specifications of the motor and the control unit are given in Appendix 1.

### 3.2.2 Settling Tank

In this study, a 800mm x 800mm x 800mm wooden settling tank is used for the purpose. The settling tank is used in order to eliminate flow irregularity due to small change in fan speed and to satisfy steady flow through the pipeline system. A honeycomb is attached at the exit part of the settling tank according to BS 1042 in order to eliminate flow irregularities and to provide uniform flow. [31-32].

### 3.2.3 Pipeline System

In order to realize two different test cases, two separate setups constructed are designed, constructed and used in this study. Pipeline system is composed of a PVC pipeline whose inner and outer diameters are 104 mm and 110 mm, respectively and acrylic glass pipes whose inner and outer diameters are 100 mm and 110 mm, respectively. The inner diameters of the pipes are different, so that special flanges are manufactured for contact points between PVC pipe and acrylic pipe as shown in figure 3.4.

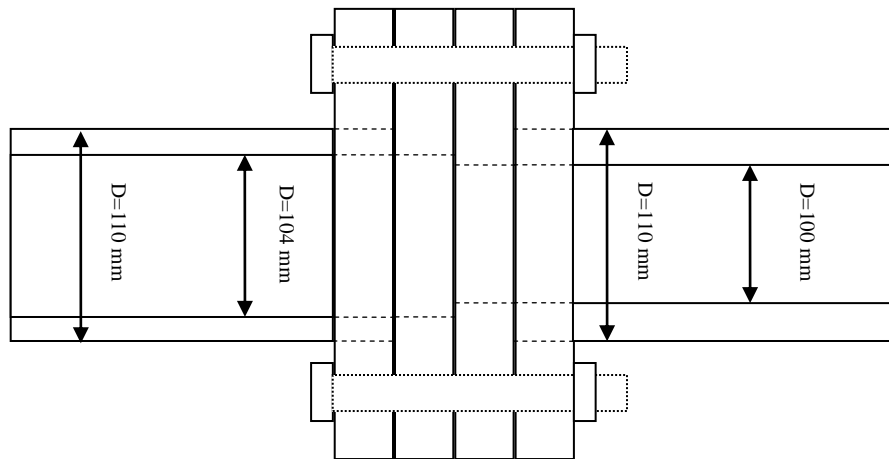


Figure 3.4 Flange between PVC pipe and acrylic glass pipe

In the test case 1 minimum fluidization velocities are determined. On the other hand, in test case 2, flow dynamics during pneumatic conveying of a variety of particles is investigated when a feeder feeds particles to the pipeline in a controlled fashion. The reference test section in which the pitot tube is used in order to measure the cross sectional velocity distribution of air flow is at reference test section,  $X_R/D = 38.46$  from the exit section of the settling tank. At this reference measurement section, the flow is found to be fully developed one for all test runs. A vertical acrylic glass pipeline whose length is  $X_V/D=20$  is used in order to estimate minimum fluidization velocity in case 1 for a variety of particle as well as flow visualization.

Three pressure transmitters are used for the measurement of the local static pressures which are located at  $X_V/D = 1.5$ ,  $X_V/D = 2.5$ ,  $X_V/D = 3.5$ . Four same pressure transmitters are used for determination of local static pressures in horizontal test case when the particle feeder is charging system with solid particles. Pressure transmitters are located  $X_H/D = 2$ ,  $X_H/D = 18$ ,  $X_H/D = 32$  and  $X_H/D = 48$  from the exit section of the particle feeder for the test case 2 as shown in figure 3.3.

### **3.2.4 Particle Feeder**

A particle feeder is used in order to induce solid particles into air flowing through the pipeline system. This unit driven by a 0.75 kW coupled electric motor and an AC control unit consists of a metal block with an inner diameter 220 mm. The feeder operates in the way described below:

A certain amount of particle is loaded from the top of the feeder and closed by a cover. Then, electric motor is operated by AC control unit at a required rotational speed. Discharge of solid particles is monitored with respect to time during the experiments. The required particle ratio in the pipe is attained and controlled by an AC motor variable speed controller which is coupled to the particle feeder. The technical drawings of the particle feeder are given in figure 3.5 and 3.6. The specifications of the electric motor and the speed controller of the particle feeder unit are given in Appendix 2.

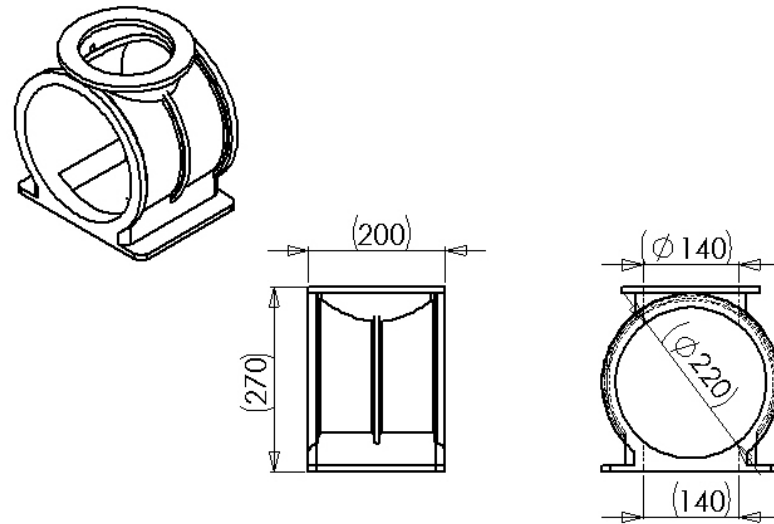


Figure 3.5 Metal block (body) of particle feeder

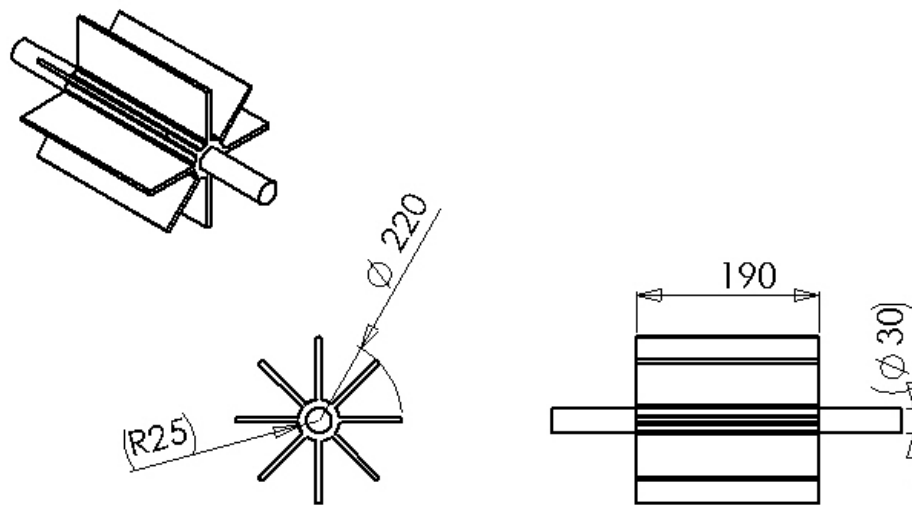


Figure 3.6 Blade of particle feeder



### 3.2.4.1 Modification of Particle Feeder

Particle feeders are generally suitable for industrial applications. Therefore, to meet different requirements, feeder unit is modified in this study.

A custom design -cone shaped- metal which has 20 mm diameter hole at the lower part is welded on top of the particle feeder as shown in figure 3.7. Also three custom design orifice plates with diameters 10 mm, 15 mm, 20 mm are manufactured. The orifice plates are mountable. Loaded particles are induced to the pipeline system via these orifices. This enables us to calibrate particle feeder as a laboratory scale. The details of modified system are given in figure 3.7.

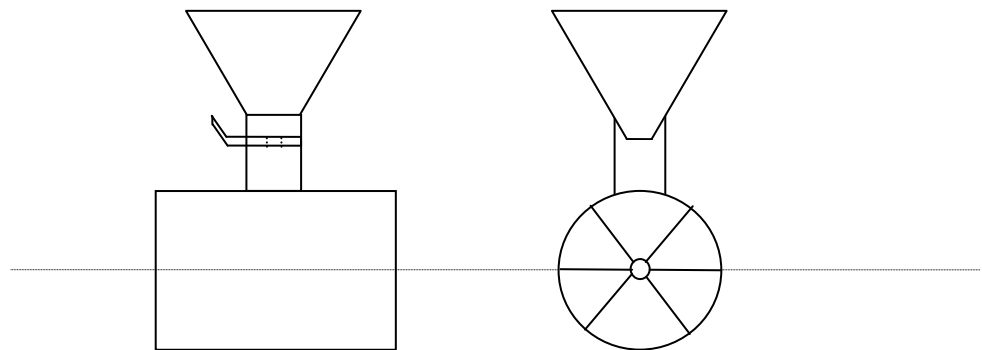


Figure 3.7 Modification of particle feeder

### 3.3 Measurement Devices and Methods

A pitot tube, a traverse mechanism, manometers, pressure transmitters, a data acquisition and an evaluation software program are used in this study to acquire and process data.

### 3.3.1 Pitot Tube and Traverse Mechanism

A pitot tube which is hold by a traverse mechanism is used in order to measure air velocity at this specific location inside the pipe. An L shaped copper pitot tube of 2 mm outer diameter and 1 mm inner diameter is mounted at  $X_R/D=38.46$  downstream of the settling tank exit section. At a significant frequency of the blower unit, the pitot tube is traversed along the pipe cross section. The local dynamic pressure is measured by means of an inclined leg alcohol manometer pitot tube and static tapping in each traversed location. The local velocities are evaluated using the values of dynamic pressures. After the traversing process, local velocity distribution  $u(r)$  is obtained with respect to radial position as shown in figure 3.8. The volume flow rate is calculated from equation 3.1. Then mean velocity,  $U_m$  and location of  $U_m$  where  $r = 39$  mm are calculated by using equation 3.2. Finally,  $u/U_{max}$  are plotted with respect to  $r/R$  and composed with the theoretical Prandtl's one-seventh power law as shown in figure 3.9. The maximum deviation from the  $1/7^{th}$  power law is found to be 5.202%.

$$Q = 2\pi \int_0^K u(r)rdr \quad (3.1)$$

$$u_{mean} = 2\pi \int_0^K u(r)rdr / \pi R^2 \quad (3.2)$$

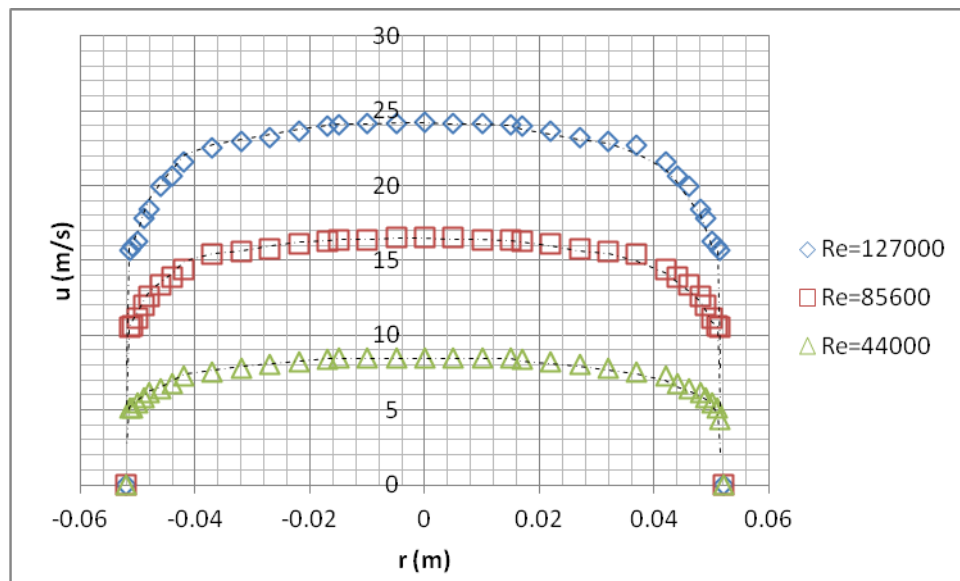


Figure 3.8 Cross sectional velocity distribution

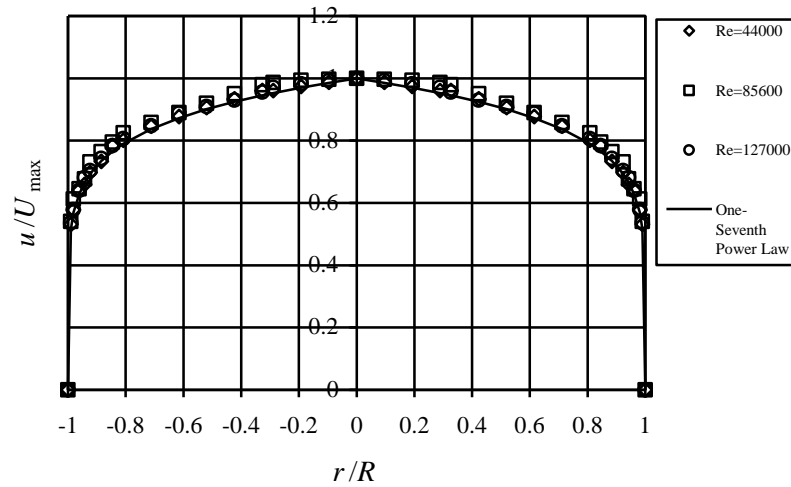


Figure 3.9 Cross sectional velocity distribution and 1/7<sup>th</sup> power law

### 3.3.2 Manometers

The pitot tube and the static tapping are used to determine total pressure and static pressure, respectively. An inclined manometer is used to determine the difference between the static and total pressures which gives dynamic pressure. Local velocities are then calculated using equations 3.3 and 3.4.

$$P_{dyn} = P_{total} - P_{static} = \rho_{alc} g h \sin \theta \quad (3.3)$$

$$\Delta P = P_{dynamic}$$

Also;

$$P_{dynamic} = 0.5 \rho_{air} u^2 \quad (3.4)$$

Density of alcohol  $\rho_{alc}$ , gravity  $g$ , alcohol height  $h$ , manometers inclination angle  $\theta$  and air density  $\rho_{air}$  are the parameters used to calculate local velocity  $u$  in the pipeline. Air velocities are tabulated with regarding to continuity equation and given as m/s in table 3.1.

Table 3.1 Blower calibration

f (Hz)	$U_{air}$ (m/s) PVC Pipe	$U_{air}$ (m/s) Acrylic Pipe	f (Hz)	$U_{air}$ (m/s) PVC Pipe	$U_{air}$ (m/s) Acrylic Pipe
4	3.37	3.65	18	15.09	16.32
5	4.13	4.47	19	16.07	17.38
6	4.57	4.94	20	16.76	18.13
7	5.51	5.96	21	17.64	19.08
8	6.46	6.99	22	18.49	19.99
9	7.29	7.89	23	19.29	20.86
10	8.27	8.94	24	20.06	21.70
11	9.14	9.89	25	20.80	22.50
12	9.94	10.75	26	21.78	23.56
13	10.67	11.54	27	22.64	24.49
14	11.53	12.47	28	23.30	25.20
15	12.32	13.33	29	23.86	25.81
16	13.22	14.29	30	24.41	26.41

A 30-tube tilting manometer is used for calibration of the pressure transmitters. All static pressures are determined with the multi tube manometer and the data are recorded. So that, the pressure transmitters are calibrated with respect to its calibration scale regarding the values that already taken with the multi tube manometer. This process is detailed in the calibration of pressure transmitter section.

### 3.3.3 Pressure Transmitters

Pressure transmitters transform mechanical pressure signals into electrical signals. In this study, WIKA SL-1 pressure transmitters are used to measure local static pressures which are located at  $X_V/D = 1.5$ ,  $X_V/D = 2.5$ ,  $X_V/D = 3.5$  in test case 1; and  $X_H/D = 2$ ,  $X_H/D = 18$ ,  $X_H/D = 32$  and  $X_H/D = 48$  in test case 2 as shown in figure 3.1 and figure 3.3. The operation range of the transmitters is  $\pm 2000$  Pa. Its analog output signal is in the range of 0-10 V. A power supply of 0-25 VDC drives the transmitter. It has a response time is of 1  $\mu$ s and a full scale accuracy of less than

0.5 %. The transmitter can operate in the temperature range of -30 °C and +80 °C. The technical specifications of the pressure transmitter are given in appendix 3.

### **3.3.4 Data Acquisition and Software Program**

In this experimental study, a 16-bit, 1-MHz A/D converter (NI USB-6353 X series DAQ, USB Board with 32 single-ended, 48 differential analog inputs and 4 analog outputs) is used in order to collect the pressure data. It is easily connected to the computer via an USB port. NI USB-6353 X series DAQ, USB daq board is instructed by a LabView software program. The technical specifications of the card are given in appendix 4.

The data is collected by using a devised program which is named as FDRIPCS.vi (Flow Dynamics Research In Pneumatic Conveying System) in LabView 2009SP1® environment. The devised program collects all raw data as Volt and records them into a file in a personal computer. Also, the statistical analysis such as RMS (root mean square), arithmetic mean and standard deviation are performed by FDRIPCS.vi for each pressure transmitter. The block diagram and the front panel of the program are given in figure 3.10 and 3.11. Attention is paid to the transmitters during the data collection process because of the sensitivity of measurement.

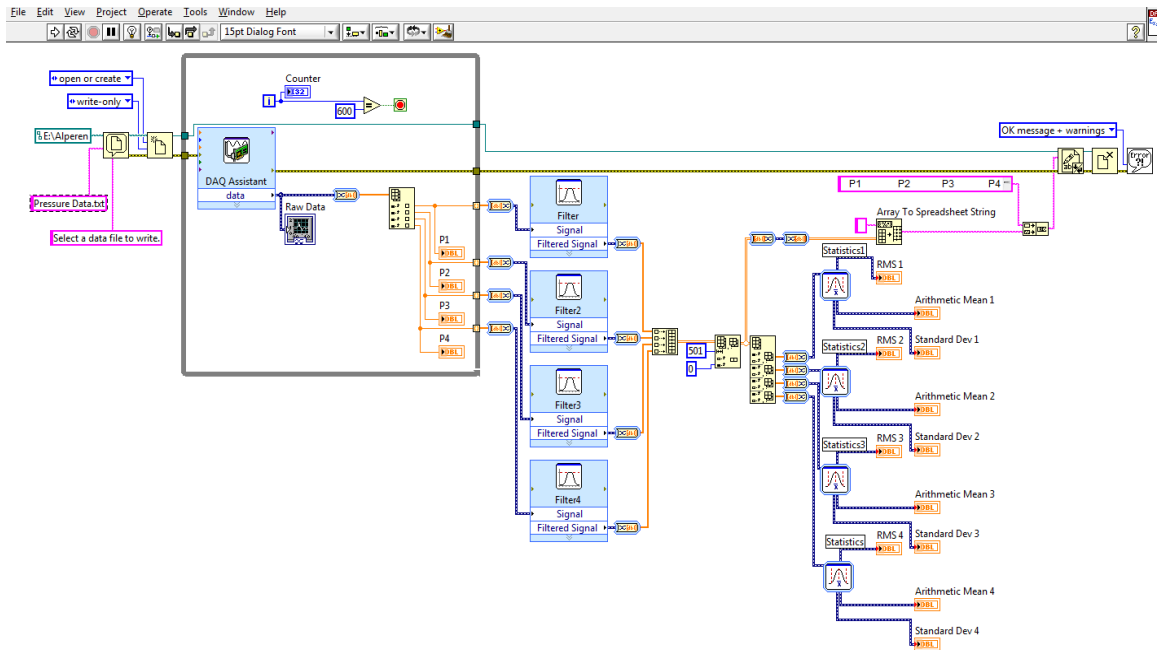


Figure 3.10 Block diagram of FDRIPCS.vi

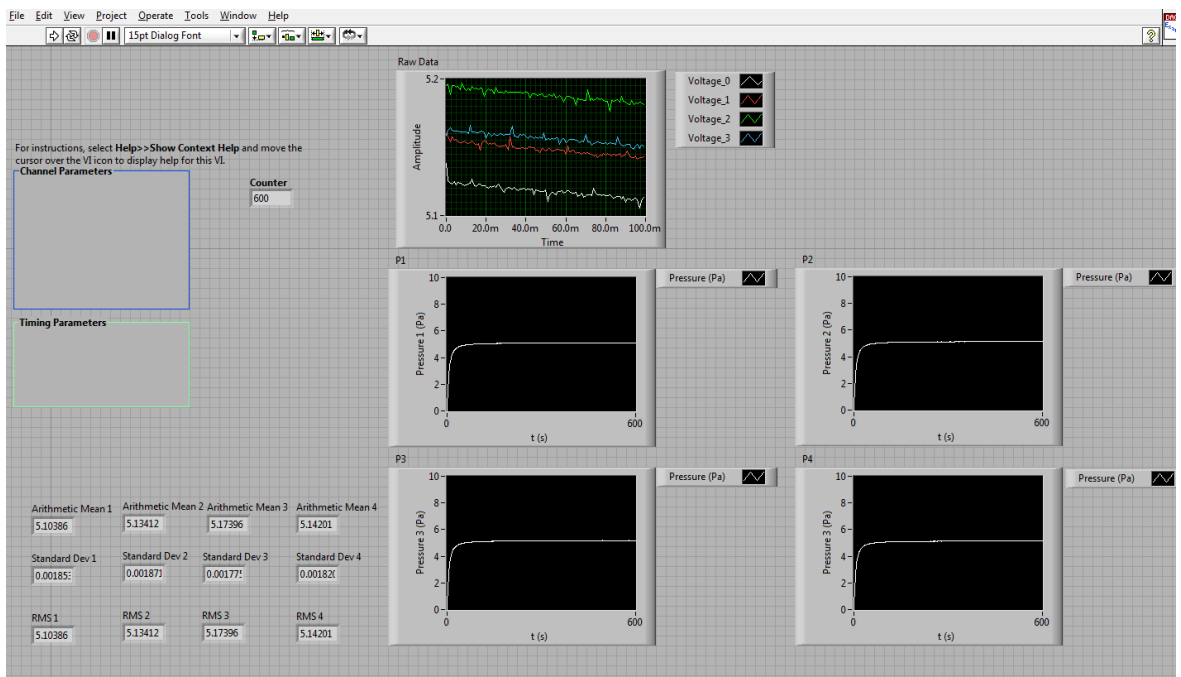


Figure 3.11 Front panel of FDRIPCS.vi

### 3.4 Properties of the Tested Solid Particles

There are numerous different types of particles which can be investigated for the flow mode characteristics used in pneumatic conveying systems. Of course, it is impossible & impractical to cover all type of particles; therefore, a selection is made on the bases of a wide range of each particle parameter coverage. Specific attention was given to the physically important parameter such as density, particle size.

In this study, sizes of solid particles are categorized by a custom design sieve with eight different meshes which have diameters of 0.1 mm, 0.4 mm, 1.0 mm, 1.25 mm, 1.5 mm, 2.0 mm, 2.5 mm and 3.0 mm, as shown in figure 3.12. The average particle diameter,  $d_p$  is taken as %50 of the weight of sieved particles.

The densities of particles  $\rho_s$  are calculated in fluid mechanics laboratory and the  $\rho_{blp}$  densities are determined by following ASTM standard code B212-76 [33]. The relation between loose-poured bulk density  $\rho_{blp}$  (apparent density), particle density  $\rho_s$  and voidage  $\varepsilon$ , is given in equation 3.5:

$$\rho_{blp} = (1-\varepsilon) \rho_s \quad (3.5)$$

Seven different type solid particles are used at the test runs and they are categorized with respect to their loose-poured bulk densities and sizes as shown in table 1. The ranges of solid particles whose diameter  $d_p$  and loose-poured bulk density  $\rho_{blp}$  are  $100 \mu\text{m} < d_p < 3000 \mu\text{m}$  and,  $200 \text{ kg/m}^3 < \rho_{blp} < 900 \text{ kg/m}^3$ .



Figure 3.12 Different mesh size sieves



Table 3.2 - Physical Characteristics of Solid Particles

Particle	Code	Size range ( $\mu\text{m}$ )	$d_p$ ( $\mu\text{m}$ )	Shape	$\rho_s$ ( $\text{kg/m}^3$ )	$\rho_{blp}$ ( $\text{kg/m}^3$ )	( $\epsilon$ )
Semolina	SE	400-1000	700	Roughly spherical	1459	850	0.417
Wheat	W	2000-2500	2250	Roughly spherical	1356	950	0.299
Polyethylene	PE	2500-3000	2750	Roughly spherical	910	550	0.396
Zeolite 1	Z1	100-400	250	Roughly spherical	1450	1000	0.45
Zeolite 2	Z2	400-1000	700	Roughly spherical	1450	920	0.365
Sand (Garnet)	S	150	150	Roughly spherical	4110	2400	0.416
Tea Flakes	T	1250-1500	1375	Flament	433	200	0.538

### 3.5 Calibration

#### 3.5.1 Pressure Transmitter Calibration

The multi-tube alcohol manometer and four pressure transmitters (Wika SL-1) are used in order to measure static pressures in acrylic glass pipe. The transmitters are mounted on acrylic glass pipe at locations of  $X_v/D= 1.5, 2.5, 3.5$  for test case 1 as shown in figure 3.1. Same procedure is used for test case 2 at locations of  $X_H/D= 2, 18, 32$  and  $48$  (figure 3.3). First, static pressures are measured by multi-tube alcohol manometer. Then volt is measured by pressure transmitters at the same frequency where taken from AC control unit. These data are collected by means of a DAQ board and FDRIPCS.vi custom design program in Labview® environment. 1000 data are collected for each test run but only 100 data are took into consideration because of the stability of transmitters. In this way volt and pressure are measured with good accuracy at all random velocities. Finally all data are plotted with regarding to calibration of pressure transmitter which is linear between 0 – 10 volt corresponding to  $\pm 2000$  Pa. The maximum and minimum deviation of transmitter is 3.025% and 1.408%. Transmitter calibrations are shown in figure 3.13.

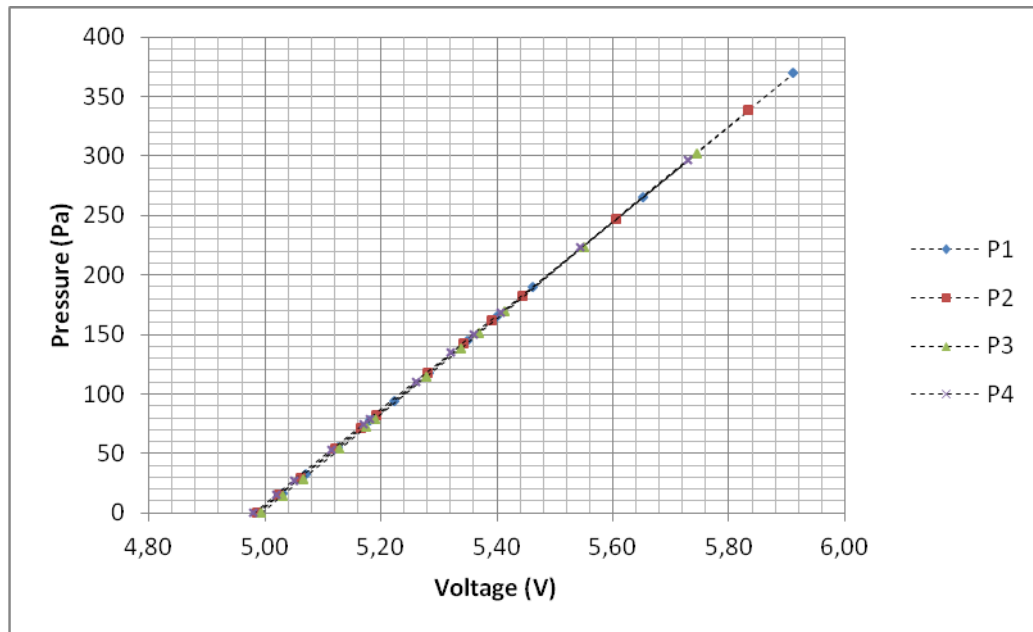


Figure 3.13 Calibration of pressure transmitters

### 3.5.2 Particle Feeder Calibration

Mass flow rate of particles must be known during the transportation in the pipeline. Because of this reason, particle feeder calibration is very important, in order to determine mass flow rate of particles. The required air mass flow rate can be adjusted to transport materials if materials flow rates are known.

Three orifice plates are used to adjust mass flow rate of particles. Cone metal is loaded with 500 gr of particles at the beginning of each test run for three different orifice plates. Each discharge time is calculated by stop watch and recorded. Tea flakes is not discharged from the cone because of their low density and also polyethylene is not discharged because of its shape. Wheat is discharged only from orifice plates of 15 mm and 20 mm. All data are tabulated and given in of kg/s in Table 3.3.

Table 3.3 Calibration of Particle Feeder

<b>Particle Mass Flow Rate, <math>\dot{m}_p</math> (kg/s)</b>			
	Orifice Diameters		
Material	10 mm	15 mm	20 mm
Z1	0.0061	0.0163	0.0294
Z2	0.0055	0.0108	0.0252
W	-	0.0166	0.0250
T	-	-	-
SE	0.0149	0.0312	0.0434
S	0.0285	0.0566	0.1111
PE	-	-	-

### 3.6 Uncertainty Analysis of Measurement Devices

The uncertainty analysis is conducted in order to confirm the validity and accuracy of the measurements during experimental study. An uncertainty may originate from causes such as the lack of accuracy in measurement equipment, random variation in the measurands and approximations in data reduction relations. According to the ANSI/ASME [33] and ISO GUM [34], the elemental errors are grouped into three categories; data acquisition errors, data reduction errors and calibration errors. There are some kinds of errors which may lead to uncertainty in the experimental measurements. One of them is random error which can occur because of personal fluctuations, random electronic fluctuations in the apparatus or instruments and various influences of friction. The second one is fixed (bias) error which can cause repeated readings in order to be in error which is sometimes called as systematic error [35].

The uncertainty of pressure measurement carried out by the WIKA SL-1 pressure transmitter is evaluated using the procedure given in [33-37]. The accuracy, non-linearity, non-repeatability, and one-year stability of the pressure transmitters are given as less than 0.5 %, 0.2 %, 0.1 % and 0.3 %, respectively. The bias and precision errors are evaluated by means of equations which are given in Table 3.4 for 5 V mean reading covering 20 tests as shown in Table 3.5. The confidence level is taken as 95 %. For 19 degrees of freedom and 95 % confidence level, t equals to 2.093. The uncertainty of the measurement of the raw pressure data in voltage is found as  $\pm 0.8$  %. After the calibration of the raw pressure data, the uncertainty of the processed data in Pa unit is found to be  $\pm 1.3$  %.

Table 3.4 Statistical parameters used in uncertainty analysis

<b>Description</b>	<b>Formula</b>
Mean of the sample population	$\bar{x} = \frac{1}{N} \sum_{i=1}^N x_i$
Precision index (Sample standard deviation)	$S_x = \left[ \frac{1}{N-1} \sum_{i=1}^N (x_i - \bar{x})^2 \right]^{1/2}$
Precision limit for a sample (t is calculated from t-distribution table for 95% confidence limit and the number of degrees of freedom, $\nu = N - 1$ )	$P_x = tS_x$
Bias limit in a measured variable	$B_x = \left( \sum_{i=1}^k B_i^2 \right)^{1/2}$
Overall Uncertainty in a measured variable	$w_x = \left[ B_x^2 + (tS_x)^2 \right]^{1/2}$

Table 3.5 Uncertainty analyze of pressure measurements based on the method in [33-37]

Source of uncertainty	Bias Limit		Precision Index		Degrees of freedom
	%	Volt	%	Volt	#
<b>Data Acquisition</b>					20
Accuracy	0.5	0.025	-	-	
Repeatability	-	-	0.1	0.005	
<b>Data Reduction</b>					
Linearity	0.2	0.01	-	-	
Stability	-	-	0.3	0.015	
Uncertainty of pressure measurement; $w_x = [0.027^2 + 0.033^2]^{1/2} = 0.043 \text{ V (0.8\%)}$					

The uncertainty analyses utilized for the measurements of alcohol density, air density, dynamic pressure, atmospheric pressure, local velocity and static pressure are based on the well-known equation given as follows [34-35];

$$w_R = \left[ \sum_{i=1}^J \left( w_{x_i} \frac{\partial R}{\partial x_i} \right)^2 \right]^{1/2} = \left[ \left( \frac{\partial R}{\partial x_1} w_1 \right)^2 + \left( \frac{\partial R}{\partial x_2} w_2 \right)^2 + \dots + \left( \frac{\partial R}{\partial x_n} w_n \right)^2 \right]^{1/2} \quad (3.6)$$

where  $w_R$  is uncertainty in result,  $R$  is result as a function of independent variables of  $x_1, x_2, \dots, x_i \dots x_n$  and  $w_1, w_2, \dots, w_{x_i} \dots w_n$  are uncertainties of the independent variables. The uncertainty values of the experimental study ranges are evaluated by means of Equation (3.6) and tabulated in Table 3.6.

Table 3.6 Uncertainty of measurements utilized in the study with the method in [33-37]

Measured data in the experiment	Unit	Overall uncertainty (nominal)	Overall uncertainty (%)
$P_{alc}$	kg/m <sup>3</sup>	4.66	0.6
$\rho_{air}$	kg/m <sup>3</sup>	$1.95 \times 10^{-3}$	0.18
$P_{dyn}$	Pa	20.19	3.31
$P_{atm}$	Pa	66.7	0.07
$u(r)$	m/s	0.558	1.66
P	V	0.043	0.8
	Pa	7.8	1.3

### 3.7 Conclusion

By means of the previous studies, it is well understood that the minimum fluidization velocity is one of the crucial parameter to determine the flow mode in pneumatic conveying systems. However, transitions between the flow modes are not clearly defined yet. Hence, this study is started to fill this gap, namely, to find new relationships in determining flow modes. Towards this aim, three different experimental test cases are performed:

Test case 1- Vertical Test Section

Test case 2- Horizontal Test Section

Test case 3- Continuous regime for Horizontal Test Section with the use of particle feeder (continuous conveying)

Particle sizes, loose-poured bulk densities and particle densities are already calculated and explained in the solid particles section. Minimum fluidization velocity and local pressure change are determined in vertical test section.

Different solid particles are used with different bed heights in vertical test section. Pressure drops are measured during the experimental test runs. The aim is to find a relationship between pressure drop and minimum fluidization velocity. Also, it is aimed to determine the  $U_{mf}$  only with pressure drop. Test runs are repeated for the horizontal test sections while the system is fed by a rotary valve feeder. The measured minimum fluidization velocities are compared in vertical and horizontal cases. Different types of flow modes such as plug, suspension are tested for the new practical application with continuous particle feeding in horizontal test section.

## CHAPTER 4

### EXPERIMENTS ON THE STATE OF MINIMUM FLUIDIZATION AND FLOW MODE DETERMINATION

#### 4.1 Introduction

In this chapter, methodology for minimum fluidization state (velocity) determination is explained for the test case 1, test case 2 and continuous conveying. Additionally, the effects of  $\rho_{blp}$  and  $d_p$  of particles which are used in all test cases are investigated to determine the flow modes in pneumatic conveying systems.

#### 4.2 Methodology for the Minimum Fluidization State Determination

There is no exact determination for the minimum fluidization velocity in the literature. In this study, two different test set-up and two different system are constructed to determine minimum fluidization state under the influence of solid particles type, size and amount. In the test case 1, solid particles which are given in table 3.1 with required properties are used with three different bed lengths (10 mm, 30 mm and 50 mm) in the form of a cylindrical bed in a vertical test chamber. Bed lengths are symbolized respectively L10, L30 and L50. The experimental study was conducted by measuring the local static pressures in the vertical test chamber at varying air flow rates with the range of  $3.65 \text{ m/s} < U_{air} < 24.83 \text{ m/s}$ . At each  $U_{air}$  the field was observed with the measurement of the local static pressures the preliminary experiments; measurements indicate that variation of local static pressures at  $X_v/D= 1.5$ ,  $X_v/D= 2.5$ ,  $X_v/D= 3.5$  and  $X_v/D= 8.5$  can be used as a determination tool for the flow inside. The measurements of local static pressure at  $X_v/D= 2.5$   $P_2$  is given as a function of  $P_1$  at  $X_v/D= 1.5$  for different  $U_{air}$  with the range of  $3.65 \text{ m/s} < U_{air} <$



24.83 m/s in figure 4.1. The visual observation for the minimum fluidization state is verified by the local static pressure measurements, the static pressure at before the bed  $X_v/D= 1.5$  is called as  $P_1$  and the static pressure at  $X_v/D= 2.5$  after the bed is called as  $P_2$ . In the experiments the local static pressures at location  $X_v/D > 2.5$  defined as  $P_3$  and  $P_4$  have no effects on state. Therefore variation of  $P_1$  and  $P_2$  is used for the state determination.

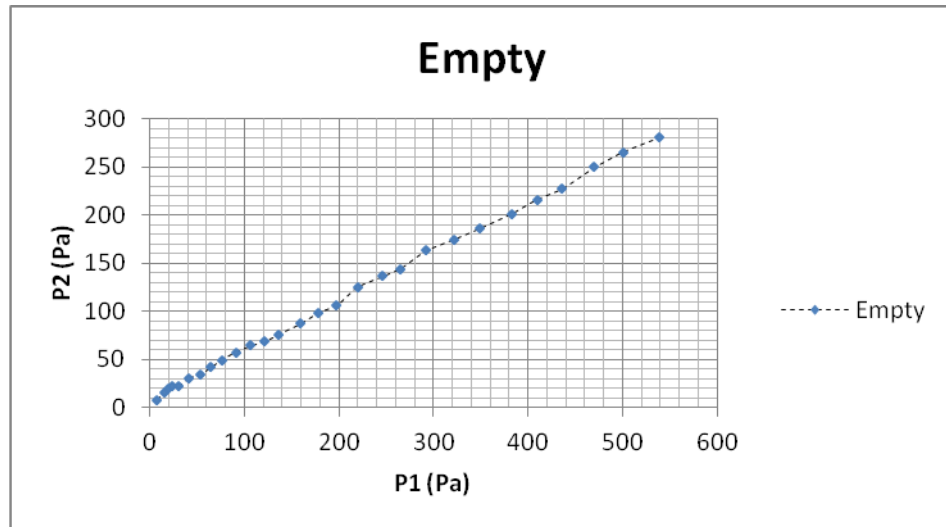


Figure 4.1 Local static pressure variation in empty pipe in Test case 1

In test case 2 first, measurement of local static pressures along the horizontal test section was conducted in empty pipe. Local static pressures are given as a function of  $U_{air}$  for empty pipe in figure 4.2. A horizontal bed in the form of a prismatic configuration with the use of SE, S, W, T and PE was located at the position  $X_H/D= 10$ . The amount and shape of the prismatic configuration were recorded. The air flow velocity  $U_{air}$  was changed gradually in the range of  $3.65 \text{ m/s} < U_{air} < 24.83 \text{ m/s}$ . At each  $U_{air}$  the field and structure of particles configuration was visually observed. The measurements of local static pressures  $P_1$  at  $X_H/D= 2$  before the prismatic configuration and  $P_2$  at  $X_H/D= 18$ ,  $P_3$  at  $X_H/D= 32$  and  $P_4$  at  $X_H/D= 48$ , after the configuration are used to analyze the minimum fluidization state. The experiment was performed with the increase of  $U_{air}$   $3.65 \text{ m/s} < U_{air} < 24.83 \text{ m/s}$ . So

that, the distribution of solid particles is observed and also local static pressures  $P_1$ ,  $P_2$ ,  $P_3$  and  $P_4$  are determined with the aid of pressure transmitters and recorded.

In the horizontal test case visual observation of prismatic configuration of solid particles is also analyzed by determining flow dynamics through the measurement of amount of mass,  $\dot{M}_p$  transported at each  $U_{air}$ . The collected amount of  $\dot{M}_p$  was measured by recording time with collection through assay balance at the end of the horizontal test section. In order to deduce about the influence of particle characteristics results on minimum fluidization velocity are given in a comparative base.

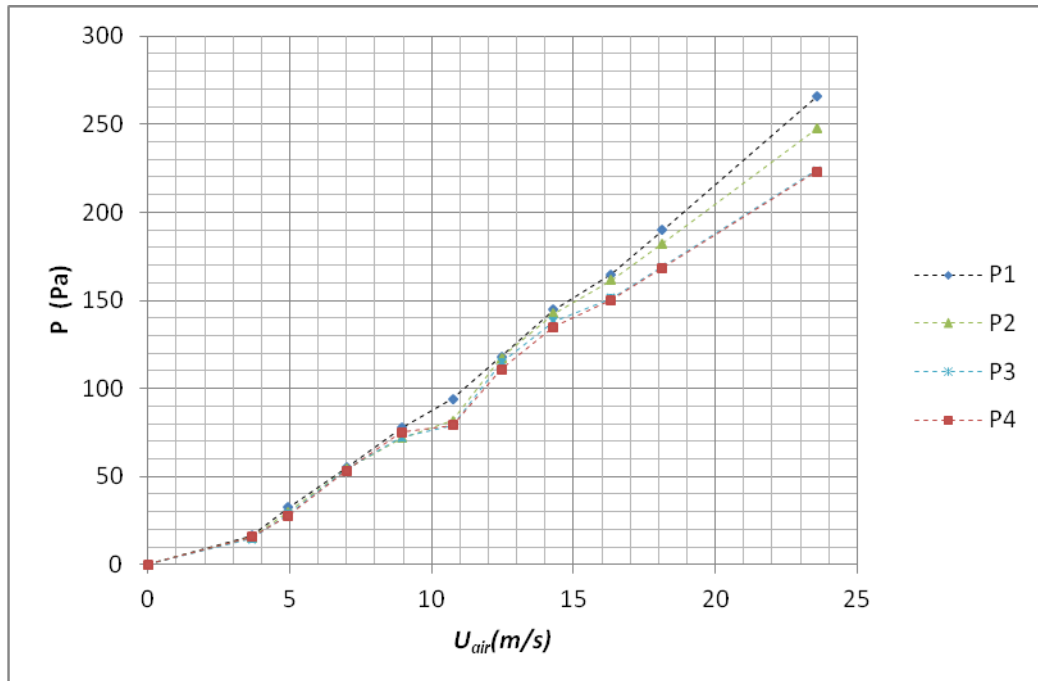


Figure 4.2 Local static pressure variation in empty pipe in Test case 2

For the final test case a sample dynamic verification experimental study was conducted. This test based upon the experimental measurements of the first and second test cases in order to complete flow mode analysis. In this test case, three solid particles which are S, W and SE are used to observe flow modes during the continuous conveying with particle feeder. The particle feeder induced the known

amount of particles into the pipeline system with determined mass flow rates,  $\dot{m}_p$ . Particle feeder induces different  $\dot{m}_p$  of particles (S, SE, W) into the air flow pipeline.

The measurements of local static pressures at defined points through the horizontal line after the particle feeder were measured together with the amount of particle transported by air. The measurements were started at the maximum  $U_{air}$  to observe a fully suspended- dilute phase inside the horizontal test section. The measurements were repeated by reducing  $U_{air}$ . At each  $U_{air}$  the measurements together with visual observation of the test section are used for flow mode analysis. The least;  $U_{air}$  at no particle conveying point was also referred to determine a critical state for the flow mode.

Therefore, the flow field observation with the static pressure measurements is compared with test case 1 and test case 2.

### 4.3 Results in the Vertical Test Case

In case 1 of this study, the minimum fluidization velocities,  $U_{mf}$  of seven different particles of SE, S, W, T, Z1, Z2 and PE used in this part constructed L10, L30 and L50 given in Table 4.1, are determined experimentally in case of different flow rates from 0.029 m<sup>3</sup>/s to 0.195 m<sup>3</sup>/s.  $U_{mf}$  was not observed with S at L50.  $U_{mf}$  of each particle is determined for three different bed lengths of L10, L30 and L50 in the vertical test column, resulting in 21 separate cases.

For each test case, a vertical test chamber (Fig. 3.2) is filled with particles to the desired bed length and the vertical test chamber is mounted at  $X_V/D=20$  from the 90 degree elbow. Then the blower is operated and controlled by means of an AC speed control unit and the steady and uniform air flow is generated throughout the pipeline.  $U_{air}$  is increased until all particles in the vertical test chamber are just suspended in which this phenomenon is called as start to fluidization. At this time,  $U_{air}$  is measured by means of the pitot tube at the reference test section. This  $U_{air}$  is taken as minimum fluidization velocity. At the same time, static pressures  $P_1$ ,  $P_2$  and  $P_3$  at  $X_V/D=1.5$ , 2.5 and 3.5 respectively are measured and acquired by means of a

devised program, FDRIPCS.vi. The statistical analyses are also performed by the devised program.

After the observation of  $U_{mf}$ , the fan speed is increased systematically up to the maximum flow rate of  $0.207 \text{ m}^3/\text{s}$  until the flow becomes fully suspended.  $U_{mf}$  values based on visual observation during the experiment indicated that: the  $U_{mf}$  was in the range of  $3.65 \text{ m/s} < U_{mf} < 24.83 \text{ m/s}$ . Minimum  $U_{mf}$  with T of  $d_p = 1375 \text{ }\mu\text{m}$  and  $\rho_{blp} = 200 \text{ kg/m}^3$  at L10 and maximum  $U_{mf}$  with W of  $d_p = 2250 \text{ }\mu\text{m}$  and  $\rho_{blp} = 950 \text{ kg/m}^3$  at L50. S with  $d_p = 150 \text{ }\mu\text{m}$  and  $\rho_{blp} = 2400 \text{ kg/m}^3$  at L50 is supposed to be maximum value of  $U_{mf}$ . Therefore it seems that the  $\rho_{blp}$  is more important parameters than  $d_p$  to define flow modes in vertical test setups. However,  $U_{mf}$  could not be obtained for S at L50.

Figures 4.3 illustrated a sample visual observation of each stage during a test run for Z1. As can be seen from the figure 4.3.a, Z1 particles are stationary in the air flow while  $U_{mf} \gg U_{air}$ . Z1 particles are caused to blockage effect to the air flow in this figure which is called as unstable zone. On the other hand in figure 4.3.b particles are started to remove from the perforated plate when  $U_{air} = U_{mf}$  which is called as transition of fluidized dense phase state. When  $U_{air}$  increases particles are started to fluidize and flow mode is stated through  $U_{air} \gg U_{mf}$  as shown in figure 4.3.c and 4.3.d. This phenomenon is called as fluidized dense phase.

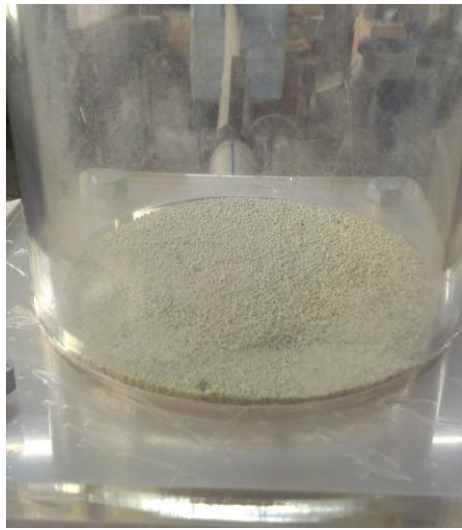
For each particle, the static pressures  $P_1$  at  $X_V/D = 1.5$  and  $P_2$  at  $X_V/D = 2.5$  which are 50 mm below and above the bottom perforated plate, are investigated for each bed length as shown in figures through Figure 4.4 – 4.6. As illustrated in figures, although the value at  $P_1$  increases continuously due to increase in air flow rate, the value of  $P_2$  is seen to be zero up to minimum fluidization velocity is obtained. When the particles just begin to bubble, the value of  $P_2$  begins to increase.

In this sample figures; three particles are selected due to a wide range of loose poured bulk density,  $\rho_{blp}$ , in which the loose poured bulk densities of T, PE and W are  $200 \text{ kg/m}^3$ ,  $550 \text{ kg/m}^3$ ,  $950 \text{ kg/m}^3$  respectively. As shown in figure 4.4, 4.5 and

4.6, the particles which have a lower loose poured bulk density,  $\rho_{blp}$  fluidizes earlier than the heavier ones. This results in lower values of static pressure at the inlet of bed and  $U_{air}$ .

Table 4.1 Minimum fluidization velocities corresponding to the visual observation of the shape

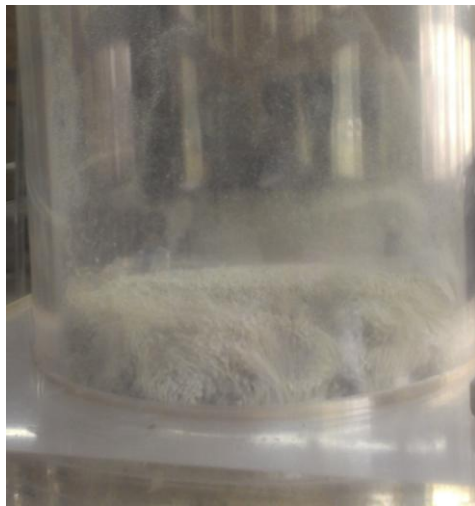
Particles	$U_{mf}$ (m/s)	Air Flow Rate (m <sup>3</sup> /s)
Z1 (10 mm)	7.44	0.058
Z1 (30 mm)	15.87	0.125
Z1 (50 mm)	21.70	0.170
Z2 (10 mm)	8.42	0.066
Z2 (30 mm)	17.38	0.136
Z2 (50 mm)	23.56	0.185
W (10 mm)	9.89	0.078
W (30 mm)	18.13	0.142
W (50 mm)	24.83	0.195
S (10 mm)	6.17	0.048
S (30 mm)	21.70	0.170
S (50 mm)	-	-
SE (10 mm)	6.99	0.055
SE (30 mm)	17.38	0.136
SE (50 mm)	21.70	0.170
PE (10 mm)	7.89	0.062
PE (30 mm)	13.81	0.108
PE (50 mm)	18.13	0.142
T (10 mm)	3.65	0.029
T (30 mm)	8.20	0.064
T (50 mm)	11.22	0.088



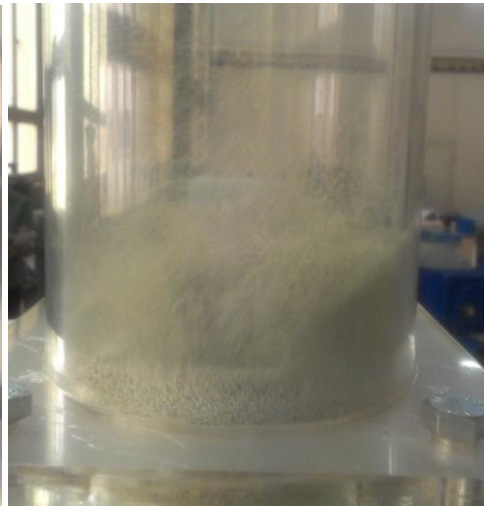
a)



b)



c)



d)

Figure 4.3 Visual observation of Z1 at L10 a) unstable zone b) just start of fluidization state c) - d) fluidized dense phase

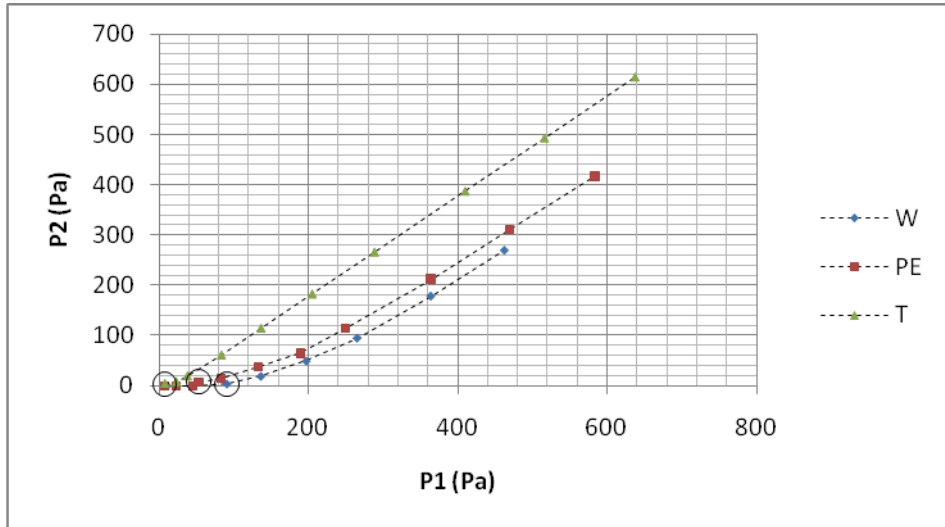


Figure 4.4 Pressure variation for W, PE and T at L10

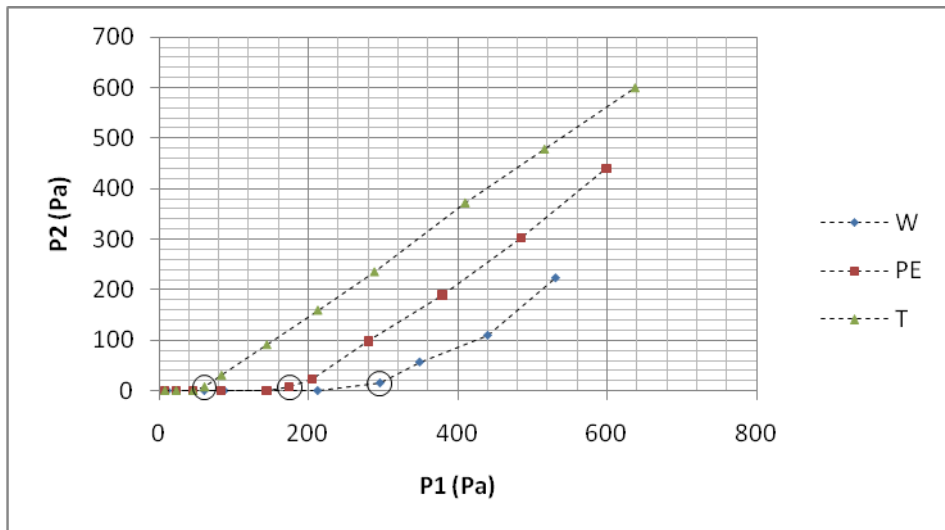


Figure 4.5 Pressure variation for W, PE and T at L30

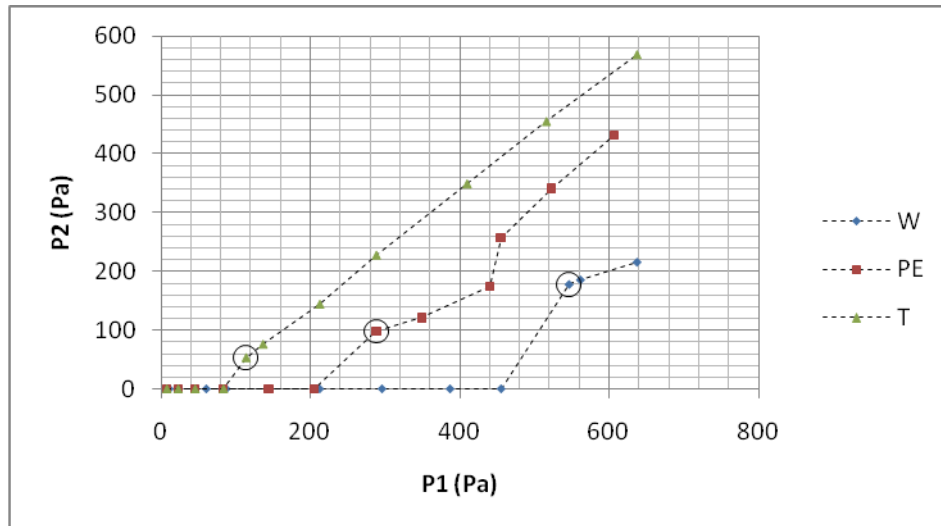


Figure 4.6 Pressure variation for wheat W, PE and T at L50

Minimum fluidization velocity  $U_{mf}$  is a direct function of L for covered particles Z1, Z2, T, W, SE, PE, S are given in table 4.1. Decrease in L is seen with a reduction of  $U_{mf}$ . The same amount of air flow is not enough to transport particles with L10, L30 and L50. Because of this reason  $U_{mf}$  values increase when the bed lengths are increased. The  $U_{mf}$  is determined in reference to variation of  $P_2$  versus  $P_1$ . The behaviour of  $P_2$  as a function of  $P_1$  is such that before the state of  $U_{air} = U_{mf}$  which is specified by a circle in related plots,  $P_2$  does not vary with  $P_1$ . The state of  $U_{air} = U_{mf}$  is associated with a sudden increase in  $P_2$  as a function of  $P_1$ .  $P_2$  versus  $P_1$  graphs for covered particles are given in figures from 4.7 to 4.13.

L seems to be governing parameter on  $U_{mf}$  determination for Z1, Z2, T, W, SE, PE, S. This influence is dominant in comparison with the corresponding effect of L for PE and T. As can be seen from figure 4.10 and 4.12 the change in L is not seriously influencing  $P_2$  versus  $P_1$  plots. The reason of this observation is due to the  $\rho_{blp}$  of PE and T, and possibly shape and size  $d_p$ . On the other hand as can be seen from figure 4.13,  $P_2$  versus  $P_1$  variation is much more influenced by L.

In figures 4.7 and 4.8  $P_2$  of Z1 and W particles are given as a function of  $P_1$ . The loose poured bulk density  $\rho_{blp}$  of Z1 is higher than that for W. But the  $U_{mf}$  of W



is seen to be higher than that for Z1 at L10, L30 and L50. This can be related to the small particle size  $d_p$  of Z1 with regarding to W. SE and Z2 are seems in the same characteristics in figure 4.9 and 4.11.  $U_{mf}$  of the SE is less than Z2 at L10, L30 and L50 although the  $d_p$  of SE is equal to Z2 which is referred in table 4.1. It seems the reason of difference can be related with  $\rho_{blp}$  values of Z2 and SE. The reason of the low  $U_{mf}$  for SE may be because of that  $\rho_{blp}$  is more effective than  $d_p$  for the determination of minimum fluidization states.

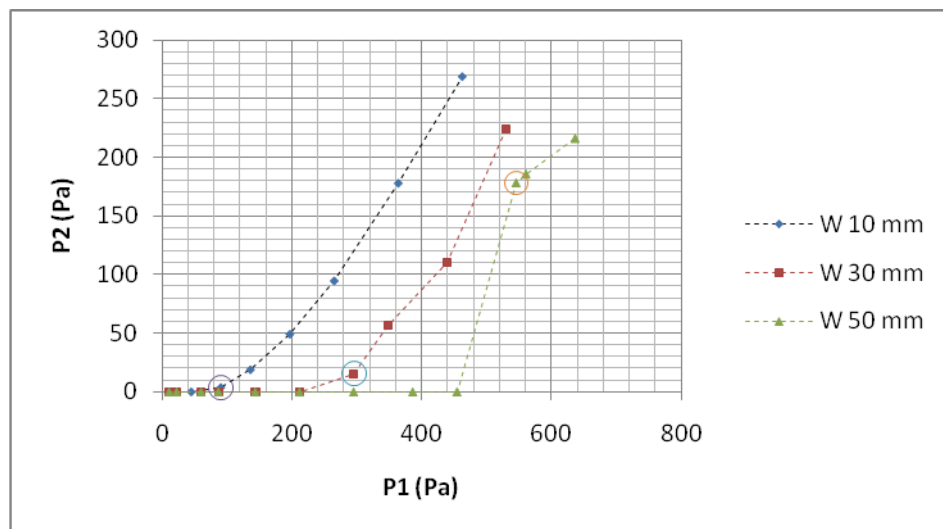


Figure 4.7 Minimum fluidization state change as a function of bed thickness for W particles

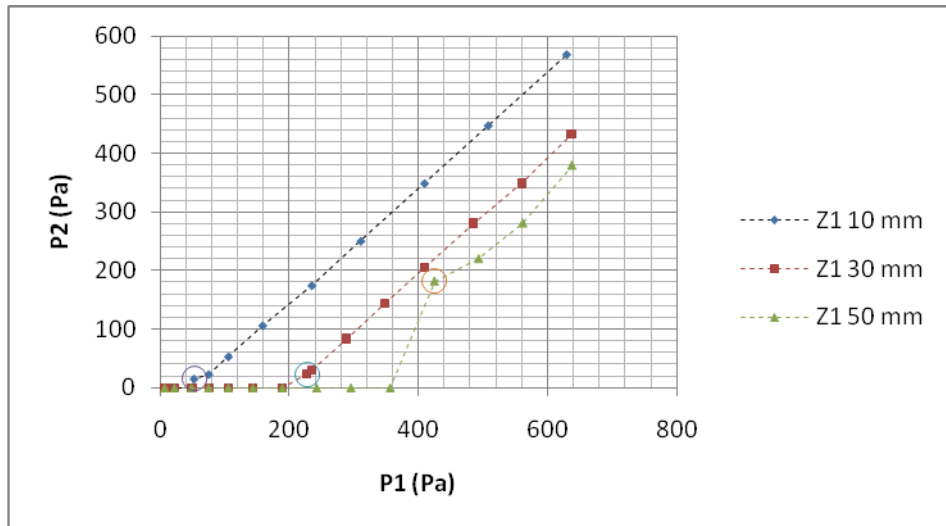


Figure 4.8 Minimum fluidization state change as a function of bed thickness for Z1 particles

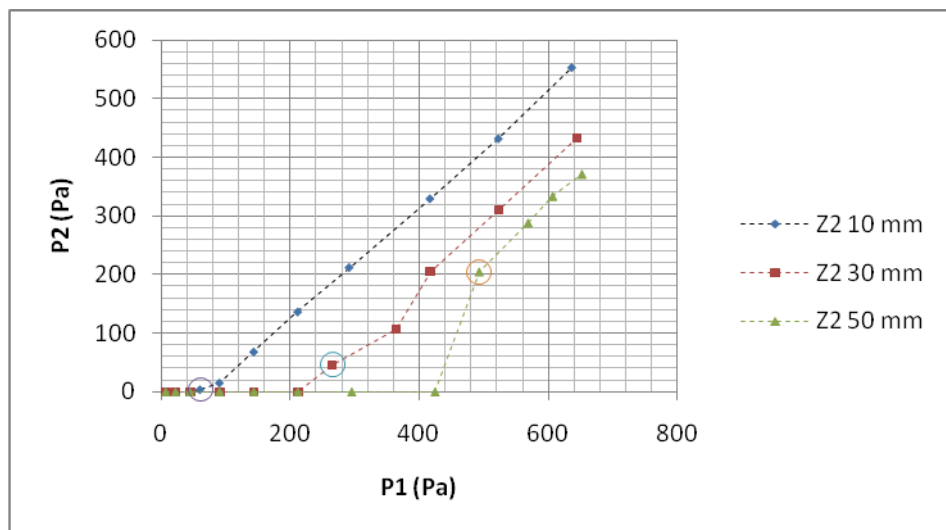


Figure 4.9 Minimum fluidization state change as a function of bed thickness for Z2 particles

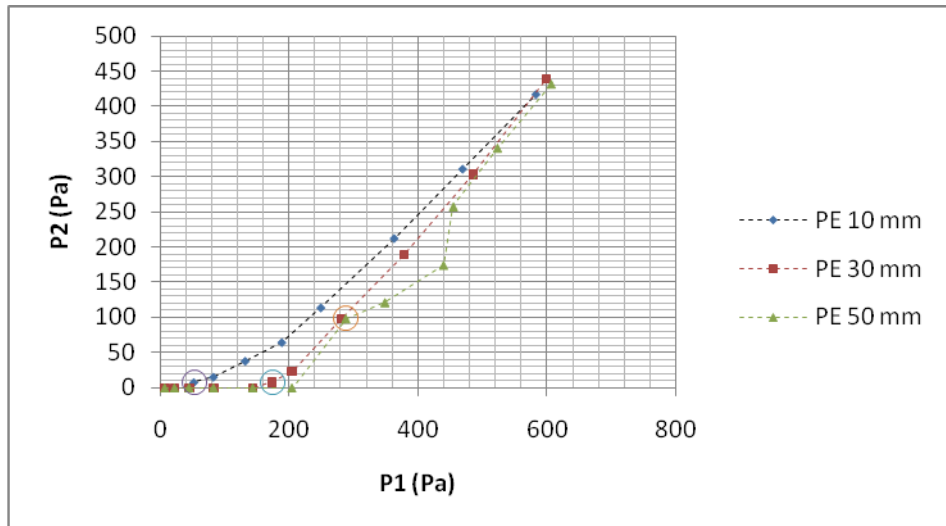


Figure 4.10 Minimum fluidization state change as a function of bed thickness for PE particles

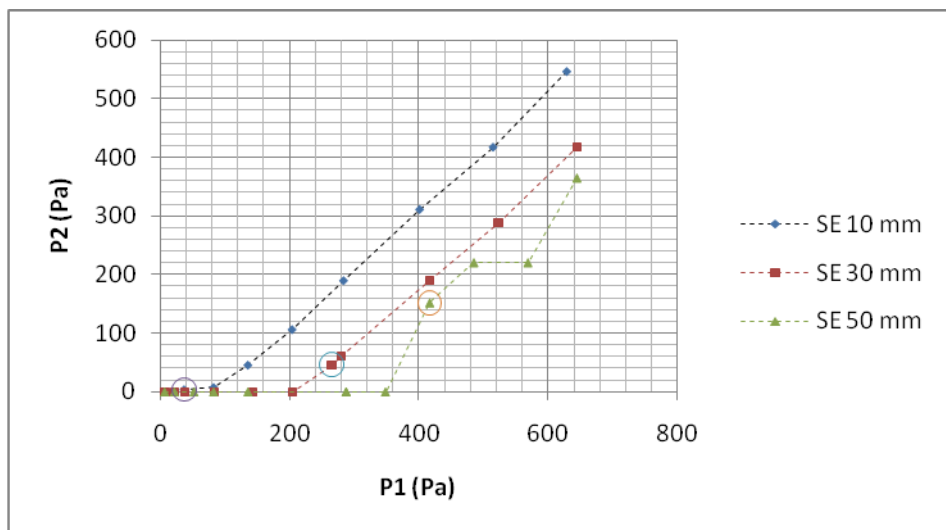


Figure 4.11 Minimum fluidization state change as a function of bed thickness for SE particles

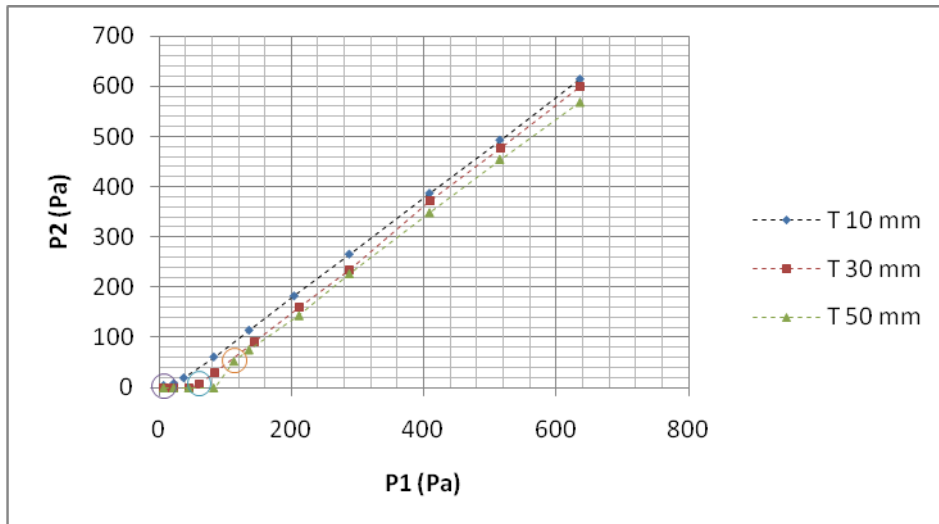


Figure 4.12 Minimum fluidization state change as a function of bed thickness for T particles

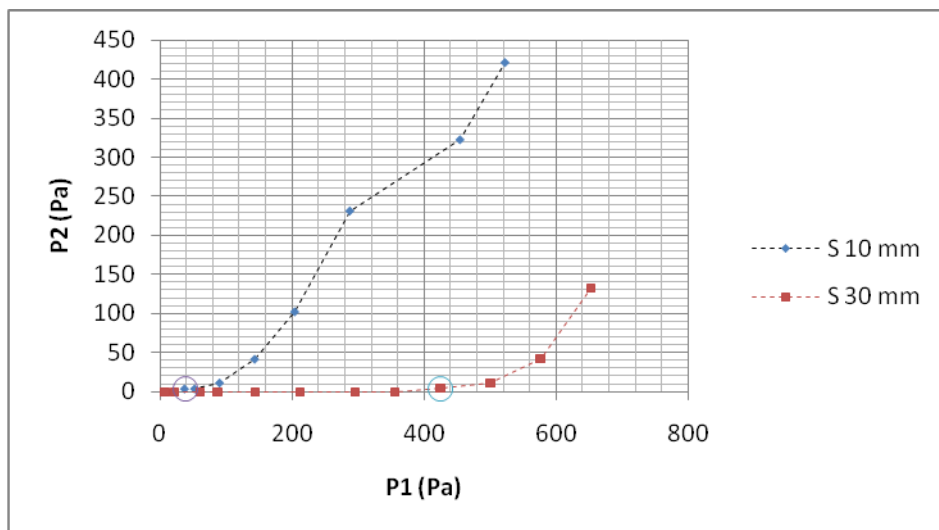


Figure 4.13 Minimum fluidization state change as a function of bed thickness for S particles

Flow modes are clearly observed in test case 1. In the beginning of the experiment of case 1, particles are filled into the vertical pipe and stayed stable in the pipe with the help of perforated plate. While the air flow rate is not enough to fluidize solid particles in the pipe  $U_{air} \ll U_{mf}$ , unstable zone is observed. At

minimum fluidization velocity of solid particles  $U_{air} = U_{mf}$ , fluidized dense phase is observed and then with increasing the air flow rate, all particles are suspended in the air flow with  $U_{air} > U_{mf}$ . This flow mode is called as dilute phase. So that, all flow modes are observed for covered particles in each L at vertical test case. The value of  $U_{mf}$  is not observed for S particles at the bed length of L50.

#### 4.4 Results in the Horizontal Test Case

Minimum fluidization velocities are determined with a new proposed method in test case 1 and explained in the previous section. In test case 2, a similar method is performed to determine minimum fluidization velocities, which are directly related to the flow modes. Since the horizontal test case is different from that of vertical one, minimum fluidization velocities are given with  $U'_{mf}$  for the test case 2. For each test case, horizontal acrylic glass pipe is filled with mass of W, S, SE, PE and T particles as 500 gr, 1000 gr, 500 gr, 500 gr and 100 gr respectively with the use of a 10 mm diameter hole at  $X_H/D=10$  from the beginning of the acrylic glass pipe until the pipe has full of particle as shown in figure 4.14.

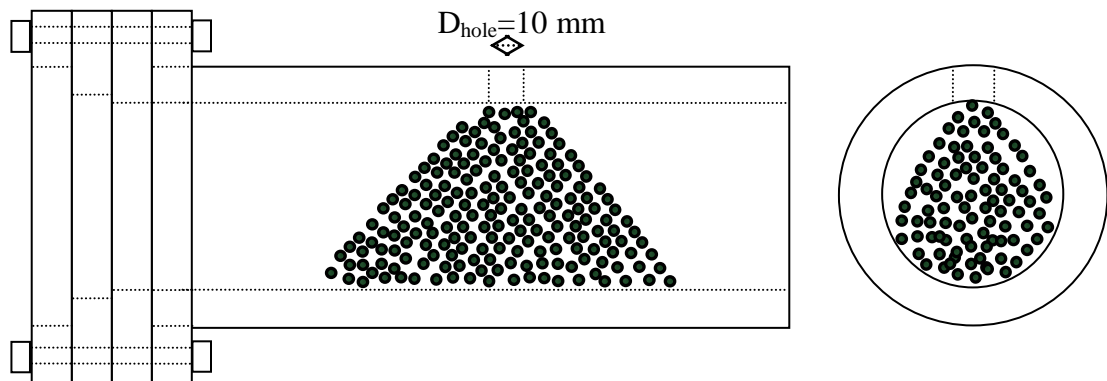


Figure 4.14 Horizontal test case with particles

$U_{air}$  is increased and at each  $U_{air}$  field was observed. The  $U_{air}$  is taken as  $U'_{mf}$  which are given in table 4.2 when the air velocity  $U_{air}$  at which first particles over the top of triangular horizontal bed carried. The carried  $\dot{M}_p$  and time were used to determine  $\dot{M}_p$ . During the process, the  $U_{air}$  is measured by means of the pitot tube

at the reference test section. Each  $U_{air}$  is recorded for the different positions of solid particles. At the same time, local static pressures at  $X_H/D=2, 18, 32$  and  $48$  which are given in figure 3.3 are measured and acquired by means of a devised program, FDRIPCS.vi. The statistical analyses are also performed by the devised program. The minimum and maximum  $U'_{mf}$  are observed for SE with  $d_p = 700 \mu\text{m}$  and  $\rho_{blp} = 850 \text{ kg/m}^3$  at  $U'_{mf} = 6.99 \text{ m/s}$  and the W with  $d_p = 2250 \mu\text{m}$  and  $\rho_{blp} = 950 \text{ kg/m}^3$  at  $U'_{mf} = 16.32 \text{ m/s}$ . This show the  $d_p$  values are dominant in comparison to  $\rho_{blp}$  to determine  $U'_{mf}$ . In addition to this,  $U'_{mf}$  of particles in horizontal test case are higher than  $U_{mf}$  of particles at L10 in vertical test case except for SE.

Table 4.2  $U'_{mf}$  of W, S, SE, PE and T in test case 2

Particles	Test Case 2
	$U'_{mf}(\text{m/s})$
W	16.32
S	10.75
SE	6.99
PE	12.47
T	8.94

Figures from 4.15.a to 4.15.j illustrate a sample visual observation of each stage during a test run for PE. At the beginning of the test run, acrylic glass pipe is filled with solid particle of 500 gr PE then  $U_{air}$  is increased systematically. Slug flow is observed when the  $U_{air} \ll U'_{mf}$  as shown in the figures 4.15.a and 4.15.b.  $U_{air}$  of first breaking point from the top of solid particle hill is taken as  $U'_{mf}$ .  $U'_{mf} = U_{air}$  in figures from 4.15.c to 4.15.f and the observation is called as start to fluidization. Then, solid particles hill is transformed to a long line in the acrylic glass pipe shown in figures from 4.15.g to 4.15.j. This long particles line is called as plug flow when  $U_{air} > U'_{mf}$ . Solid particles line shortens continuously depending on  $U_{air}$  before the pipe is totally discharged. At this time flow mode is observed as fully suspended-dilute phase when the  $U_{air} \gg U_{mf}$ .



a)



b)



c)



d)



e)



f)



g)



h)



i)



j)

Figure 4.15 Visual observation of polyethylene

Figure 4.16 indicated that the variation of  $P_2$  versus  $P_1$  for test case 2 for five solid particles which are W, T, SE, S and PE. In this figure, minimum fluidization states are marked with a circle symbol of “O”. Variation of  $P_2$  versus  $P_1$  was used to determine fluidization states for the test case 1 and it is shown the sudden increase in  $P_2$  represented the minimum fluidization states. On the other hand as shown in figure 4.16 in test case 2, this method does not give any remarkable results to determine fluidization state similar to test case 1.  $P_2$  increases almost gradually with  $P_1$  without a special influence of “O” point. For this reason, an alternative method is proposed and detailed in the following part.

Four different pressure transmitters are used to determine local static pressures which are detailed in the previous section. Pressure drops;  $\Delta P_2$ ,  $\Delta P_3$  and  $\Delta P_4$  are used for the determination of states for each particle. Pressure difference of  $P_1$  and  $P_2$ ,  $P_1$  and  $P_3$  and  $P_1$  and  $P_4$  are symbolized as  $\Delta P_2$ ,  $\Delta P_3$  and  $\Delta P_4$ . Then local pressure gradients  $\Delta P/L$  were obtained. Fluidization states are shown with a circle symbol as before. The local pressure drops versus  $U_{air}$  are given in figures from 4.17 to 4.21. Also local pressure gradients are shown in figures from 4.22 to 4.26 as a function of  $U_{air}$ .

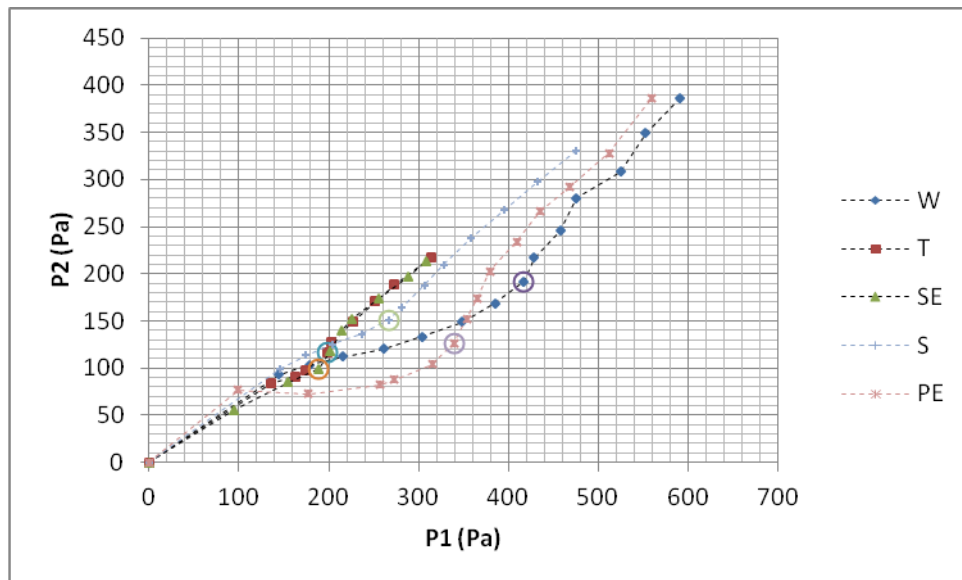


Figure 4.16 Pressure variation and minimum fluidization state change in test case 2



In vertical test case; variation of local pressure magnitudes before and after the packed cylindrical material samples as a function of  $U_{air}$  was used to determine minimum fluidization velocity and its link with flow dynamics. In horizontal test case the similar measurement practice indicated that variation of local pressures before and after the packed triangular material samples presented a different functional relationship with  $U_{air}$ . Therefore local pressure drops  $\Delta P_2$ ,  $\Delta P_3$  and  $\Delta P_4$  defined as the local pressure differences. Furthermore local pressure gradients  $\Delta P/L$  are referred to observe the local frictional effects as a function of  $U_{air}$ .

It is clearly shown, the local pressure drops as function of  $U_{air}$  for W and PE are almost in the same characteristics lines in figure 4.20 and 4.21. Local static pressure drop values are increasing with increasing air flow rate during the experiment. When the minimum fluidization occurs, the pressure drop values decrease very slowly then pressure drop is almost constant for the rest of the experiment. PE which has an average particle diameter of 2750  $\mu\text{m}$  is the biggest particle and wheat with an average diameter of 2250  $\mu\text{m}$  is the second one in this study. These particles effected the flow pattern as slug flow until the minimum fluidization state because of their big average particle diameters. After the minimum fluidization state, particles are dispersed slowly along the pipeline then the local pressure drops are became almost stable.  $U'_{mf}$  of PE is less than W but higher than the other particles which are referred in table 4.2.  $U'_{mf}$  of SE is the minimum value in table 4.2 which is also a remarkable point. In vertical test case  $\rho_{blp}$  seems to be more effective than  $d_p$ , but in horizontal test case the result seems to be opposite.

The minimum slope of local pressure drop values are shown in figure 4.17 for T. T has the lowest loose poured bulk density,  $\rho_{blp}$  of 200  $\text{kg}/\text{m}^3$  in this study. This can be reason of the low slopes. The new expectations is the maximum slope for the particle of maximum density which is sand with loose poured bulk density,  $\rho_{blp}$  of 2400  $\text{kg}/\text{m}^3$  with regarding this proposal. But, sand particles which has the minimum average diameter of 150  $\mu\text{m}$  in this study, are not generated the maximum slope of pressure drop as shown in figure 4.18. So, the slope of the pressure drop is not only

related with loose pored bulk density,  $\rho_{blp}$  it is also related with average particle diameter,  $d_p$ .

In figure 4.19, local pressure drop versus  $U_{air}$  for SE is given. In this figure, local pressure drop for SE with the maximum  $\Delta P = 117.33$  Pa. The pressure drop for W and PE are  $\Delta P = 246.27$  Pa and  $\Delta P = 212.84$  Pa, respectively as shown in figure 4.20 and 4.21. The reason of this result may be because of the fact that the average particle diameter of SE with  $d_p = 700 \mu\text{m}$  is less than W and PE with  $d_p = 2250 \mu\text{m}$  and  $d_p = 2750 \mu\text{m}$  respectively.

In horizontal test case particles are filled into the pipe then experiment is started. This is caused to the slug flow formation in the pipe in the beginning of the experiment with  $U_{air} = 0$ . Flow field is stayed stable until the first breakaway points from the prismatic shape of particles at  $U'_{mf} \gg U_{air}$ . After this points, particles are spreaded into the pipe, then it is provided to transition of plug flow when the  $U_{air} = U'_{mf}$ . Following that long plugs are occurred when the  $U_{air} > U'_{mf}$  in through the pipe line and it is called as plug flow. With the increasing of  $U_{air}$  all particles are started to flow in the air flow and again plug flow is occurred at  $U_{air} \gg U'_{mf}$ .

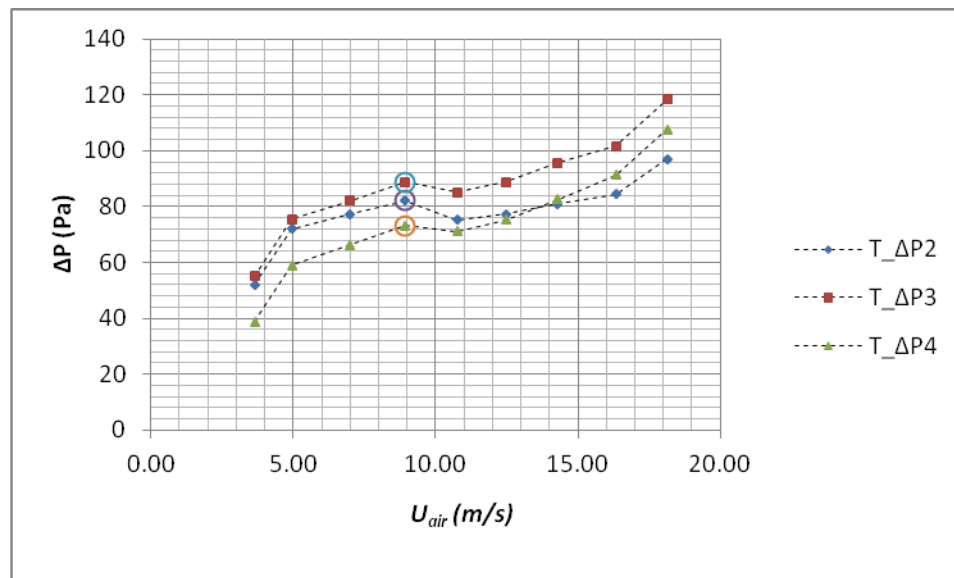


Figure 4.17  $\Delta P$  as a function of  $U_{air}$  for T

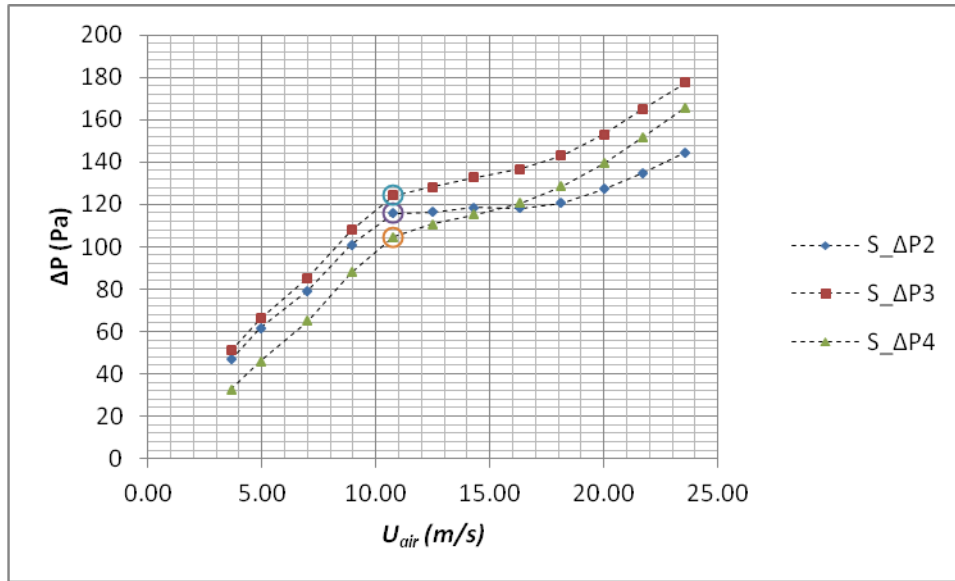


Figure 4.18  $\Delta P$  as a function of  $U_{air}$  for S

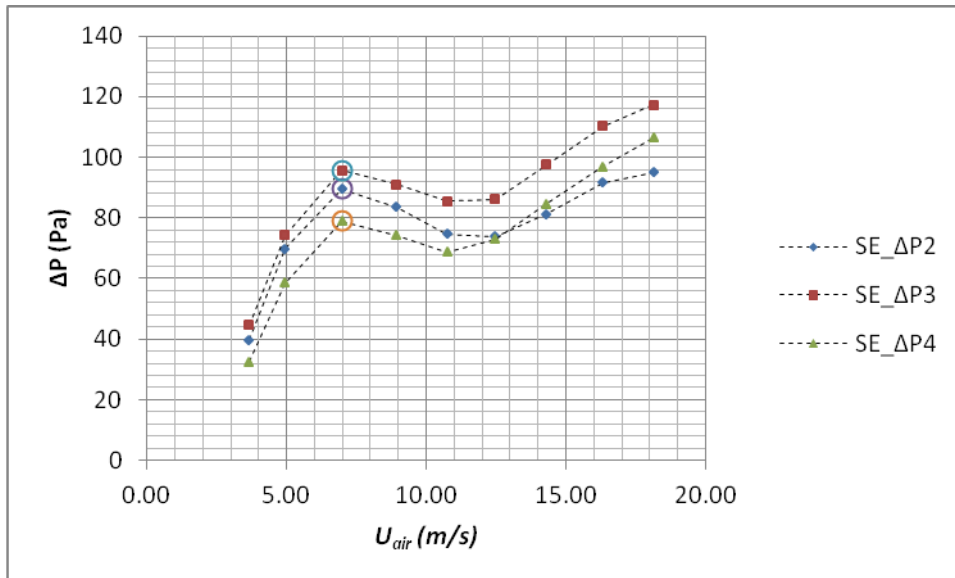


Figure 4.19  $\Delta P$  as a function of  $U_{air}$  for SE

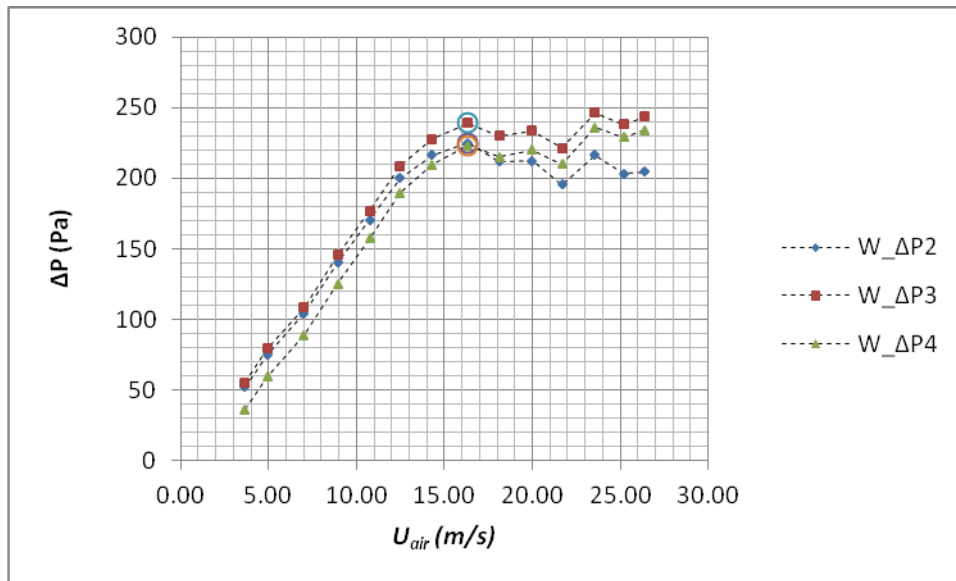


Figure 4.20  $\Delta P$  as a function of  $U_{air}$  for W

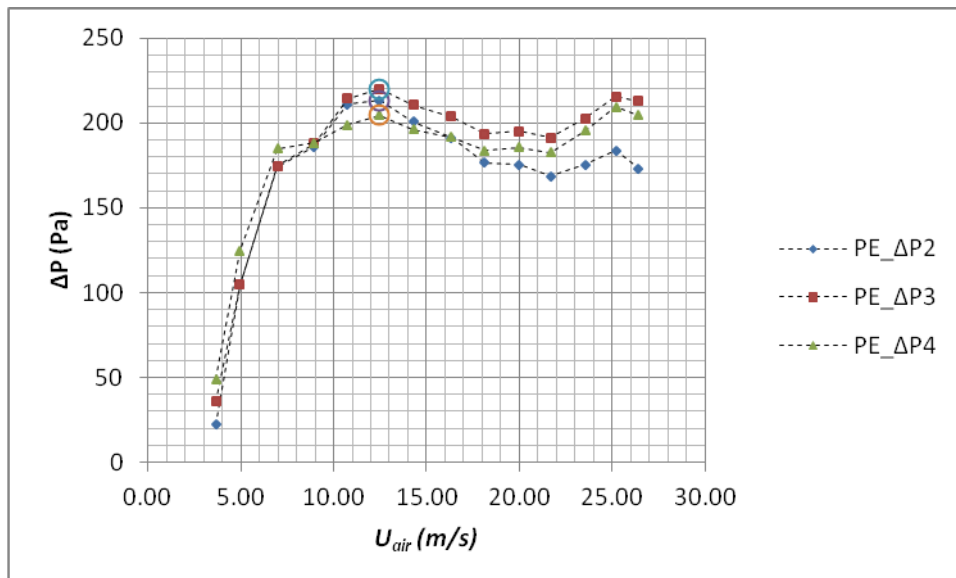


Figure 4.21  $\Delta P$  as a function of  $U_{air}$  for PE

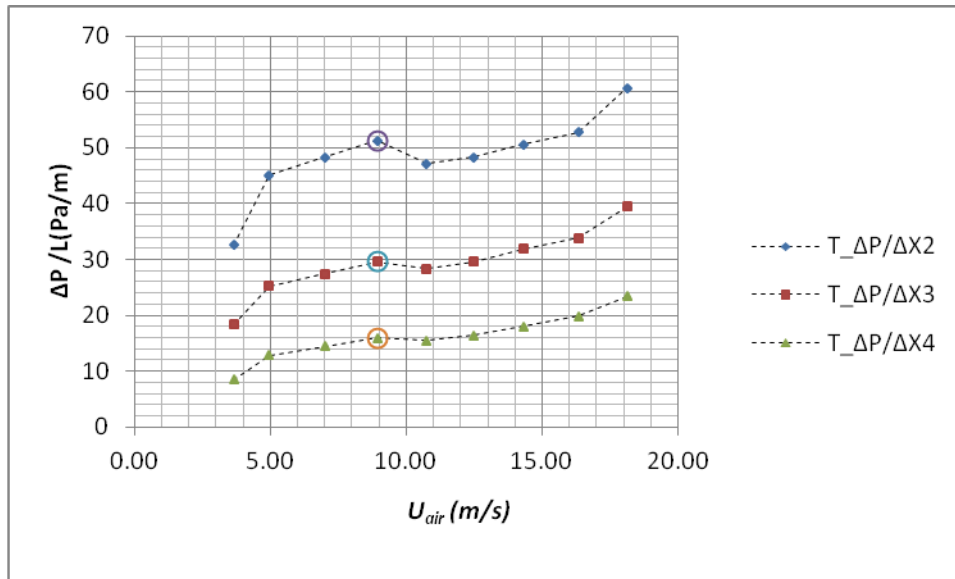


Figure 4.22  $\Delta P/L$  as a function of  $U_{air}$  for T

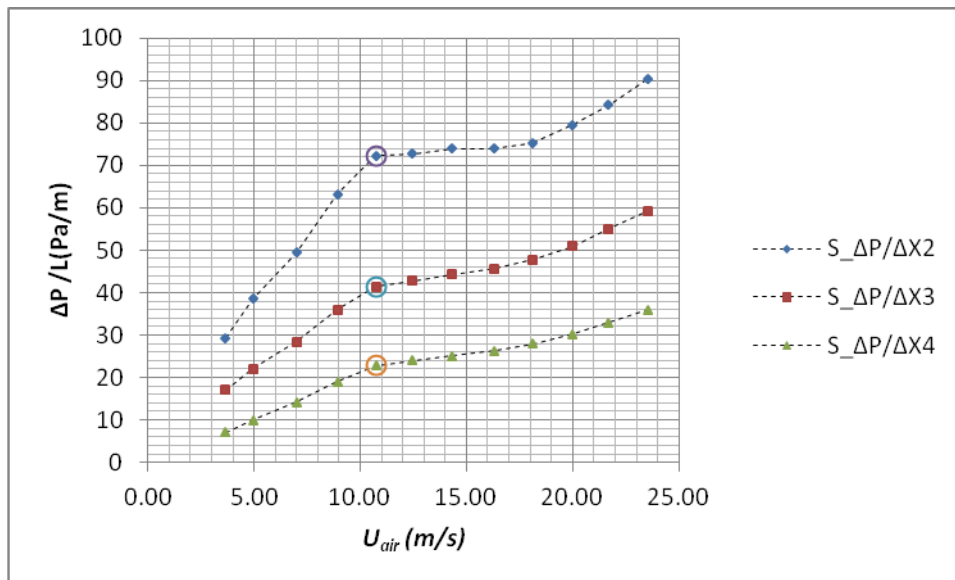


Figure 4.23  $\Delta P/L$  as a function of  $U_{air}$  for S

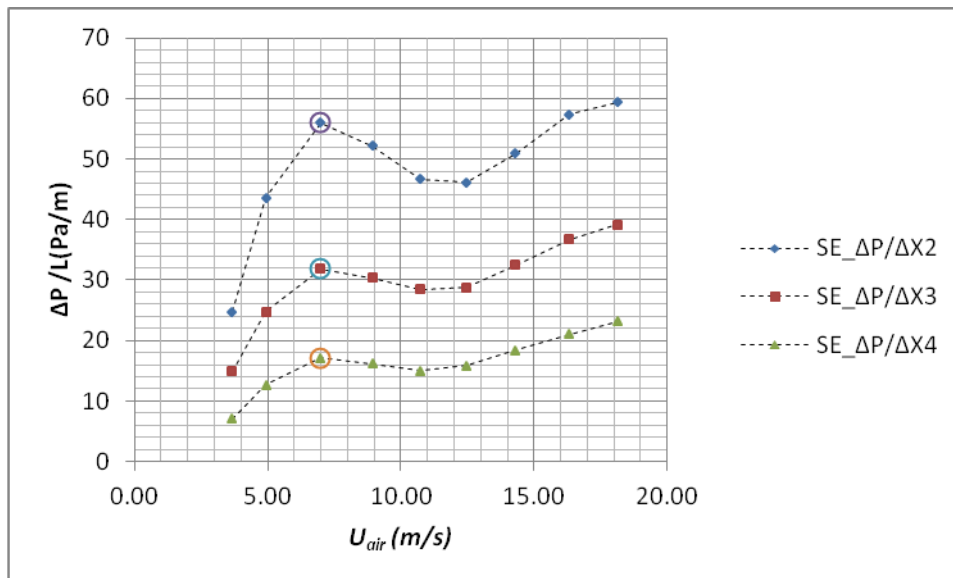


Figure 4.24  $\Delta P/L$  as a function of  $U_{air}$  for SE

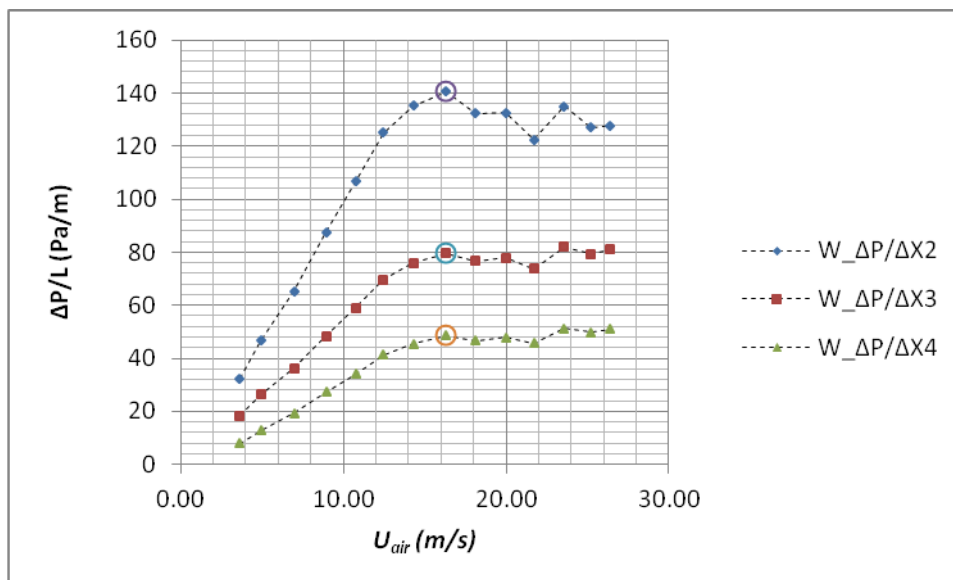


Figure 4.25  $\Delta P/L$  as a function of  $U_{air}$  for W

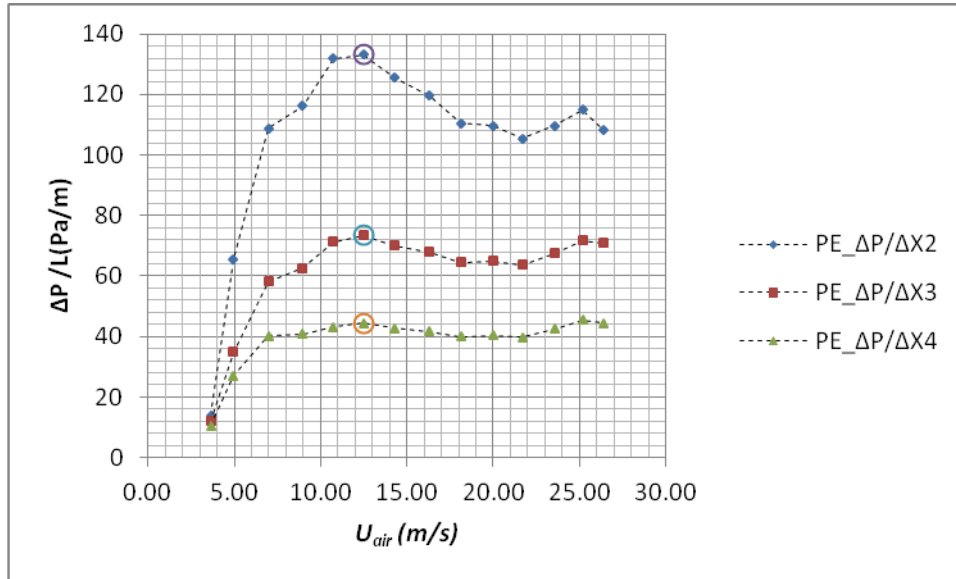


Figure 4.26  $\Delta P/L$  as a function of  $U_{air}$  for PE

#### 4.5 Results in Continuous Conveying with Particle Feeder

In this test case, S, W and SE (with the  $\rho_{blp}$  of  $2400 \text{ kg/m}^3$ ,  $950 \text{ kg/m}^3$ ,  $850 \text{ kg/m}^3$  and  $d_p$  of  $150 \text{ }\mu\text{m}$ ,  $2250 \text{ }\mu\text{m}$ ,  $2750 \text{ }\mu\text{m}$ , respectively) are used to observe flow modes during the continuous conveying with particle feeder where located at  $X_H/D=0$ . The particle feeder induced the known amount of particles into the pipeline system with determined mass flow rates,  $\dot{m}_p$  with the ranges of  $0.0149 \text{ kg/s} < \dot{m}_p < 0.111 \text{ kg/s}$ . The measurements were started at the maximum  $U_{air} = 26.41 \text{ m/s}$  to observe a fully suspended- dilute phase inside the horizontal test section until no particle conveying. During the process, local static pressure values are recorded at  $X_H/D=2, 18, 32$  and  $48$  and also conveyed particles are weighed by means of an assay balance. The measurements were repeated by reducing  $U_{air}$  for S, W and SE particles where the  $U'' = 14.29 \text{ m/s}$ ,  $14.29 \text{ m/s}$  and  $12.47 \text{ m/s}$  respectively.  $U''$  is defined as before the no particle conveying velocity in continuous conveying test section. Particle feeder having different sized orifice plates is used to induce different mass flow rates of particles,  $\dot{m}_p$  which is detailed in table 3.3, to be carried by airflow.  $U_{air}$ , and local pressure drop values  $\Delta P_2$ ,  $\Delta P_3$  and  $\Delta P_4$  are measured together with the carried mass of particles;  $\dot{M}_p/\dot{M}_a$  through the experiments. Here,  $\dot{M}_a$  is the

air mass flow rate and  $\dot{M}_p$  is the mass flow rate of particles which are carried by different values of  $U_{air}$ .

In these test runs, all particles are weighed for each  $U_{air}$  with regarding to air flow rates and orifice plates. Mass flow rates of particles with respect to air mass flow rates are tabulated in table 4.3.

Table 4.3 Mass flow rates of particles with respect to air for continuous conveying

Particle	Orifice (mm)	Max $\dot{M}_p/\dot{M}_a$ (%)	Min $\dot{M}_p/\dot{M}_a$ (%)
W	20	12.2	0.43
	15	9.47	0.38
S	20	29.14	1.08
	15	23.74	0.65
	10	14.2	0.5
SE	20	17.56	0.43
	15	11.7	0.37
	10	4.18	0.25

In continuous conveying tests only dilute phase is observed. The local pressure drop values are increased with respect to  $U_{air}$  (mean air velocity) for all particles. S which is induced into the pipeline with 10 mm, 15 mm and 20 mm orifice plates with the ranges of  $0.5\% < \dot{M}_p/\dot{M}_a < 29.14\%$  are given from figures 4.27 to 4.29 for the continuous conveying. Local pressure drops for S particles with 10 mm orifice  $\Delta P_2$ ,  $\Delta P_3$  and  $\Delta P_4$  are given with the range of  $77.14\text{ Pa} < \Delta P_2 < 177.18\text{ Pa}$ ,  $92.73\text{ Pa} < \Delta P_3 < 223.02\text{ Pa}$  and  $82.62\text{ Pa} < \Delta P_4 < 221.65\text{ Pa}$  in figure 4.27. These ranges increase for 15 mm and 20 mm respectively as  $80.15\text{ Pa} < \Delta P_2 < 191.48\text{ Pa}$ ,  $93.24\text{ Pa} < \Delta P_3 < 235.53\text{ Pa}$ ,  $84.11\text{ Pa} < \Delta P_4 < 227.93\text{ Pa}$ , and  $86.32\text{ Pa} < \Delta P_2 < 192.97\text{ Pa}$ ,  $115.32\text{ Pa} < \Delta P_3 < 236.36\text{ Pa}$  and  $105.25\text{ Pa} < \Delta P_4 < 227.54\text{ Pa}$ .  $\Delta P$  ranges of S particles indicated that the mass flow rates are directly related with local pressure drops in the pipeline. In figure 4.23,  $\Delta P_2$ ,  $\Delta P_3$  and  $\Delta P_4$  are 77.14 Pa, 92.73 Pa and 82.11 Pa while  $\dot{M}_p/\dot{M}_a = 0.5\%$ . Magnitudes are increasing in figures 4.28 and



4.29  $\Delta P_2$ ,  $\Delta P_3$  and  $\Delta P_4$  are 80.15 Pa, 93.24 Pa and 84.11 Pa respectively for  $\dot{M}_p/\dot{M}_a = 0.65\%$  and  $\Delta P_2$ ,  $\Delta P_3$  and  $\Delta P_4$  are 86.32 Pa, 115.32 Pa and 105.25 Pa for  $\dot{M}_p/\dot{M}_a = 1.08\%$ .

SE particles are induced into the pipeline also with 10 mm, 15 mm and 20 mm orifice plates with the ranges of  $0.25\% < \dot{M}_p/\dot{M}_a < 17.56\%$  are given from figure 4.26 to figure 4.28 for the continuous conveying. Local pressure drops for SE particles with 10 mm orifice  $\Delta P_2$ ,  $\Delta P_3$  and  $\Delta P_4$  are given with the range of  $57.24\text{ Pa} < \Delta P_2 < 160.98\text{ Pa}$ ,  $65.72\text{ Pa} < \Delta P_3 < 203.69\text{ Pa}$  and  $58.58\text{ Pa} < \Delta P_4 < 203.60\text{ Pa}$  in figure 4.30. These ranges increase for 15 mm and 20 mm as of  $59.12\text{ Pa} < \Delta P_2 < 170.94\text{ Pa}$ ,  $69.78\text{ Pa} < \Delta P_3 < 212.82\text{ Pa}$ ,  $64.74\text{ Pa} < \Delta P_4 < 214.01\text{ Pa}$ , and  $63.55\text{ Pa} < \Delta P_2 < 175.37\text{ Pa}$ ,  $74.01\text{ Pa} < \Delta P_3 < 216.19\text{ Pa}$  and  $68.06\text{ Pa} < \Delta P_4 < 217.06\text{ Pa}$  respectively. In figure 4.30,  $\Delta P_2$ ,  $\Delta P_3$  and  $\Delta P_4$  are 57.24 Pa, 65.72 Pa and 58.58 Pa for  $\dot{M}_p/\dot{M}_a = 0.25\%$ . Magnitudes are increasing in figures 4.31 and 4.32 such that  $\Delta P_2$ ,  $\Delta P_3$  and  $\Delta P_4$  are 59.12 Pa, 69.78 Pa and 64.74 Pa for  $\dot{M}_p/\dot{M}_a = 0.37\%$  and  $\Delta P_2$ ,  $\Delta P_3$  and  $\Delta P_4$  values are 63.55 Pa, 74.01 Pa and 68.06 Pa for  $\dot{M}_p/\dot{M}_a = 0.43\%$ .

W particles are induced into the pipeline with only 15 mm and 20 mm orifice plates with the ranges of  $0.38\% > \dot{M}_p/\dot{M}_a > 12.20\%$  and the results are shown in figures 4.33 and 4.34 for the continuous conveying. W is not discharged from the 10 mm orifice plate. Local pressure drops for wheat particles with 15 mm orifice  $\Delta P_2$ ,  $\Delta P_3$  and  $\Delta P_4$  are given with the range of  $66.70\text{ Pa} < \Delta P_2 < 170.99\text{ Pa}$ ,  $73.05\text{ Pa} < \Delta P_3 < 211.20\text{ Pa}$  and  $71.45\text{ Pa} < \Delta P_4 < 214.26\text{ Pa}$  as given in figure 4.33. These ranges increase for 20 mm plate as  $71.18\text{ Pa} < \Delta P_2 < 176.56\text{ Pa}$ ,  $79.46\text{ Pa} < \Delta P_3 < 212.66\text{ Pa}$ ,  $75.32\text{ Pa} < \Delta P_4 < 215.54\text{ Pa}$ . In figure 4.29,  $\Delta P_2$ ,  $\Delta P_3$  and  $\Delta P_4$  are 66.70 Pa, 73.05 Pa and 71.45 Pa respectively for  $\dot{M}_p/\dot{M}_a = 0.38\%$ . Magnitudes are increasing in figure 4.34, namely  $\Delta P_2$ ,  $\Delta P_3$  and  $\Delta P_4$  are 71.18 Pa, 79.46 Pa and 75.32 Pa for  $\dot{M}_p/\dot{M}_a = 0.43\%$ .

For the general view of the link between the local pressure drop and  $\dot{M}_p/\dot{M}_a$  for S, W and SE particles, they are in the similar characteristics.  $\Delta P$  increases as  $\dot{M}_p/\dot{M}_a$  increases. However, local pressure drop values are differently affected by

solid particles because of their loose poured bulk densities,  $\rho_{blp}$  and particle sizes,  $d_p$ . Due to their small size, SE particles generated lower local pressure drop values in comparison to W particles for the same  $\dot{M}_p/\dot{M}_a = 0.43\%$ . On the other hand the local pressure drop values for S at  $\dot{M}_p/\dot{M}_a = 5.33\%$  are seen to be higher than that for SE at  $\dot{M}_p/\dot{M}_a = 5.44\%$ . Local pressure drop values are given  $\Delta P_2$ ,  $\Delta P_3$  and  $\Delta P_4$  as 114.22 Pa, 136.09 Pa, 123.05 Pa (for S) and 88.50 Pa, 109.21 Pa, 99.46 Pa (for SE). It is predicted due to the loose poured bulk density,  $\rho_{blp}$  of S ( $2400 \text{ kg/m}^3$ ) being higher than that of SE ( $850 \text{ kg/m}^3$ ).

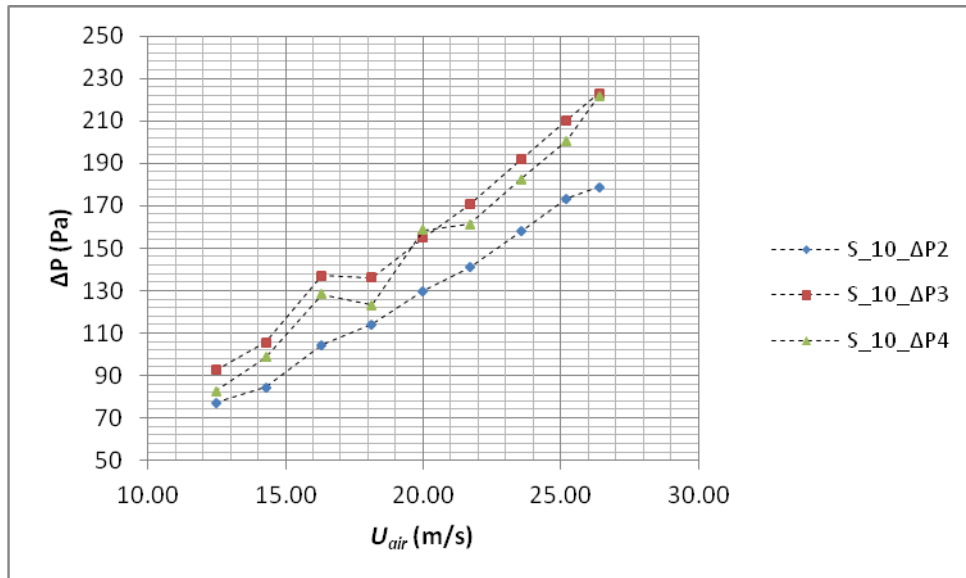


Figure 4.27  $\Delta P$  as a function of  $U_{air}$  for S particles with the range of  $0.50 < \dot{M}_p/\dot{M}_a < 14.20$

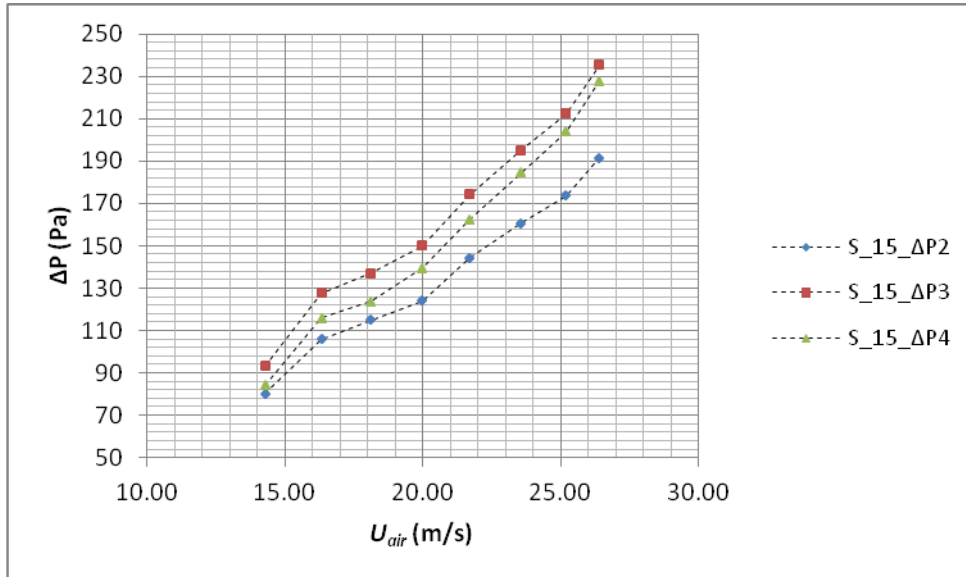


Figure 4.28  $\Delta P$  as a function of  $U_{air}$  for S particles with the range of  $0.65 < \dot{M}_p/\dot{M}_a < 23.74$

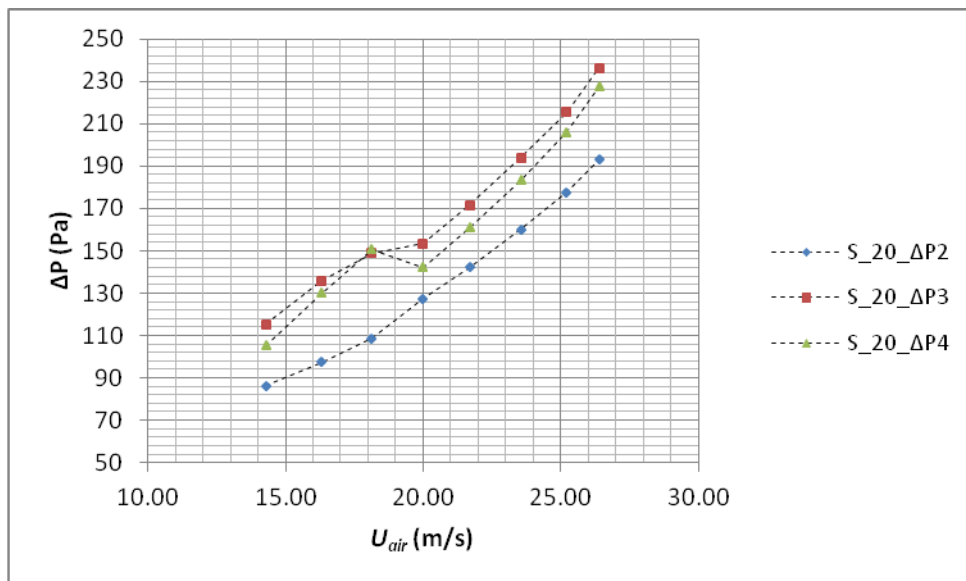


Figure 4.29  $\Delta P$  as a function of  $U_{air}$  for S particles with the range of  $1.08 < \dot{M}_p/\dot{M}_a < 29.14$

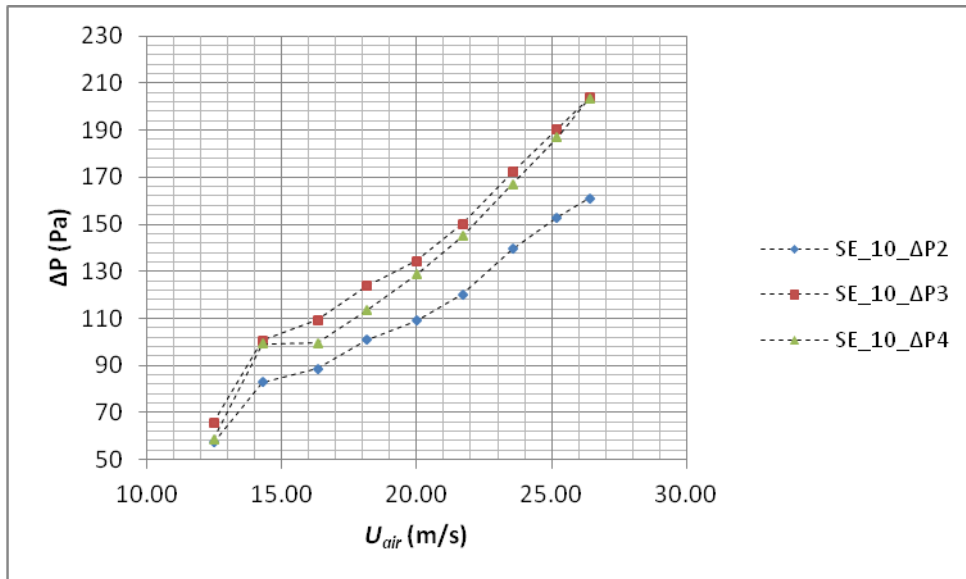


Figure 4.30  $\Delta P$  as a function of  $U_{air}$  for SE particles with the range of  $0.25 < \dot{M}_p/\dot{M}_a < 4.18$

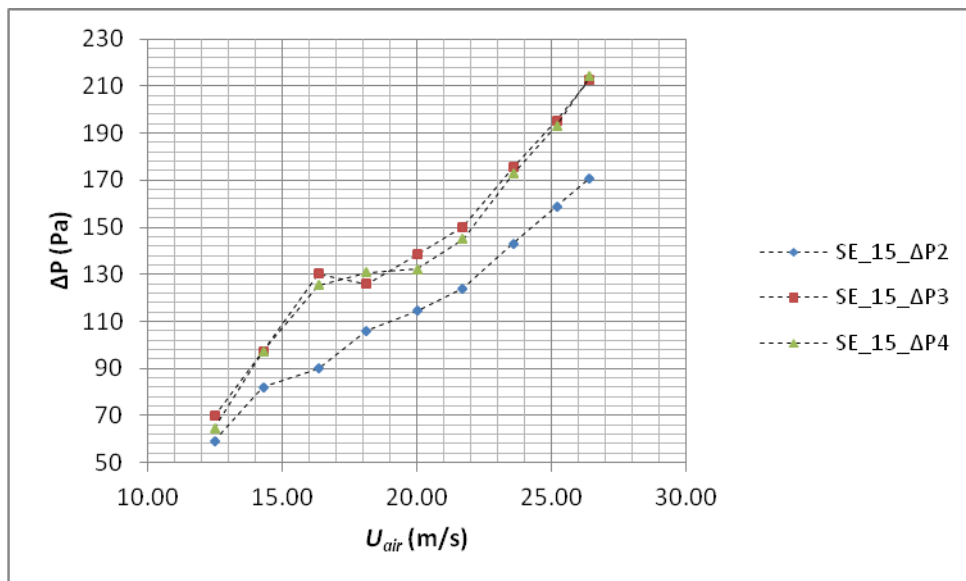


Figure 4.31  $\Delta P$  as a function of  $U_{air}$  for SE particles with the range of  $0.37 < \dot{M}_p/\dot{M}_a < 11.70$

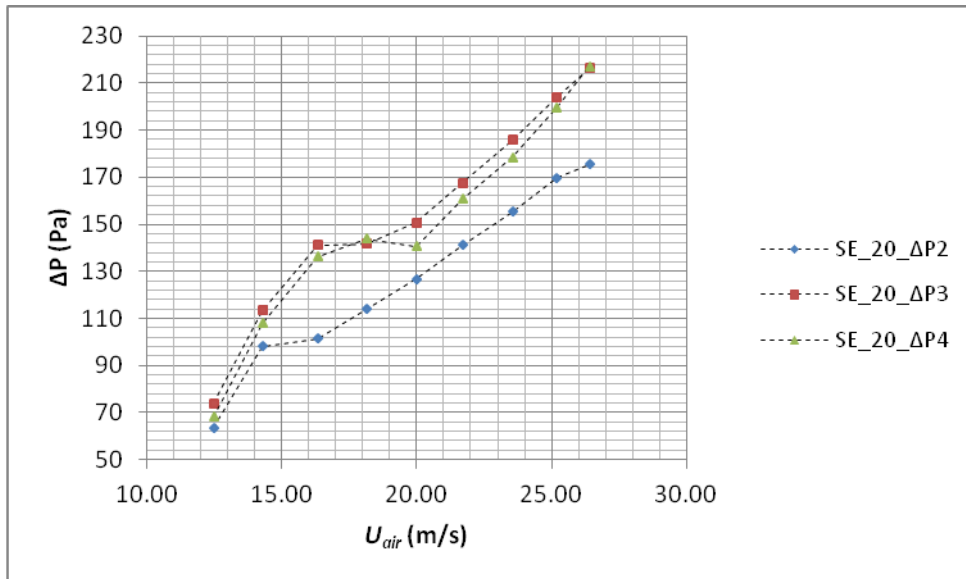


Figure 4.32  $\Delta P$  as a function of  $U_{air}$  for SE particles with the range of  $0.43 < \dot{M}_p/\dot{M}_a < 17.56$

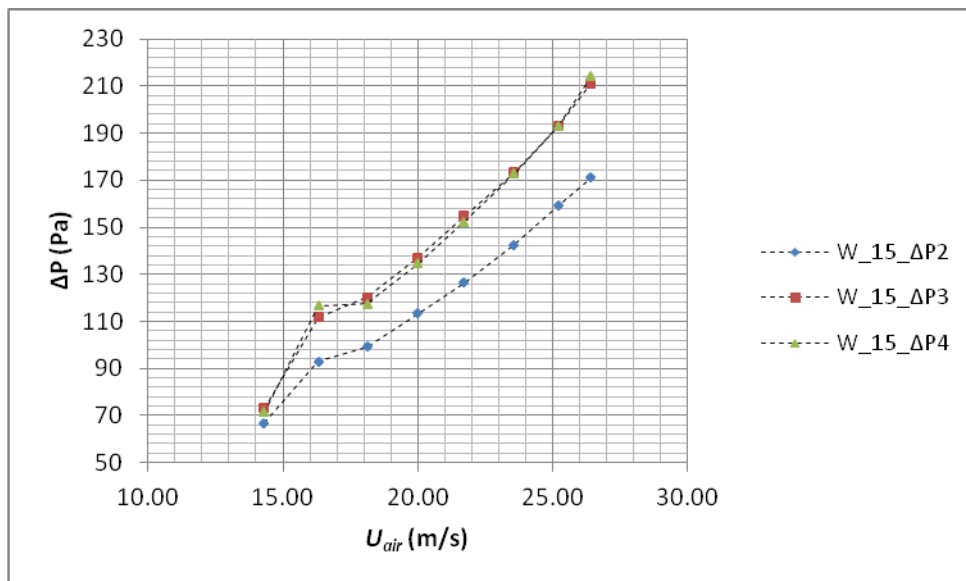


Figure 4.33  $\Delta P$  as a function of  $U_{air}$  for W particles with the range of  $0.38 < \dot{M}_p/\dot{M}_a < 9.47$

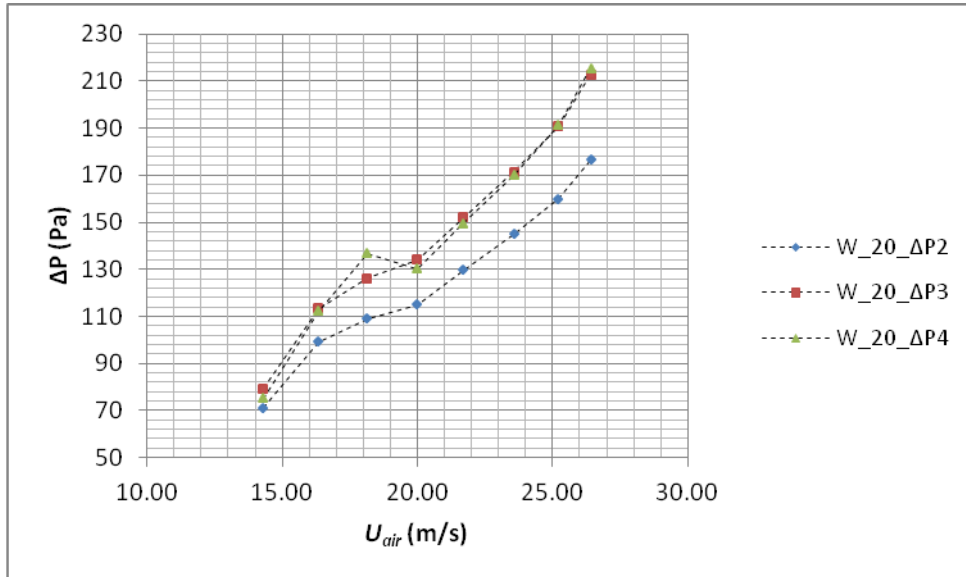


Figure 4.34  $\Delta P$  as a function of  $U_{air}$  for W particles with the range of  $0.43 < \dot{M}_p/\dot{M}_a < 12.20$

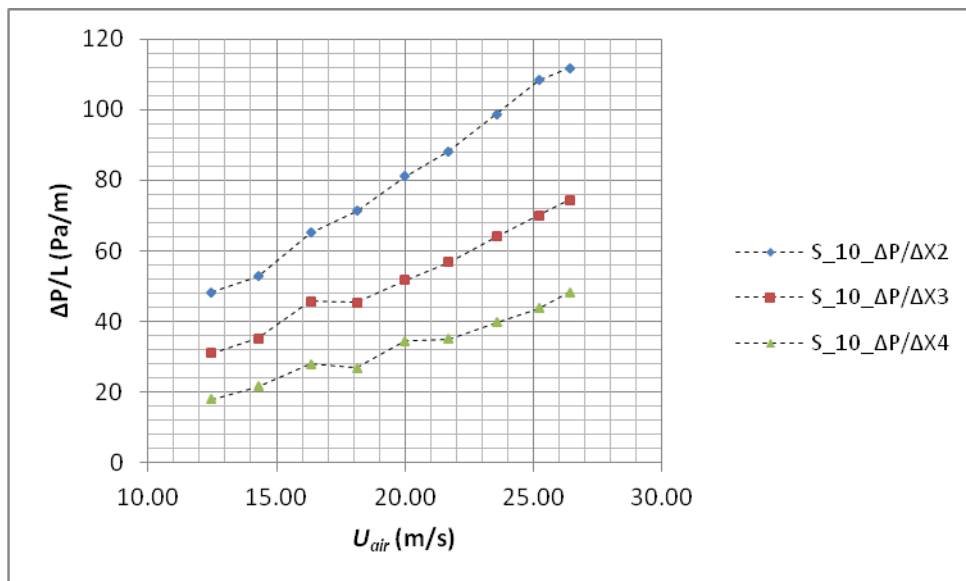


Figure 4.35  $\Delta P/L$  as a function of  $U_{air}$  for S particles with the range of  $0.50 < \dot{M}_p/\dot{M}_a < 14.20$

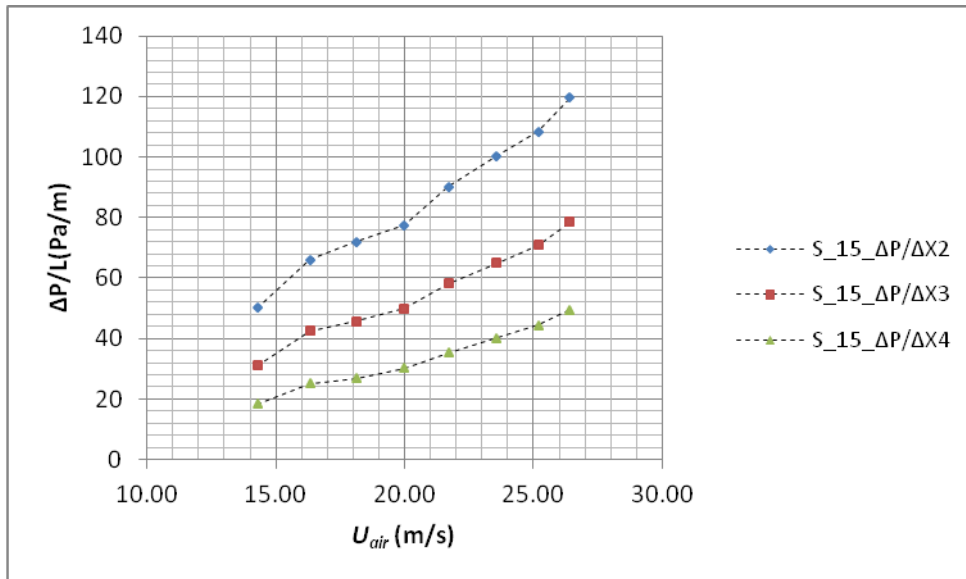


Figure 4.36  $\Delta P/L$  as a function of  $U_{air}$  for S particles with the range of  $0.65 < \dot{M}_p/\dot{M}_a < 23.74$

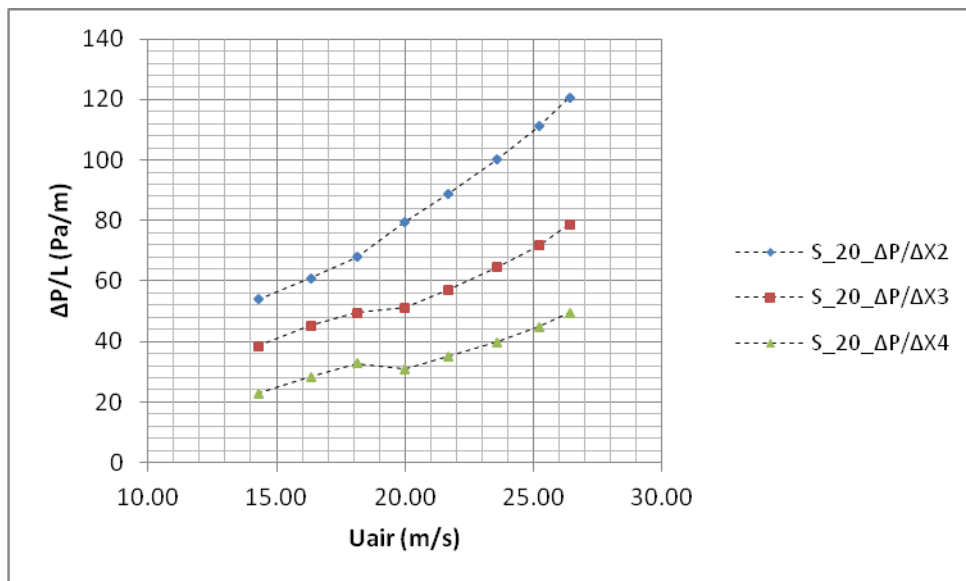


Figure 4.37  $\Delta P/L$  as a function of  $U_{air}$  for S particles with the range of  $1.08 < \dot{M}_p/\dot{M}_a < 29.14$

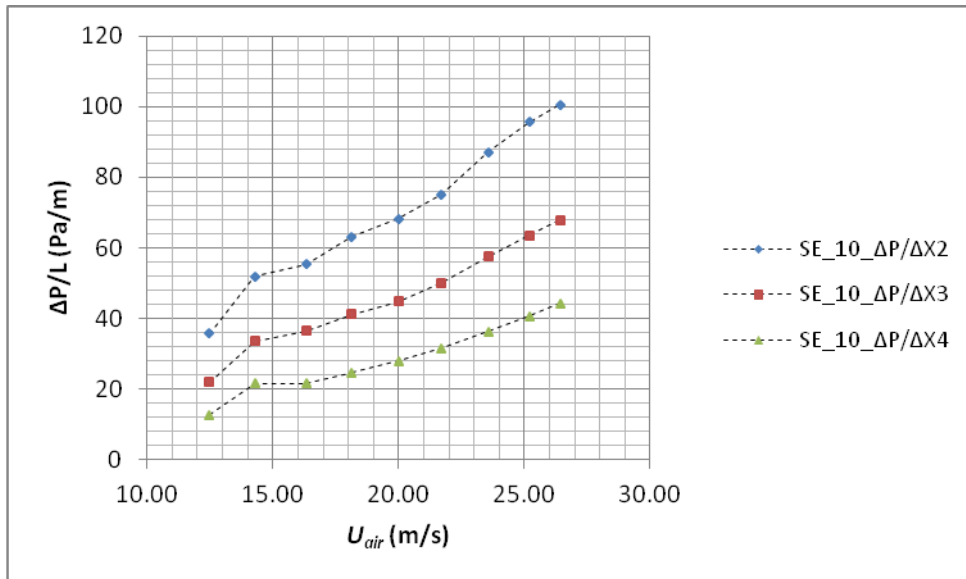


Figure 4.38  $\Delta P/L$  as a function of  $U_{air}$  for SE particles with the range of  $0.25 < \dot{M}_p/\dot{M}_a < 4.18$

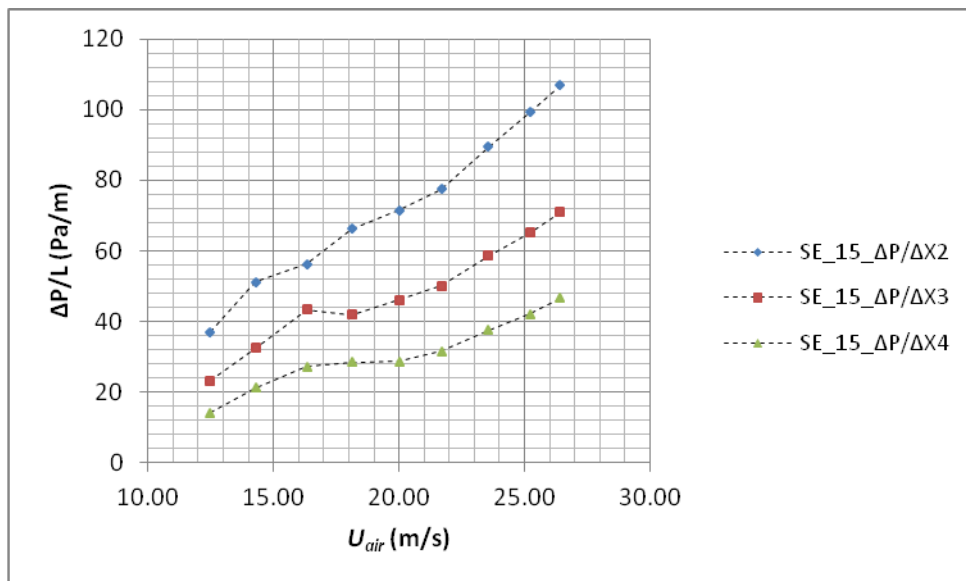


Figure 4.39  $\Delta P/L$  as a function of  $U_{air}$  for SE particles with the range of  $0.37 < \dot{M}_p/\dot{M}_a < 11.70$



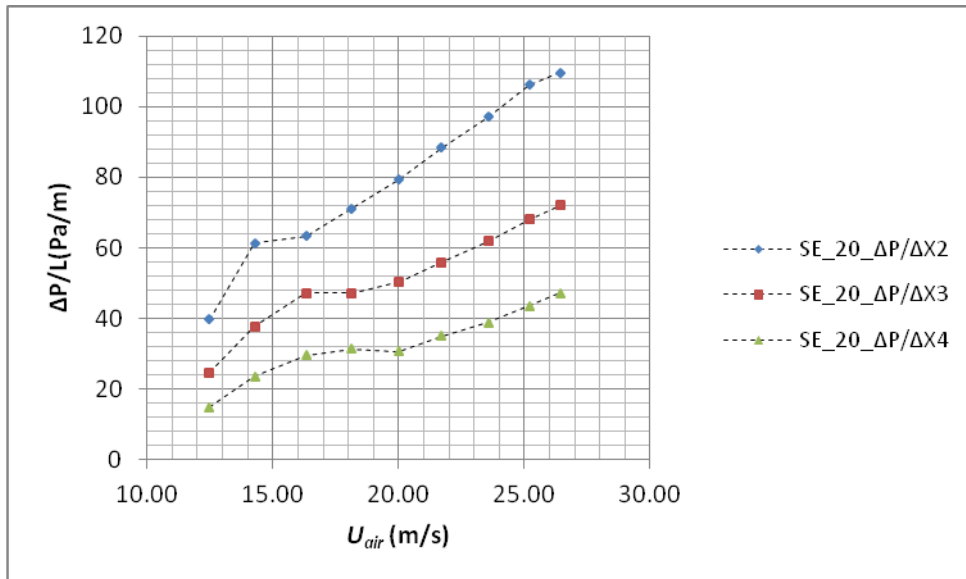


Figure 4.40  $\Delta P/L$  as a function of  $U_{air}$  for SE particles with the range of  $0.43 < \dot{M}_p/\dot{M}_a < 17.56$

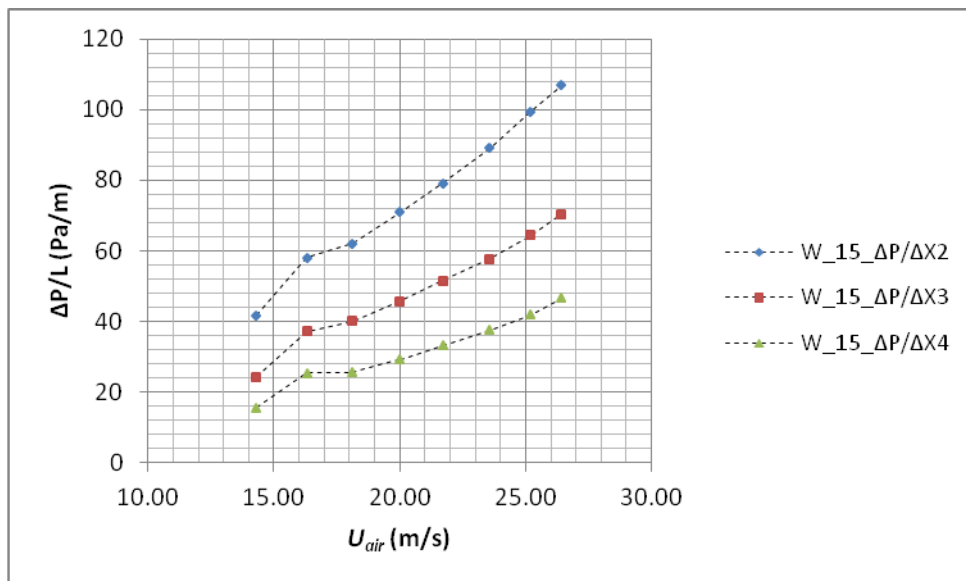


Figure 4.41  $\Delta P/L$  as a function of  $U_{air}$  for W particles with the range of  $0.38 < \dot{M}_p/\dot{M}_a < 9.47$

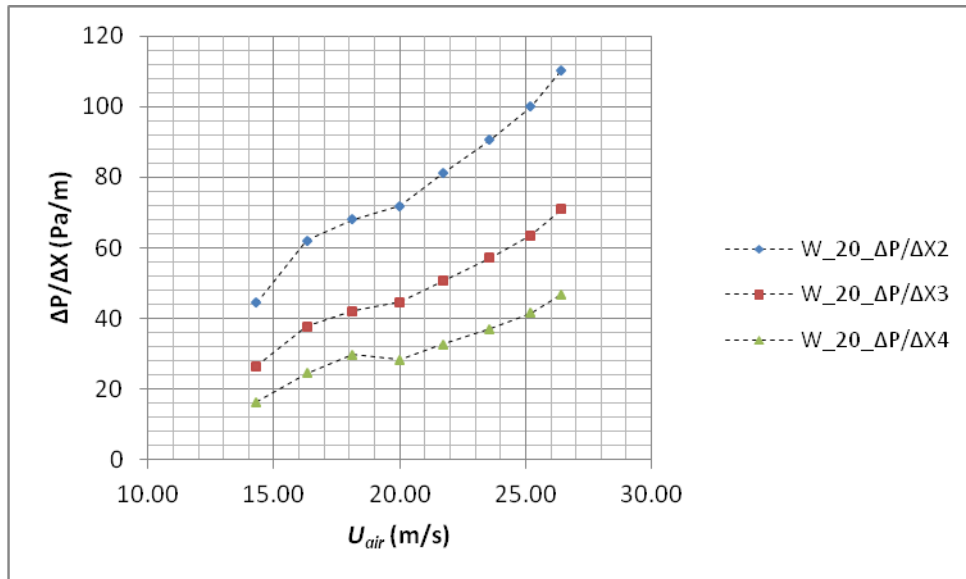


Figure 4.42  $\Delta P/L$  as a function of  $U_{air}$  for W particles with the range of  $0.43 < \dot{M}_p/\dot{M}_a < 12.20$

#### 4.6 Conclusion

The methodology for the determination of minimum fluidization velocities are presented for the vertical and horizontal test cases and also continuous conveying. In order to determine the flow modes,  $\Delta P$  and  $\Delta P/L$  are plotted as a function of  $U_{mf}$  for the covered particles in reference to visual observations of the flow field. Moreover, the effects of loose poured bulk densities and average diameters are investigated to determine the flow modes in pneumatic conveying systems.

## CHAPTER 5

### CORRELATIONS FOR FLOW MODE ANALYSIS

#### 5.1 Introduction

In this chapter, flow modes analyses are found through the variation of permeability with  $\dot{M}_p/\dot{M}_a$ . And also a correlation is performed in terms of fluidized dense phase at onset of fluidization.

#### 5.2 Flow Mode Analysis through Variation of Permeability, $\dot{M}_p/\dot{M}_a$

In this study three experimental test set-ups which are vertical, horizontal and continuous feeding are constructed to analyze flow modes. Minimum fluidization velocities, local static pressures, pressure drops and pressure gradients are used to determine flow modes. In this part, the relationship between permeability,  $P_f$  which is given in equation 2.2 and  $\dot{M}_p/\dot{M}_a$  that is also given in table 4.3 for continuous conveying are considered.

##### 5.2.1 Determination of Plug-Slug Flow Modes through Test Case 2 (Horizontal)

In figures 5.1, 5.2 and 5.3  $P_{f2}$ ,  $P_{f3}$  and  $P_{f4}$  values are shown as a function of  $\dot{M}_p/\dot{M}_a$  for SE, W and S in test case 2. SE, W and S particles are given with the range of  $1.11 \% < \dot{M}_p/\dot{M}_a < 42.62 \%$ ,  $0.47 \% < \dot{M}_p/\dot{M}_a < 8.78 \%$  and  $0.72 \% < \dot{M}_p/\dot{M}_a < 51.99 \%$  respectively. For the better considering, figure 5.4 is given for S, W and SE with the ranges of  $0.15 < P_{f2} < 0.26$ ,  $0.12 < P_{f2} < 0.21$  and  $0.12 < P_{f2} < 0.31$  respectively. It seems that for W particles which are  $2250 \mu\text{m}$ , are in the slug flow region because of high  $d_p$ . On the other hand S particles with  $d_p = 150 \mu\text{m}$  and SE particles with  $d_p = 700 \mu\text{m}$  start to flow in slug flow region, but when  $P_{f2} > 0.20$

$\text{m}^2/\text{Pa}\cdot\text{s}$  they are shown in the plug flow region. This flow characteristic is almost the same for  $P_{f3}$  and  $P_{f4}$  values as a function of  $\dot{M}_p/\dot{M}_a$  with the different ranges of  $P_f$  values. In figure 5.5, when the  $P_{f3} > 0.30 \text{ m}^2/\text{Pa}\cdot\text{s}$  particles are appeared in the plug flow region. And also in figure 5.6 for the flow mode analyze, when  $P_{f4} > 0.56 \text{ m}^2/\text{Pa}\cdot\text{s}$ , particles are shown in the plug flow region.

Slug flow and plug flow occurred in horizontal test case. Purple lines indicate slug flow region and the black line indicates plug flow region for the covered particles. Variation of  $P_f$  with  $\dot{M}_p/\dot{M}_a$  is such that two separate regions are defined. In the first region  $P_f$  varies linearly with  $\dot{M}_p/\dot{M}_a$  for  $\dot{M}_p/\dot{M}_a < 8 \%$ . In the second region  $P_f$  is almost independent of  $\dot{M}_p/\dot{M}_a$ . Therefore,  $P_f$  increases with increasing  $\dot{M}_p/\dot{M}_a$  in first region and  $P_f$  retains almost at constant value for the second region.

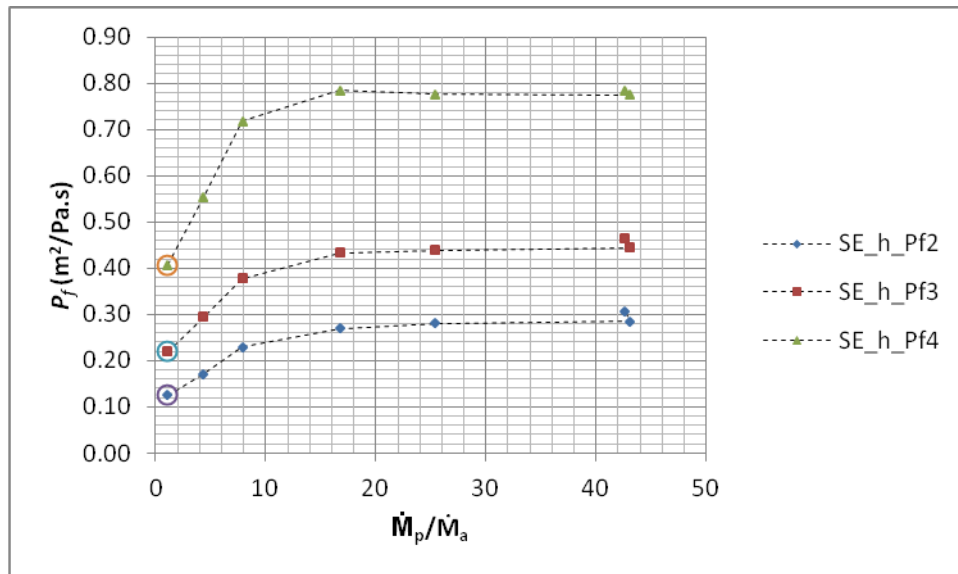


Figure 5.1  $P_f$  values as a function of  $\dot{M}_p/\dot{M}_a$  for SE in test case 2

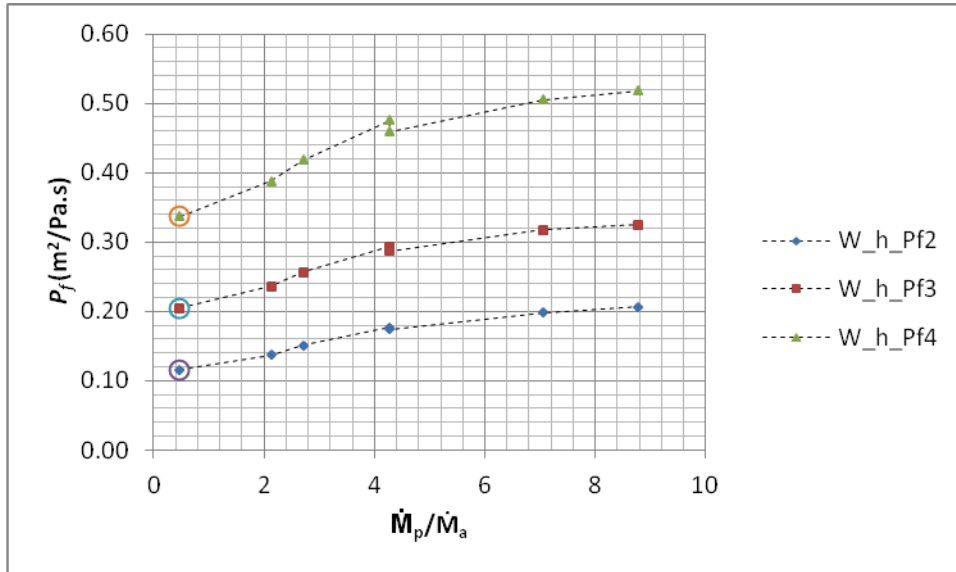


Figure 5.2  $P_f$  values as a function of  $\dot{M}_p/\dot{M}_a$  for W in test case 2

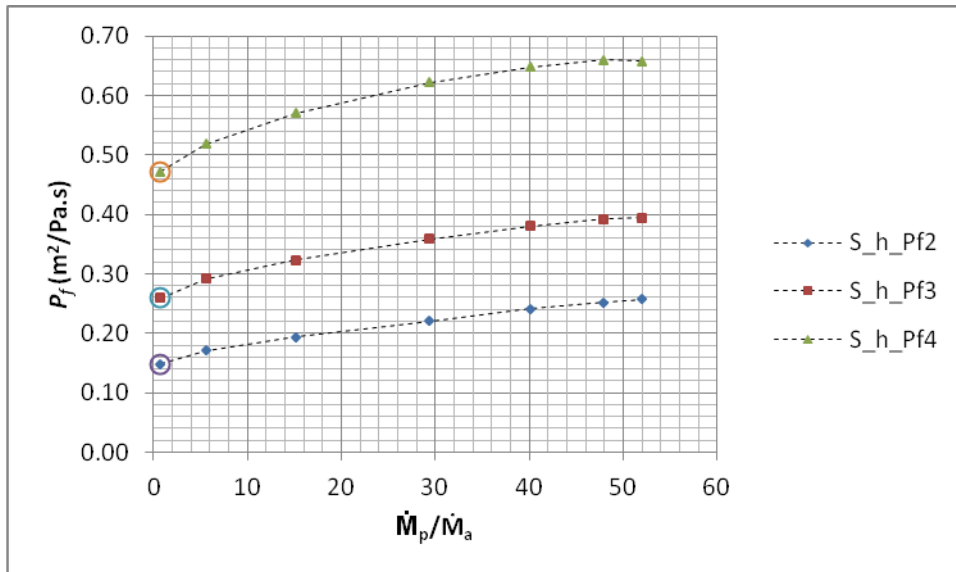


Figure 5.3  $P_f$  values as a function of  $\dot{M}_p/\dot{M}_a$  for S in test case 2

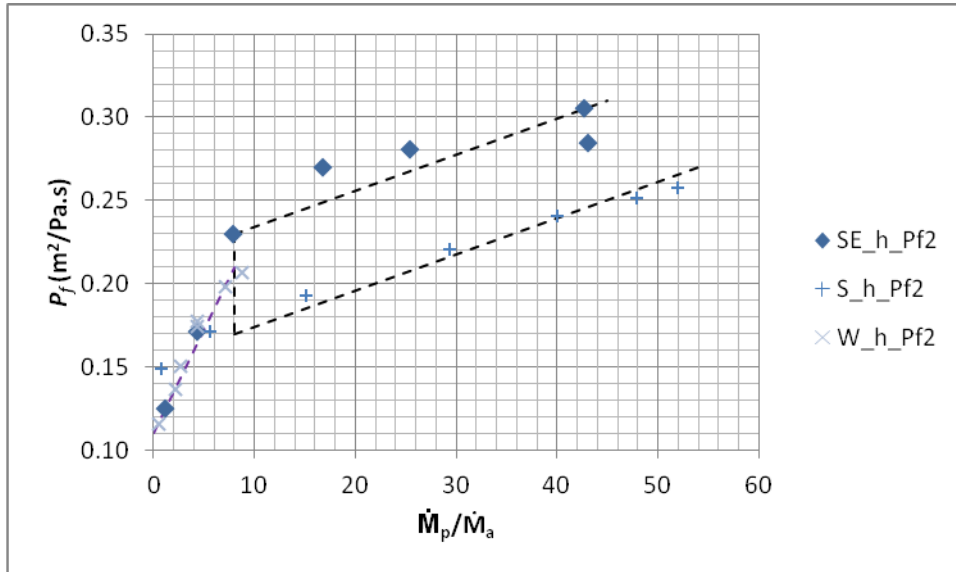


Figure 5.4  $P_{f2}$  as a function of  $\dot{M}_p/\dot{M}_a$  for S, SE and W in test case 2

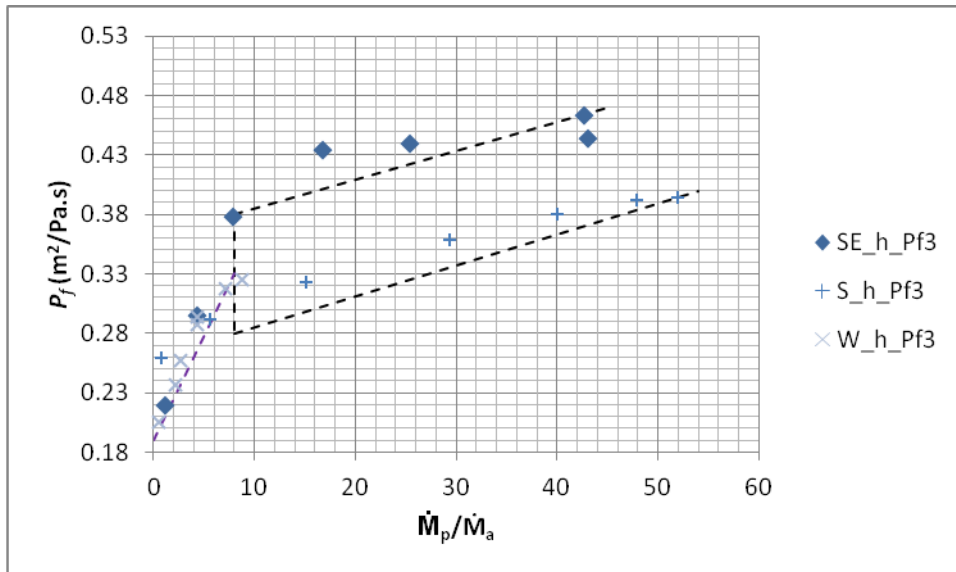


Figure 5.5  $P_{f3}$  as a function of  $\dot{M}_p/\dot{M}_a$  for S, SE and W in test case 2

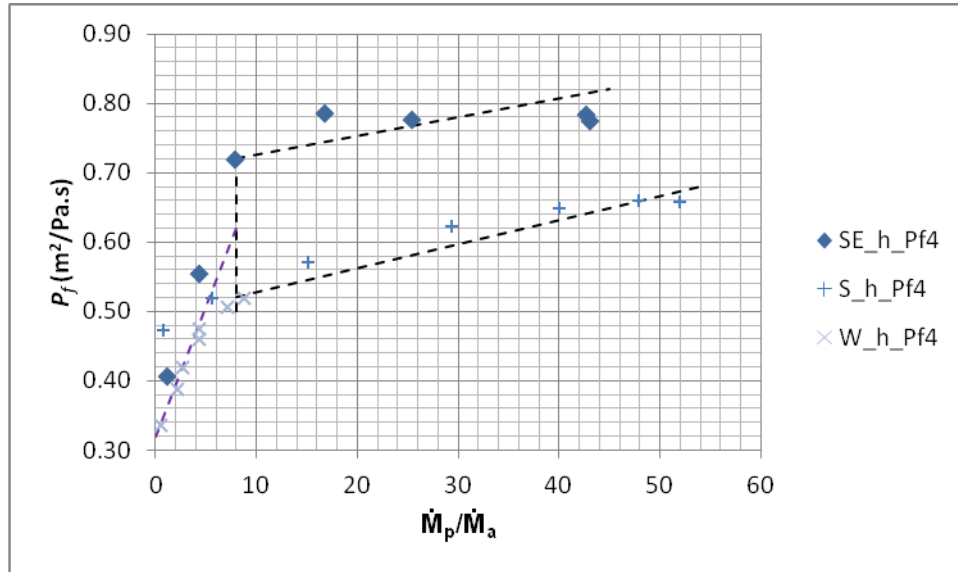


Figure 5.6  $P_{f4}$  as a function of  $\dot{M}_p/\dot{M}_a$  for S, SE and W in test case 2

### 5.2.2 Determination of Plug Flow and Dilute Phase through Continuous Conveying

In continuous conveying test case, plug flow and dilute phase are observed visually. Three particles S, SE and W are considered with the use of particle feeder in different  $\dot{M}_p/\dot{M}_a$  values.  $\dot{M}_p/\dot{M}_a$  ranges are given in table 4.2 in the previous chapter. Figures from 5.7 to 5.14,  $P_f$  values are given as a function of  $\dot{M}_p/\dot{M}_a$  values for the SE, W and S particles. In these figures, observed flow modes which are plug flow and dilute phase are clearly shown. For the SE particles for 10 mm, 15 mm and 20 mm orifices as shown in figures from 5.7 to 5.9,  $P_f$  decreases with increasing  $\dot{M}_p/\dot{M}_a$  values until the ranges of  $\dot{M}_p/\dot{M}_a < 2.4 \%$ ,  $\dot{M}_p/\dot{M}_a < 5.8 \%$  and  $\dot{M}_p/\dot{M}_a < 6.8 \%$  respectively which shows the plug flow region. Then  $P_f$  increases with respect to  $\dot{M}_p/\dot{M}_a > 2.4 \%$ ,  $\dot{M}_p/\dot{M}_a > 5.8 \%$  and  $\dot{M}_p/\dot{M}_a > 6.8 \%$  respectively which shows the dilute phase region. Plug flow region and dilute phase region are also clearly shown for W and S particles in figures from 5.10 to 5.14.

Figures from 5.15 to 5.17 are given to analyze flow modes with respect to  $P_f$  values as a function of  $\dot{M}_p/\dot{M}_a$ . In addition to this, particle characteristics can be considered in the same figures for the same  $P_f$ , also black lines are indicated that the

limit of plug flow region and dilute phase region for the covered particles.  $P_{f2}$  values of SE, W and S are given in figure 5.15 with the ranges of  $0.23 \text{ m}^2/\text{Pa.s} < P_{f2} < 0.35 \text{ m}^2/\text{Pa.s}$ ,  $0.24 \text{ m}^2/\text{Pa.s} < P_{f2} < 0.34 \text{ m}^2/\text{Pa.s}$  and  $0.22 \text{ m}^2/\text{Pa.s} < P_{f2} < 0.29 \text{ m}^2/\text{Pa.s}$  respectively. When the  $P_{f2} > 0.31 \text{ m}^2/\text{Pa.s}$ ,  $P_{f2} > 0.32 \text{ m}^2/\text{Pa.s}$  and  $P_{f2} > 0.27 \text{ m}^2/\text{Pa.s}$  for SE, W and S respectively flow mode is changed from dilute phase to plug flow. The limit of  $P_{f2}$  for SE is bigger than that of S although the  $\rho_{blp}$  of S ( $2400 \text{ kg/m}^3$ ) is greater than that of SE ( $850 \text{ kg/m}^3$ ). So that, the plug flow limits for each particle are indicated that the particle size,  $d_p$  is dominant in comparison with the loose poured bulk density,  $\rho_{blp}$ . This approach is valid for the  $P_{f3}$  and  $P_{f4}$  values as shown in figures 5.16 and 5.17. The limit of  $P_{f3}$  and  $P_{f4}$  values are given as  $P_{f3} > 0.51 \text{ m}^2/\text{Pa.s}$ ,  $P_{f3} > 0.41 \text{ m}^2/\text{Pa.s}$  and  $P_{f3} > 0.54 \text{ m}^2/\text{Pa.s}$ ,  $P_{f4} > 0.84 \text{ m}^2/\text{Pa.s}$ ,  $P_{f4} > 0.67 \text{ m}^2/\text{Pa.s}$  and  $P_{f4} > 0.87 \text{ m}^2/\text{Pa.s}$  for SE, S and W respectively.

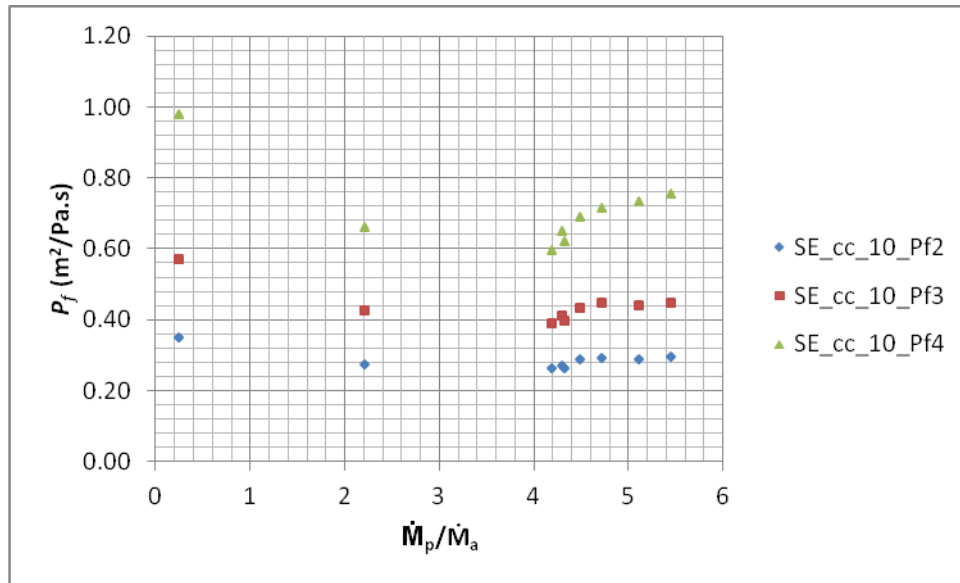


Figure 5.7  $P_f$  values as a function of  $\dot{M}_p/\dot{M}_a$  for SE with 10 mm orifice in continuous conveying



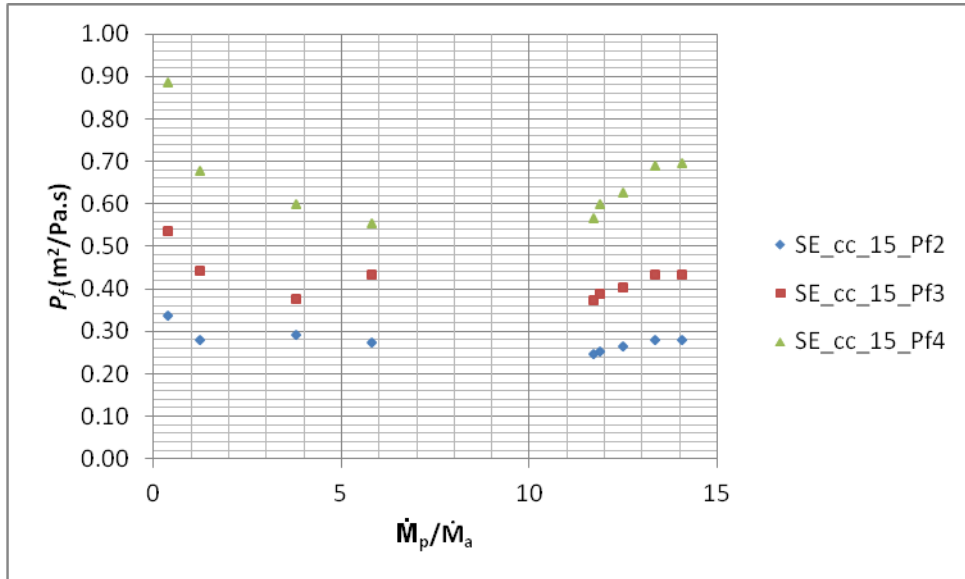


Figure 5.8  $P_f$  values as a function of  $\dot{M}_p/\dot{M}_a$  for SE with 15 mm orifice in continuous conveying

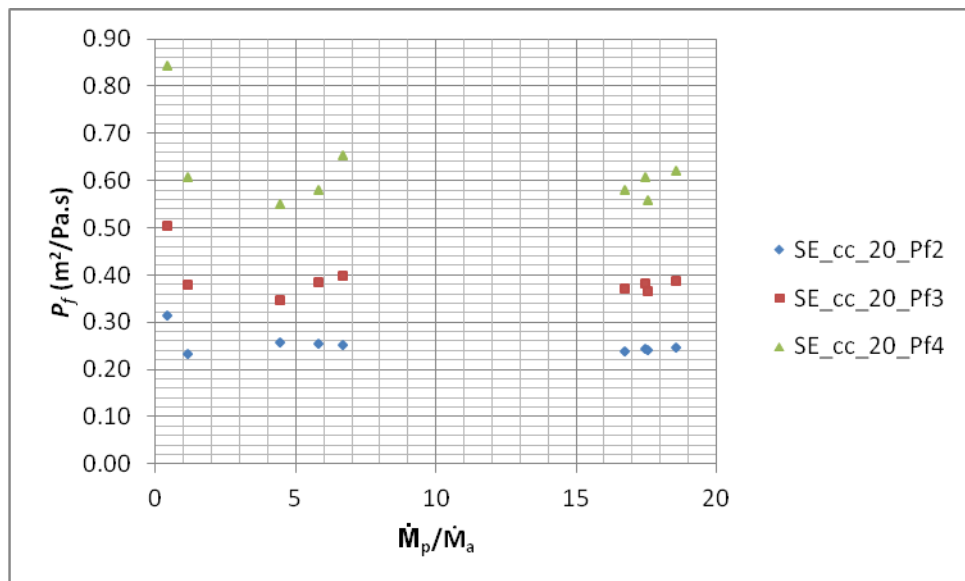


Figure 5.9  $P_f$  values as a function of  $\dot{M}_p/\dot{M}_a$  for SE with 20 mm orifice in continuous conveying

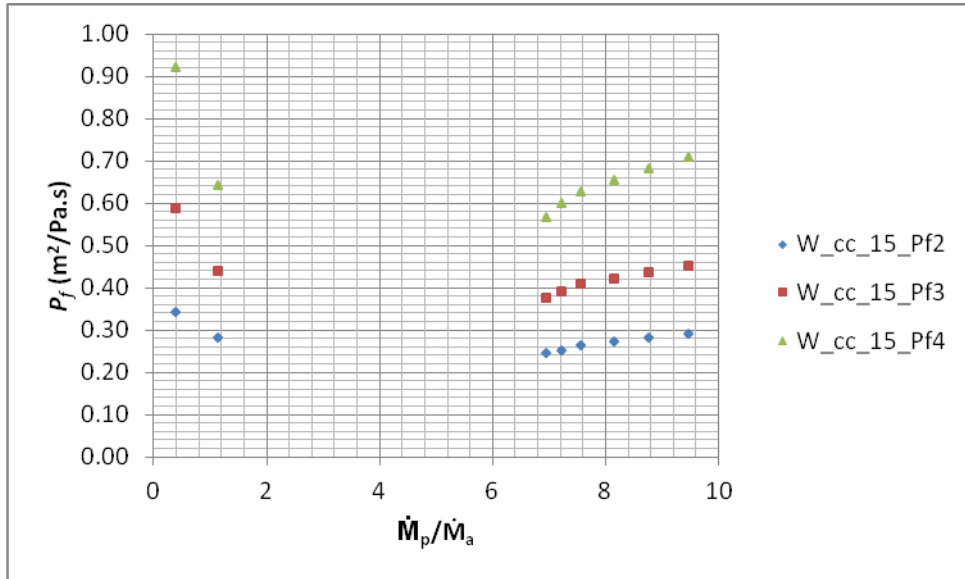


Figure 5.10  $P_f$  values as a function of  $\dot{M}_p/\dot{M}_a$  for W with 15 mm orifice in continuous conveying

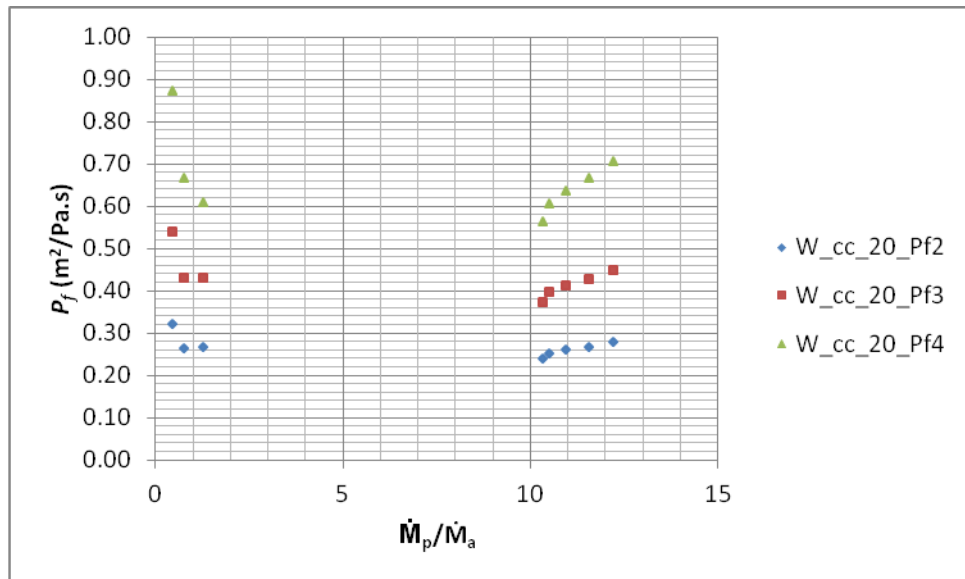


Figure 5.11  $P_f$  values as a function of  $\dot{M}_p/\dot{M}_a$  for W with 20 mm orifice in continuous conveying

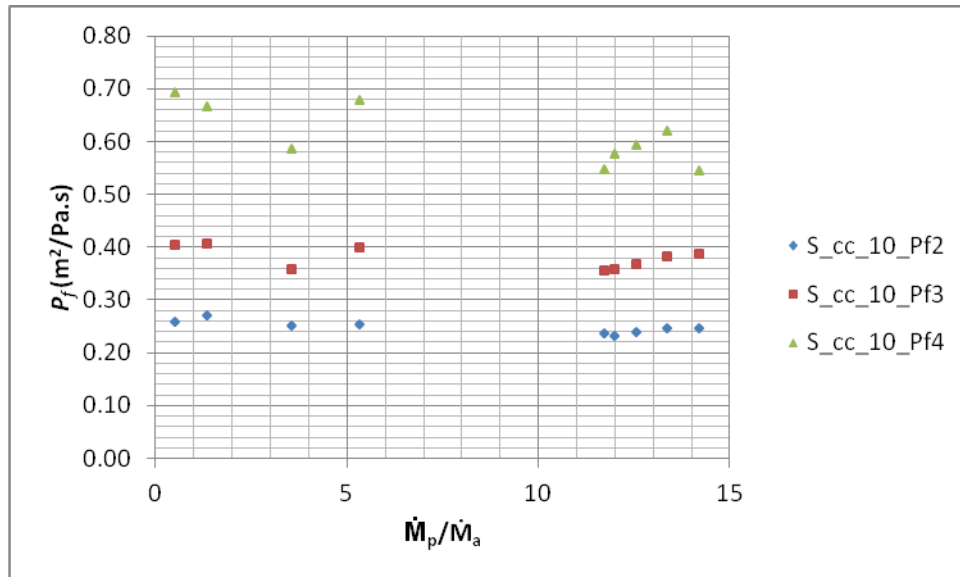


Figure 5.12  $P_f$  values as a function of  $\dot{M}_p/\dot{M}_a$  for S with 10 mm orifice in continuous conveying

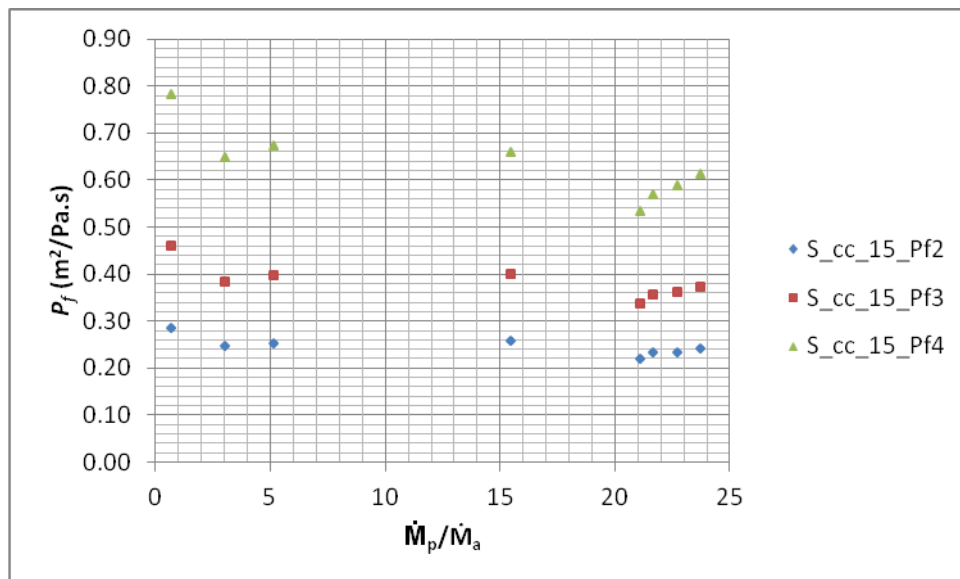


Figure 5.13  $P_f$  values as a function of  $\dot{M}_p/\dot{M}_a$  for S with 15 mm orifice in continuous conveying

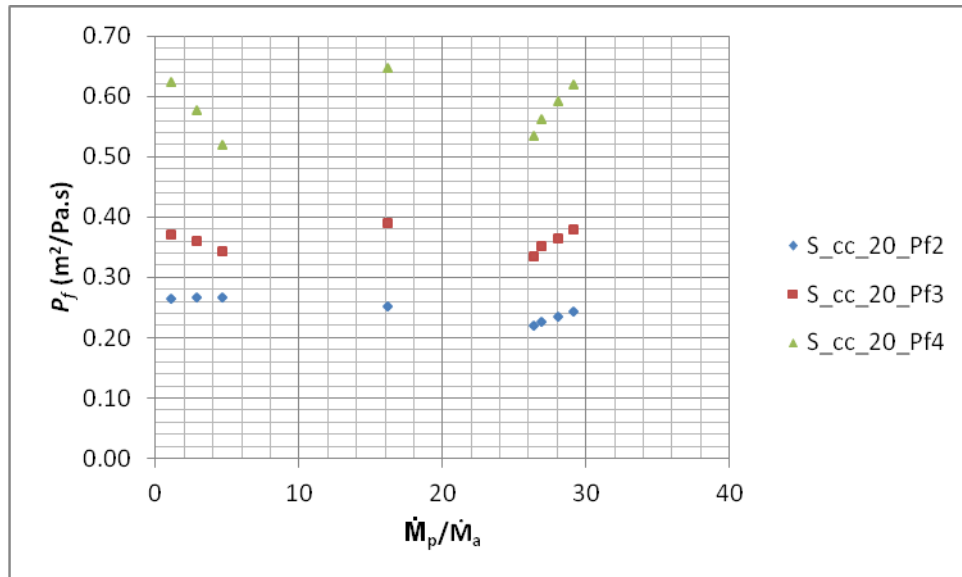


Figure 5.14  $P_f$  values as a function of  $\dot{M}_p/\dot{M}_a$  for S with 20 mm orifice in continuous conveying

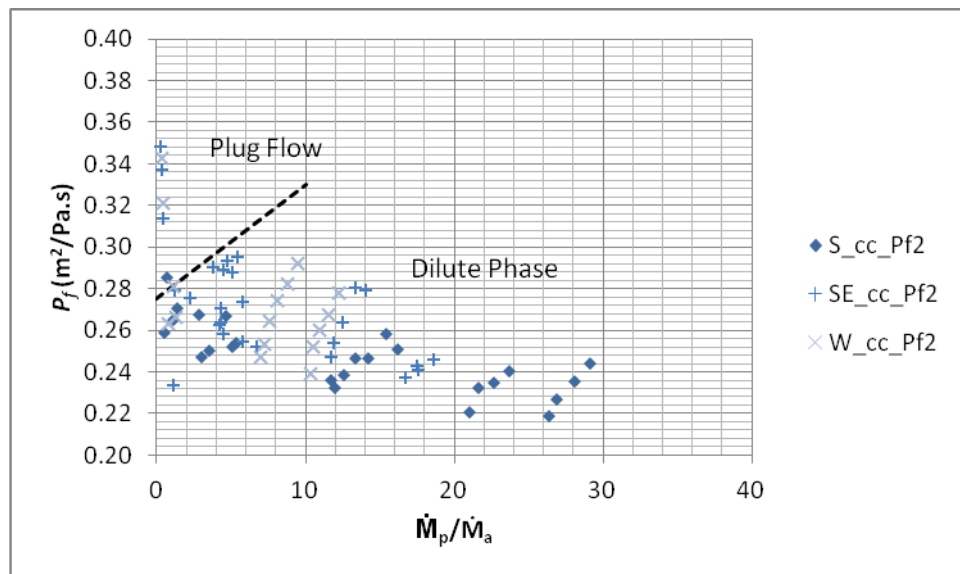


Figure 5.15  $P_{f2}$  as a function of  $\dot{M}_p/\dot{M}_a$  for SE, W and S in continuous conveying

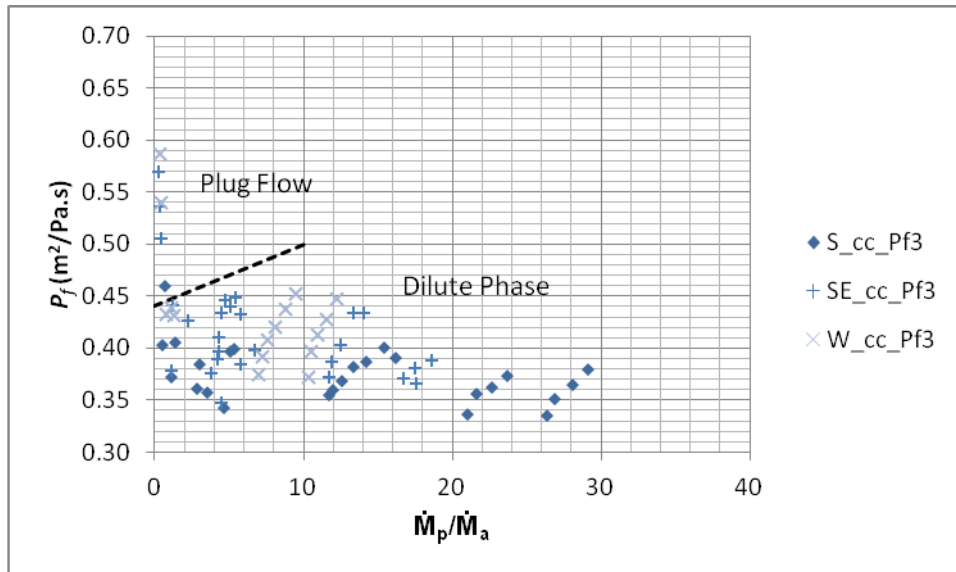


Figure 5.16  $P_{f3}$  as a function of  $\dot{M}_p/\dot{M}_a$  for SE, W and S in continuous conveying

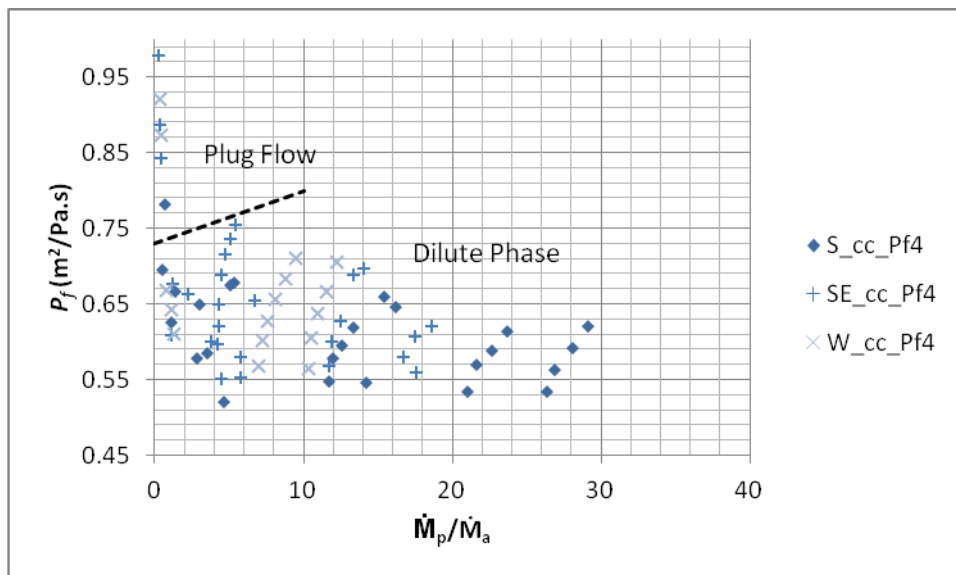


Figure 5.17  $P_{f4}$  as a function of  $\dot{M}_p/\dot{M}_a$  for SE, W and S in continuous conveying

### 5.2.3 Determination of Unstable Zone and Fluidized Dense Phase through Test Case 1 (Vertical)

In vertical test case, unstable zone and fluidized dense phase region are shown with visual observations. In figure 5.18  $P_{f\text{mf}}$  (permeability of minimum fluidization state) is given as a function of  $U_{mf}$  to determine the flow modes for the covered particles SE, Z1, Z2, S, PE, W and T. The fluidized dense phase is shown for this figure with the ranges of  $0.0052 \text{ m}^2/\text{Pa.s} < P_{f\text{mf}} < 0.0963 \text{ m}^2/\text{Pa.s}$ . However, the particle characteristics are not clearly shown in figure 5.18. Therefore, the particle influences are shown in figures from 5.19 to 5.25 for determination of the region from the unstable zone to fluidized dense phase. The loose pored bulk density  $\rho_{blp}$  is dominant in comparison to average particle diameter  $d_p$  in vertical test case, the reason of this case was expressed. in the previous chapter.

It can be stated that the  $P_{f\text{mf}}$  values of S should be minimum due to its higher  $\rho_{blp}$  value which is  $2400 \text{ kg/m}^3$ . In the same manner,  $P_{f\text{mf}}$  values of T should be maximum because of the minimum  $\rho_{blp}$  values of  $200 \text{ kg/m}^3$  when compared with others.  $P_{f\text{mf}}$  of S is,  $0.0052 \text{ m}^2/\text{Pa.s}$  which is the minimum  $P_{f\text{mf}}$  value as can be seen in figure 5.22. The maximum value of  $P_{f\text{mf}}$  for T is seen as  $0.0963 \text{ m}^2/\text{Pa.s}$  which is shown in figure 5.25. It is then deduced that the value of  $P_{f\text{mf}}$  decreases when the value of  $\rho_{blp}$  increases.

Here, it is important to investigate the interactive influences of  $\rho_{blp}$  and  $d_p$  together. For this purpose, some trial and error procedures are performed. As a result of them the function of  $\rho_{blp}^2 \cdot d_p^{2/3}$  is found to be appropriate one. In order to have better prediction for determination of flow modes in vertical test case at L10, L30 and L50, figures from 5.26 to 5.28 are plotted with procedure trial error as  $P_{f\text{mf}}$  versus  $\rho_{blp}^2 \cdot d_p^{2/3} \cdot 10^{-3}$ .

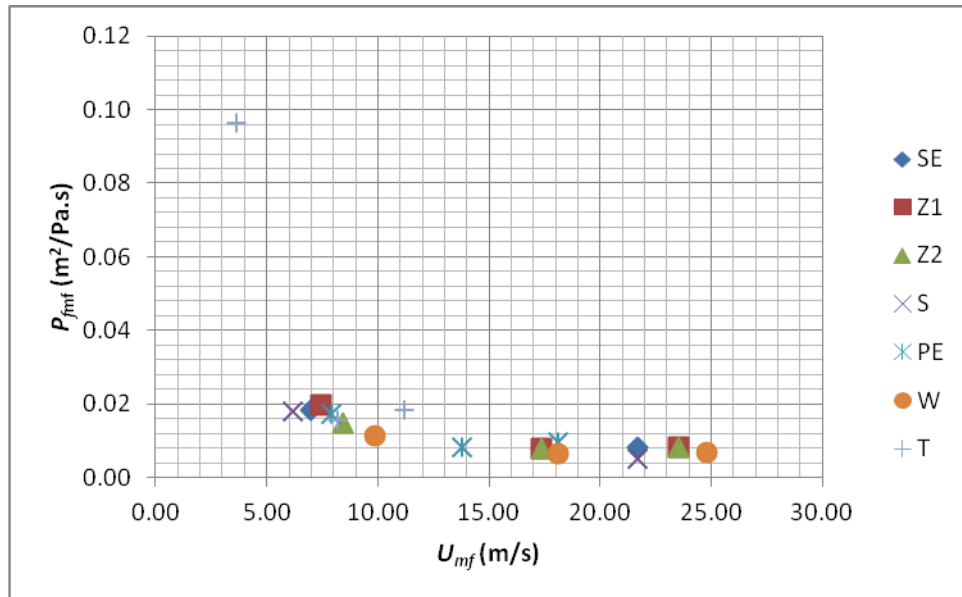


Figure 5.18  $P_{f_{mf}}$  values as a function of  $U_{mf}$  in test case 1

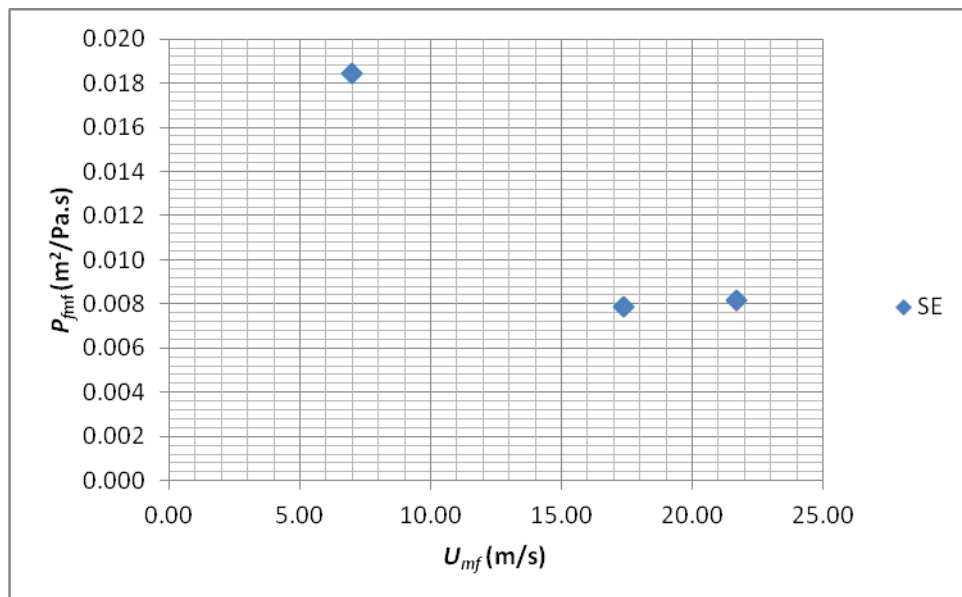


Figure 5.19  $P_{f_{mf}}$  values as a function of  $U_{mf}$  for SE in test case 1

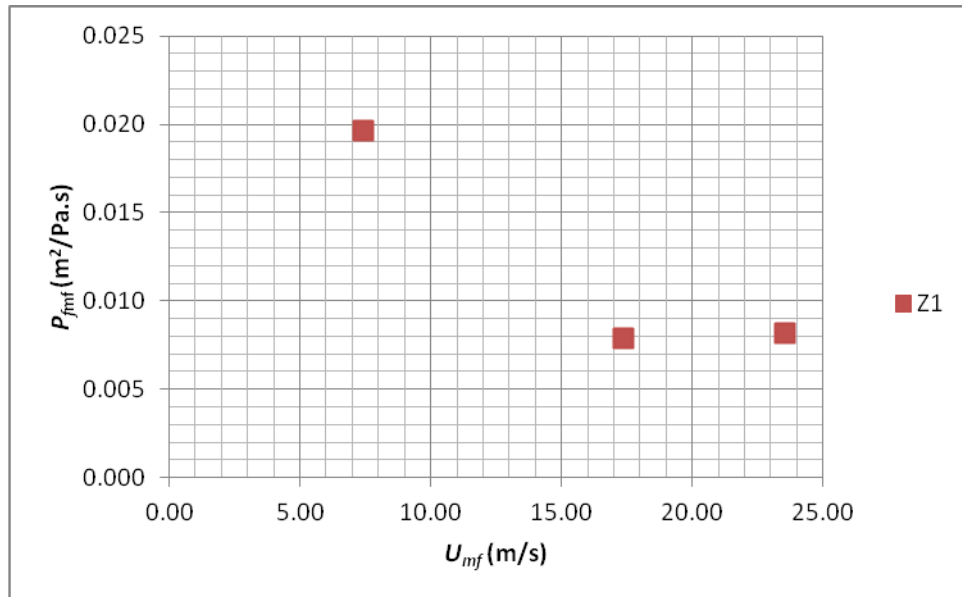


Figure 5.20  $P_{f_{mf}}$  values as a function of  $U_{mf}$  for Z1 in test case 1

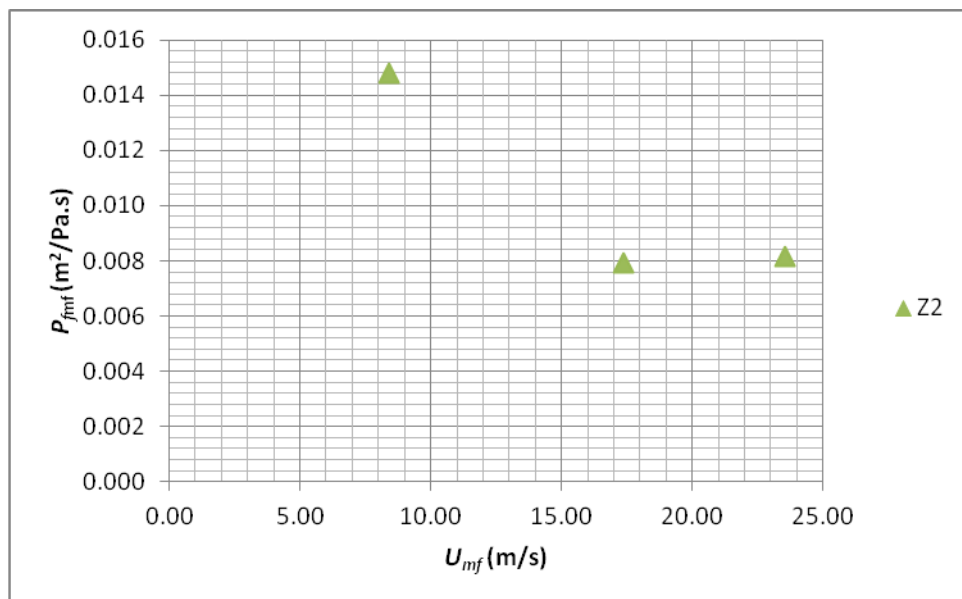


Figure 5.21  $P_{f_{mf}}$  values as a function of  $U_{mf}$  for Z2 in test case 1



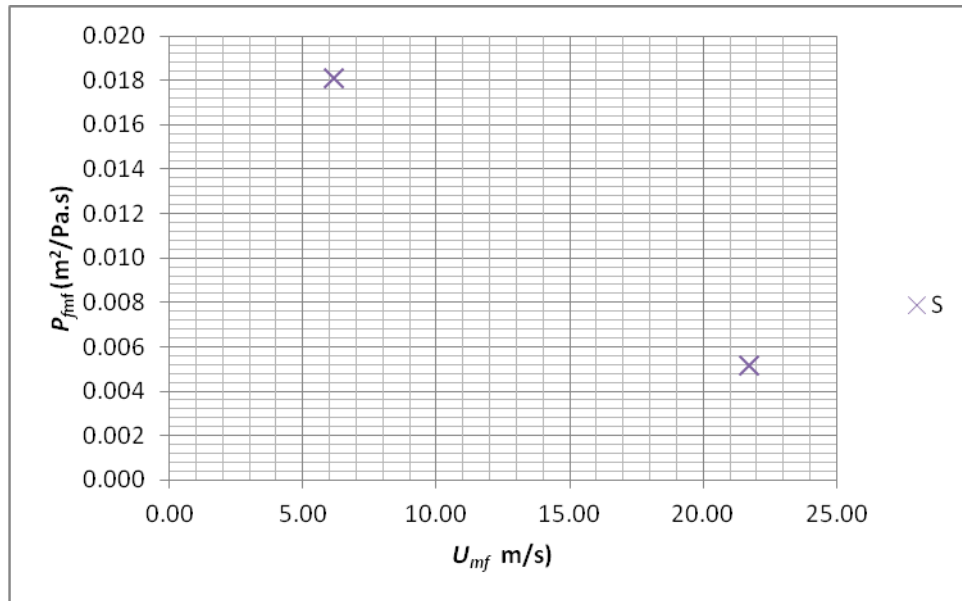


Figure 5.22  $P_{f_{mf}}$  values as a function of  $U_{mf}$  for S in test case 1

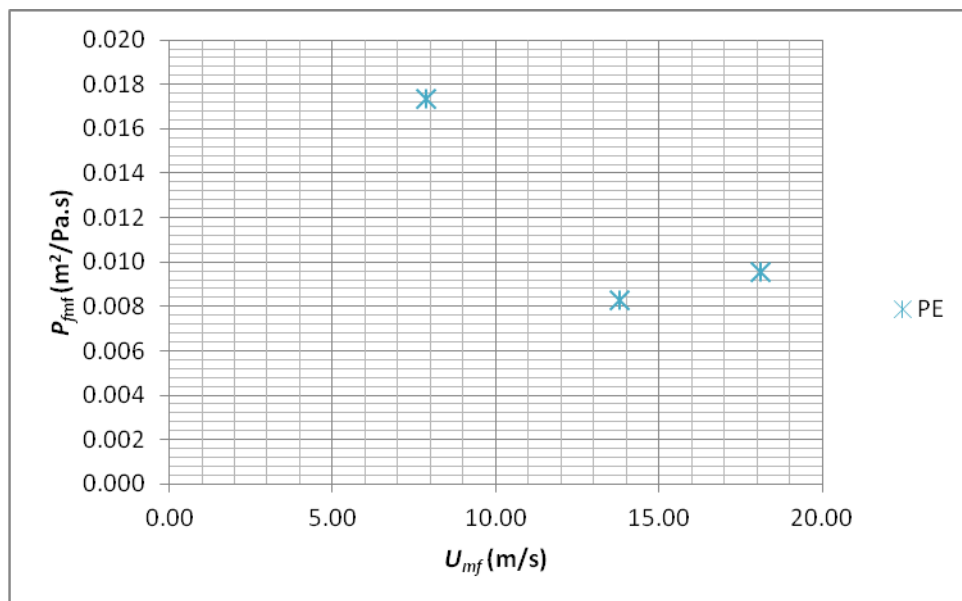


Figure 5.23  $P_{f_{mf}}$  values as a function of  $U_{mf}$  for PE in test case 1

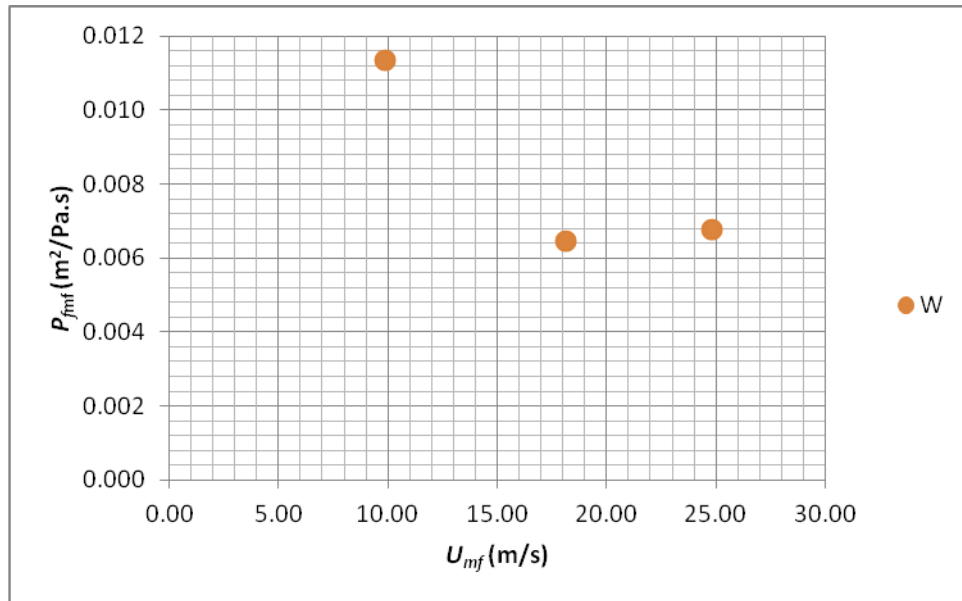


Figure 5.24  $P_{f_{mf}}$  values as a function of  $U_{mf}$  for W in test case 1

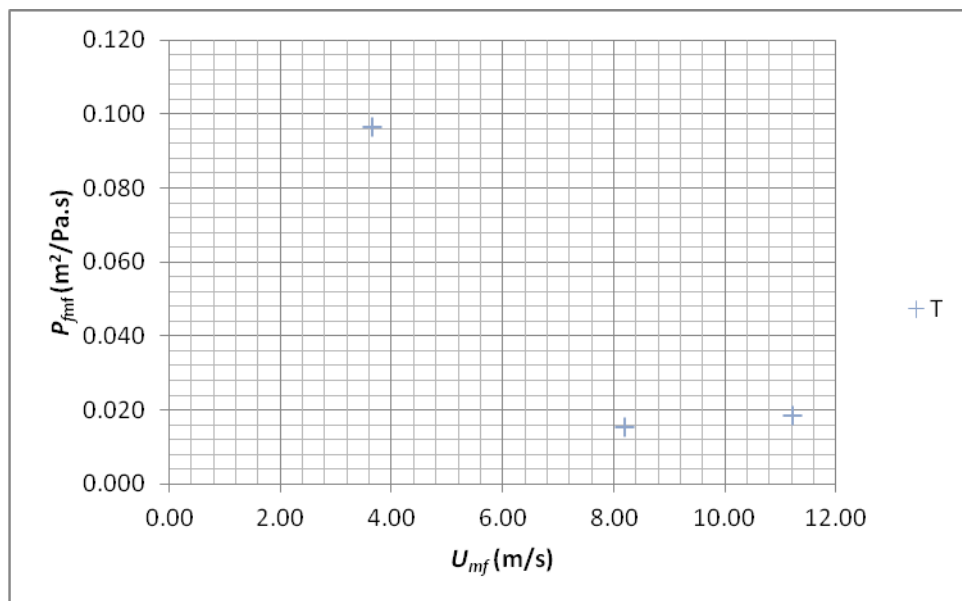


Figure 5.25  $P_{f_{mf}}$  values as a function of  $U_{mf}$  for T in test case 1

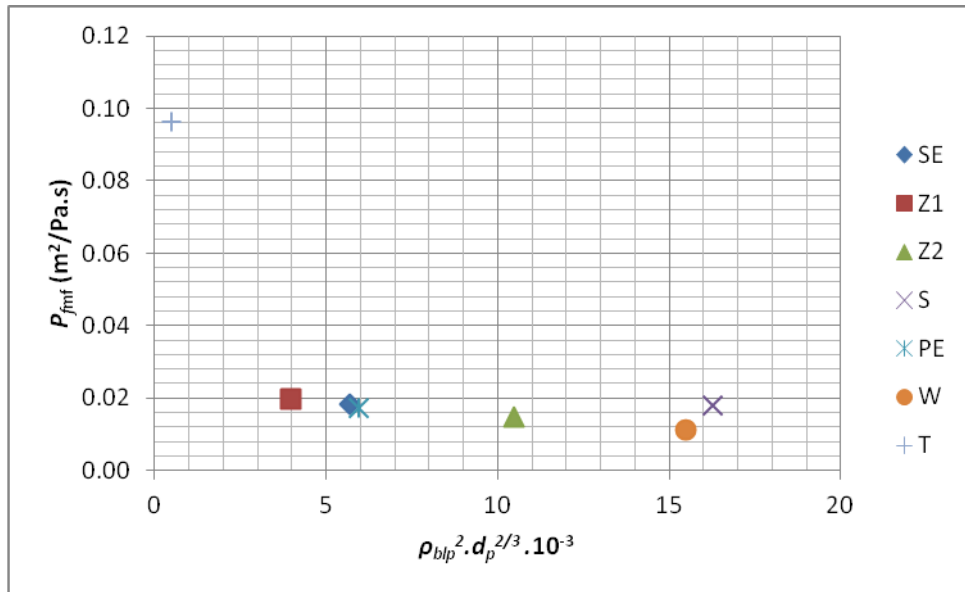


Figure 5.26  $P_{fmf}$  values as a function of  $\rho_{blp}$  and  $d_p$  for covered particles at L10 in test case 1

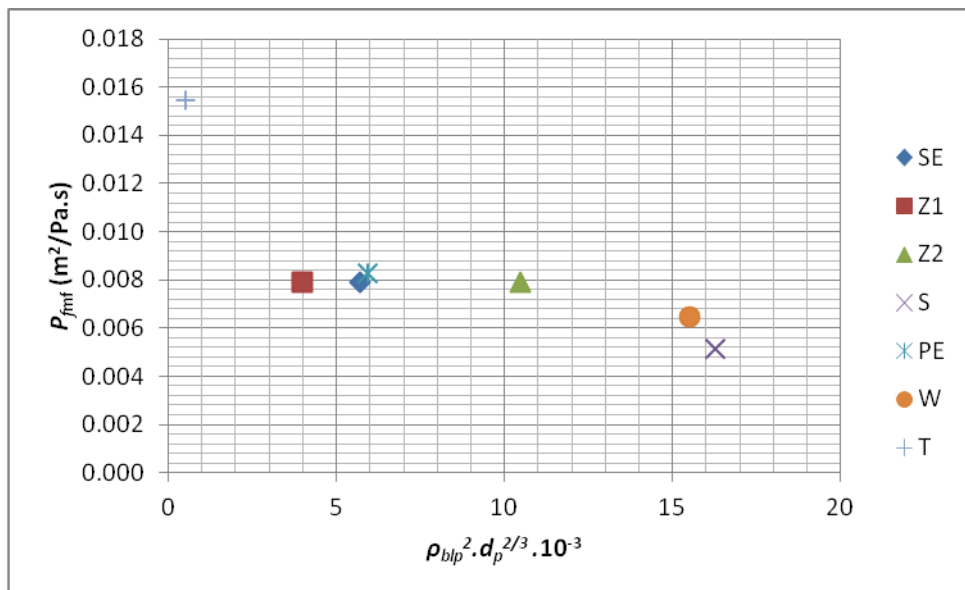


Figure 5.27  $P_{fmf}$  values as a function of  $\rho_{blp}$  and  $d_p$  for covered particles at L30 in test case 1

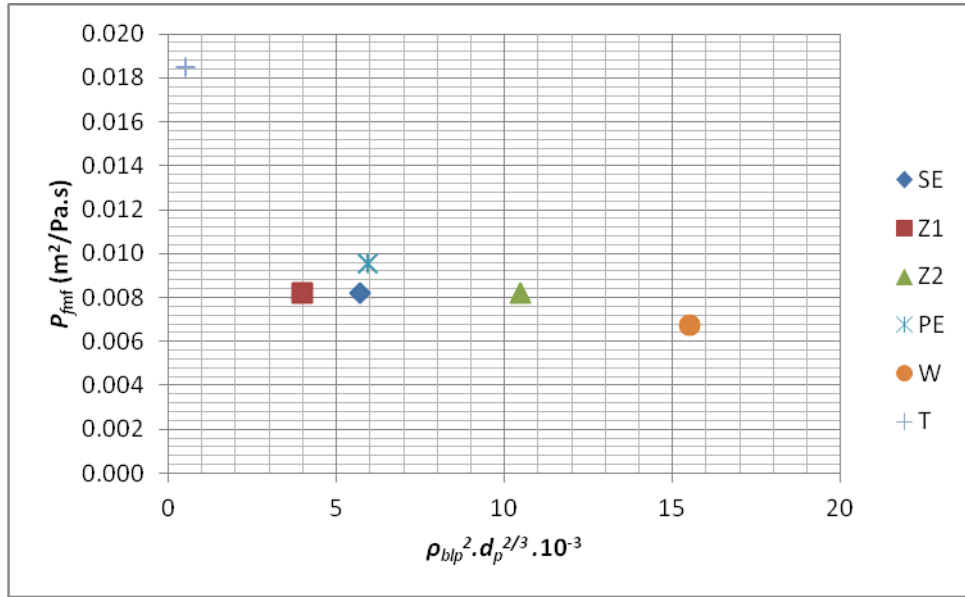


Figure 5.28  $P_{f_{mf}}$  values as a function of  $\rho_{blp}$  and  $d_p$  for covered particles at L50 in test case 1

### 5.3 A Correlation Study in terms of Fluidized Dense Phase at Onset of Fluidization

The normalized pressure of  $\Delta P_{bed}/P_{dyn}$  is considered with respect to normalized velocity of  $U_{air} / U_{mf}$  for the bed lengths of L10, L30 and L50 as shown in figures 5.29 – 5.31. The observed flow mode is transition from the unstable zone to fluidized dense phase in vertical test case.  $\Delta P_{bed}/P_{dyn}$  with the ranges of  $0.06 < \Delta P_{bed}/P_{dyn} < 1.83$  and  $U_{air} / U_{mf}$  with the ranges of  $0.2 < U_{air} / U_{mf} < 7.23$  are given in these figures.  $U_{air}$  is the superficial air velocity in acrylic glass pipe,  $U_{mf}$  is the minimum fluidization velocity of particles in test case 1,  $\Delta P_{bed}$  is the pressure difference between local static pressures  $P_1$  and  $P_2$  and  $\Delta P_{dyn}$  is the dynamic pressure related with  $U_{air}$  in the pipe.

In all figures, it is found that the flow mode is the unstable zone for  $U_{air} / U_{mf} < 1$ . For  $U_{air} / U_{mf} > 1$ , the flow mode is named as fluidized dense phase. Moreover the value of  $\Delta P_{bed}/P_{dyn}$  decreases when  $U_{air} / U_{mf}$  increases. However, the

relationship between  $\Delta P_{bed}/P_{dyn}$  and  $U_{air} / U_{mf}$  for L30 and L50 are a bit of different than that for L10. Due to the short bed length at L10, the flow becomes quickly fluidized dense phase. This means that for fluidized dense phase is occurred for low velocities in the range of  $3.65 \text{ m/s} < U_{mf} < 9.89 \text{ m/s}$  at L10 which is given in figure 5.29. But, the flow becomes fluidized dense phase at higher velocities in the range of  $8.20 \text{ m/s} < U_{mf} < 21.70 \text{ m/s}$  at L30 and  $11.22 \text{ m/s} < U_{mf} < 24.83 \text{ m/s}$  at L50 as can be seen in figures 5.30 and 5.31 respectively.

#### 5.4 Conclusion

All the results are considered to determine flow modes for the test case 1, test case 2 and continuous conveying. Unstable zone and start to fluidization dense phase occurred as shown from figures 5.29 to figure 5.31 for the test case 1. Slug flow and plug flow regions are determined for the test case 2 figures from 5.4 to 5.6. In continuous conveying, plug flow and dilute phase limit is investigated and indicated in figures from 5.15 to 5.17.

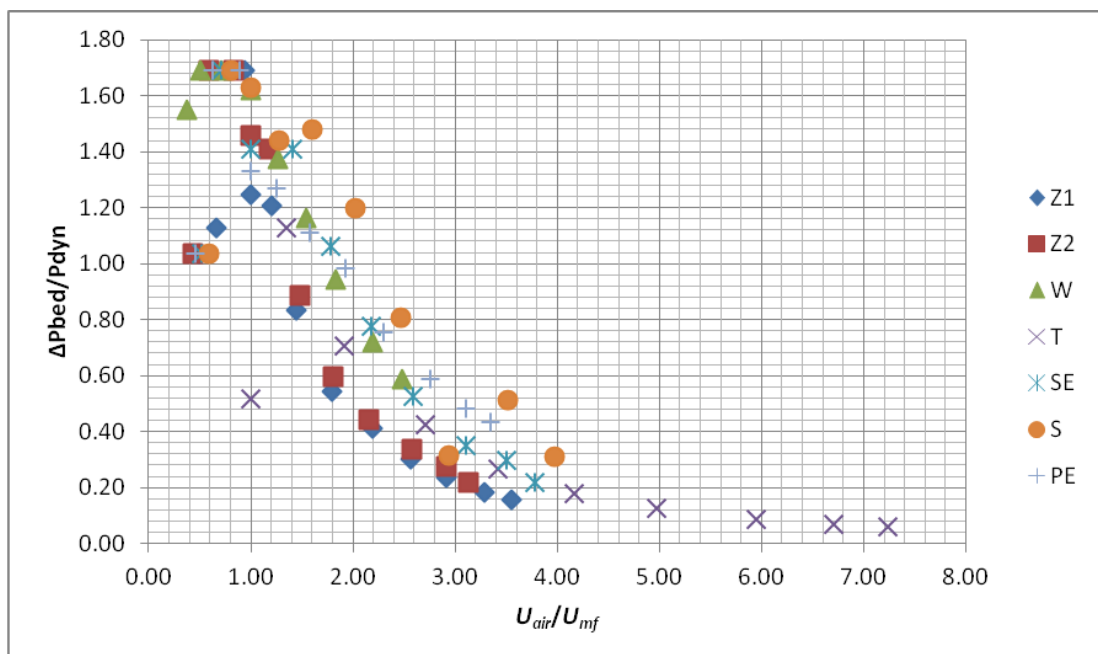


Figure 5.29 Normalized pressure and velocity values for L10

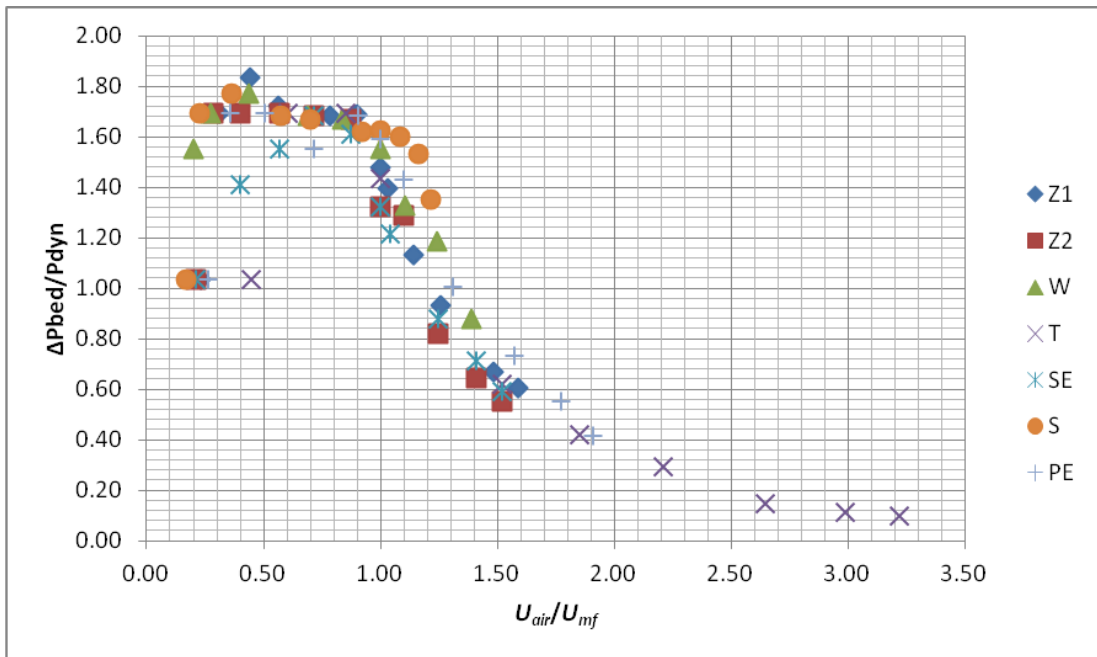


Figure 5.30 Normalized pressure and velocity values for L30

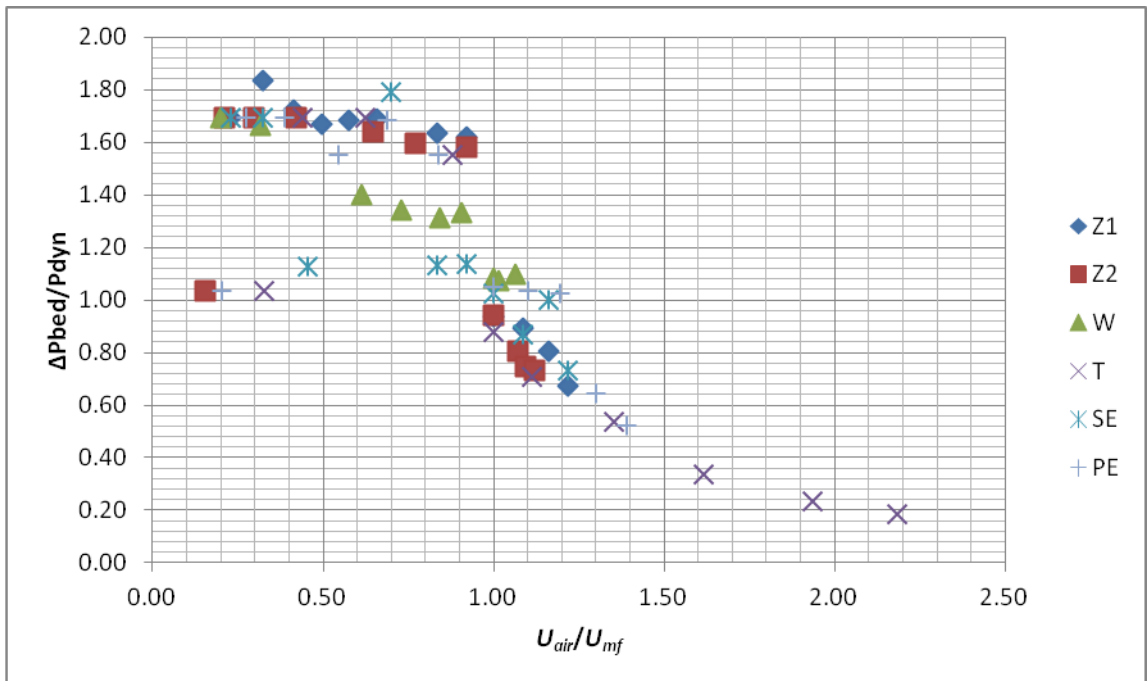


Figure 5.31 Normalized pressure and velocity values for L50

## CHAPTER 6

### CONCLUSION AND SUGGESTIONS FOR FURTHER INVESTIGATIONS

In this study three different cases which are vertical (test case 1), horizontal (test case 2) and continuous conveying test case are used to determine flow modes. Seven solid particles which are SE, W, S, T, PE, Z1 and Z2 with the range of  $200 \text{ kg/m}^3 < \rho_{blp} < 2400 \text{ kg/m}^3$  and  $150 \text{ }\mu\text{m} < d_p < 2750 \text{ }\mu\text{m}$  are used in these three cases. The used parameters are calculated with the ranges of  $17714 < \text{Re}_{mf} < 147600$ ,  $3.65 \text{ m/s} < U_{mf} < 24.83 \text{ m/s}$ ,  $0.0052 \text{ m}^2/\text{Pa}\cdot\text{s} < P_f < 0.92 \text{ m}^2/\text{Pa}\cdot\text{s}$  and  $0.25 \% < \dot{M}_p/\dot{M}_a < 51.99 \%$ .

In vertical test case unstable zone and fluidized dense phase is occurred, then in the horizontal test case slug flow and plug flow is observed and lastly plug flow and dilute phase is occurred visually in continuous conveying test case. Finally, all obtained data which were explained in the previous chapters are classified according to flow modes in pneumatic conveying systems. The flow modes are shown in figure 6.1 under the results of visual observations with respect to  $P_{f\text{ mf}}$  ( $\text{m}^2/\text{Pa}\cdot\text{s}$ ) as a function of  $\text{Re}_{mf}$  (Reynolds Number at minimum fluidization velocities). In addition to this, flow modes are given with respect to test cases in table 6.1.

Table 6.1 Limit of flow modes in test cases

Vertical Test Case			
Unstable Zone	Transition of Fluidized Dense Phase	Fluidized Dense Phase	
$U_{air} \ll U_{mf}$	$U_{air} = U_{mf}$	$U_{air} > U_{mf}$	$U_{air} \gg U_{mf}$
Horizontal Test Case			
Slug Flow	Transition of Plug Flow	Plug Flow	
$U_{air} \ll U'_{mf}$	$U_{air} = U'_{mf}$	$U_{air} > U'_{mf}$	$U_{air} \gg U'_{mf}$
Continuous Conveying Test Case			
Plug Flow		Dilute Phase	
$U_{air} \leq U''$		$U_{air} \gg U''$	

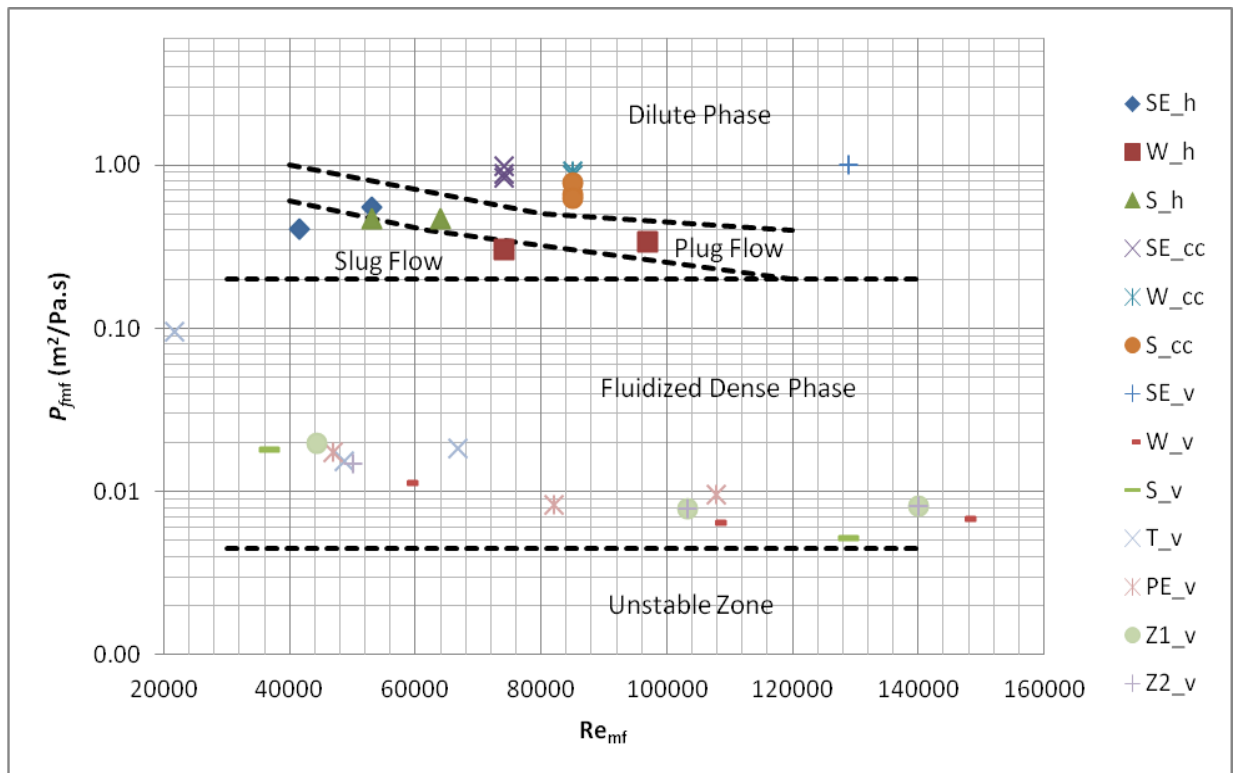


Figure 6.1 Proposed flow mode diagram with regarding  $P_{f, mf}$  as a function of  $Re_{mf}$



As a result of the systematic experimental cases consisted of 210 vertical, 65 horizontal and 72 continuous conveying measurements following concluding remarks can be deduced:

1) An increase of loose poured bulk density,  $\rho_{blp}$  causes an increase of minimum fluidization velocity,  $U_{mf}$  in vertical test case. The loose poured bulk density seems more effective in comparison to the horizontal test cases. On the other hand, increase of average particle diameter,  $d_p$  causes an increase of minimum fluidization velocity in horizontal test case. Furthermore, the average particle diameter is seen to be more effective in horizontal test case in comparison with vertical test case. These deductions on  $\rho_{blp}$ ,  $d_p$  are due to the constraints at horizontal and vertical test cases.

2) It is found that fluidized dense phase is observed in the range of  $0.0052 \text{ m}^2/\text{Pa.s} < P_f < 0.2 \text{ m}^2/\text{Pa.s}$ . Slug flow and plug flow are found to be observed for  $0.2 \text{ m}^2/\text{Pa.s} < P_f < 0.56 \text{ m}^2/\text{Pa.s}$ . On the other hand, dilute phase is detected for  $0.56 \text{ m}^2/\text{Pa.s} < P_f$ . The measurements and visual observations confirm the determined limits. This is an original contribution to the available literature.

3) Although the defined limits are valid for the covered particle characteristics and utilized methodology the comparison with the available literature. Jones [15] proposed the limits between fluidized dense phase and dilute phase as  $P_f \rho_{blp}^{0.75} \approx 300$ , and the limits between dilute phase and plug flow as  $P_f \approx 20 \times 10^{-6}$ . In this study  $P_{fmf}$  is used to determine the flow modes instead of  $P_f$ . Due to this reason the limits are found to be in a different range.

As a result of the study, some further investigations on the manner will be conducted as follows:

1) The particle characteristics should be considered particularly for the ranges of  $d_p < 100 \mu\text{m}$  and  $d_p > 3000 \mu\text{m}$ .

2) The range of study should be extended to cover of a variety of industrial applications.

3) The constructed test system should be revised to have a fully automated structure.

## LIST OF REFERENCES

- [1] Geldart D. (1973). Types of Gas Fluidization, *Powder Technology*, Vol.7, pp. 285-292.
- [2] Geldart D. (1972). *Powder Technology*, Vol. 6, pp. 201.
- [3] Dixon G. (1979). The Impact of Powder Properties on Dense Phase Flow, *In Proceedings of the international conference on pneumatic conveying*.
- [4] Molerus O. (1967). Proc. Intern. Symp. on Fluidization, Eindhoven, Netherlands Univ. Press Amsterdam.
- [5] Molerus O. (1982). Interpretation of Geldart's Type A, B, C and D Powders Taking into Account Interparticle Cohesion Force, *Powder Technology*, Vol. 33, pp. 81-87.
- [6] Molerus O. (1980). *Chem. Engng. Science* 35, Vol. 6, pp. 1331.
- [7] Mainwaring N. J., Reed A. R. (1987). Permeability and Air Retention Characteristics of Bulk Solid Materials in Relation to Modes of Dense Phase Pneumatic Conveying, *Bulk Solids Handling*, Vol. 7(3), pp. 415-425.
- [8] Fargette C., Jones M. G., Nussbaum G. (1997). Bench Scale Tests Assessment of Pneumatic Conveying Behavior of Powders, *Powder Handling and Processing*, Vol. 9(2), pp. 103-110.
- [9] Sanchez L., Vasquez N., Klinzing G. E., Dhopdakar S. (2003). Characterization of Bulk Solids to Assess Dense Phase Pneumatic Conveying, *Powder Technology*, Vol. 138, pp. 93-117.
- [10] Pan R., Wypych P., Frew I. (1998). 6<sup>th</sup> Intl. Conf. on Bulk Materials, Storage, Handling and Transport, Wollongong, AU, September.
- [11] Pan R., Frew I., Cook D. (2000). *I-Mechanical Engineering*, 65 (C566/044/2000).

- [12] Pan R. (1995). Intl. Conf. on Bulk Materials, Storage, *Handling and Transport*, Newcastle, AU, July,
- [13] Pan R. (1999). Material Properties and Flow Modes in Pneumatic Conveying, *Powder Technology*, Vol. **104**, pp. 157-163.
- [14] Williams K. C., Jones M. G. (2003). Classification Diagrams for Dense-Phase Pneumatic Conveying, *Powder Handling and Processing*, Vol. **15(6)**, pp. 368-373.
- [15] Jones M. G., Williams K. C. (2008). Predicting the Mode of Flow in Pneumatic Conveying Systems, *Particuology*, Vol. **6**, pp. 289-300.
- [16] Jackson R., (1963). *Trans. Inst. Chem. Engrs*, Vol. **41**, pp. 13.
- [17] Pigford R L., Baron T. (1965). *Ind. Eng. Chem. Fundamentals*, Vol. **4**, pp. 81.
- [18] Davies L., Richardson J.F. (1966). *Transactions of the Institution of Chemical Engineers*, Vol. **44**, T293.
- [19] H\_ Rumpf (1970). *Chemie-kg-Technik*, Vol. **42**, pp. 538.
- [20] Krupp H (1967). *Adv. in Coil. and Interf. Sci.* Vol. **1**, pp. 2.
- [21] Mathur K. B. (1971). Chapter 17. Spouted Beds, in Davidson J.F., and Harrison D. H. *Fluidization*. Academic Press, London and Newyork
- [22] Chambers A. J., Keys S., Pan R. (1998). The Influence of Material Properties on Conveying Characteristics, *In Proceedings of the 6<sup>th</sup> international conference on bulk materials storage, handling and transportation*, pp. 309-319.
- [23] Jones M.G., Mills U.K. (1990). Product classification for pneumatic conveying, *Powder Handling and Processing*, Vol. **2**, pp. 117–122.
- [24] Mi B. (1994). Low Velocity Pneumatic Transportation of Bulk Solids, PhD Dissertation, Wollongong University, AU.
- [25] Kennedy O.C. (1998). 6th International Conference on Bulk Materials Storage, Handling and Transportation, Wollongong, Australia, 8 – 30 September.
- [26] Geldart D., Wong A.C.Y. (1985). *Chemical Engineering Science* Vol. **40**, pp. 653–661.
- [27] Kwauk M. (1992). *Fluidization: Idealized and Bubbleless, with Applications*, Ellis Horwood, New York.
- [28] Sanchez L. (2001). Characterization of Bulk Solids for Dense Phase Pneumatic Conveying, MS Thesis, University of Pittsburgh.

- [29] Ergun S. (1952). "Fluid Flow Through Packed Columns," *Chemical Engineering Progress*, vol. **48**, pp. 89-94.
- [30] Tozlu A., Özahi E., Kutlar A.İ., Çarpınlioğlu M., (2012). "Modes of Flow in Pneumatic Conveying Systems," FLUIDS-HEAT'12, Recent Researches in Applied Mechanics, Greece, vol. **1**, pp. 51-57, March.
- [31] Oruç V. (2001). An experimental investigation on flow hydrodynamics in pneumatic transport of solid particles, M.Sc Thesis, Gaziantep.
- [32] BS 1042, Part 2 (1973). British Standard Methods for the Measurement of Fluid Flow in Pipes, British Standard Institution.
- [33] ANSI/ASME PTC 19.1-1985 Part 1 1986 Measurement Uncertainty (Available from ASME Order Dept., 22 Law Drive, Box 2300, Fairfield, New Jersey 07007-2300)
- [34] Joint Committee for Guides in Metrology, (2008) Evaluation of measurement data-guide to the expression of uncertainty in measurement (GUM), JCGM 100.
- [35] Holman, JP. (2012). *Experimental Methods for Engineers*. 8<sup>th</sup> ed. New York: McGraw Hill.
- [36] Coleman HW, Steele WG Jr. (1989). *Experimentation and uncertainty analysis for engineers*. New York: Wiley.
- [37] Wheeler AJ, Ganji AR. (1996). *Introduction to engineering experimentation*. New Jersey: Prentice Hall.

## APPENDIX 1

### TECHNICAL SPECIFICATIONS OF THE DRIVE UNIT OF BLOWER

#### **Electric Motor**

Input: 220-380 V, 50 Hz

Power rating: 2.95 HP/2.2 kW

Rotational speed: 2835 rpm

Protection class: IP 44 B

#### **AC Control Unit**

Controller specification: Simovert P. 6SE2008-3AA00

Input: 380/500 V, 47-63 Hz

Output: 380/500V, 0-400Hz

Power rating: 8.3 kVA, motor: 7.5HP/5.5kW

Protection class: IEC 529 IP 20

Temperature range: 0-40<sup>0</sup>C

## APPENDIX 2

### TECHNICAL SPECIFICATIONS OF THE PARTICLE FEEDER

The drive unit of particle feeder consists of an electric motor and an AC control unit which have the following specifications:

#### **Electric Motor**

Input: 220-380 V, 50 Hz

Power rating: 0.75 kW

Rotational speed: 1400 rpm

#### **AC Control Unit**

Controller specification: Simovert P. 6SE2001-1AA00

Input: 220/240 V, 50-60 Hz

Output: 0-220/240V, 0-120Hz

Power rating: 0.7 kVA, motor: 0.5HP/0.37kW

Protection class: IEC 529 IP 20

Temperature range: 0-40<sup>0</sup>C

### APPENDIX 3

#### TECHNICAL SPECIFICATION OF THE PRESSURE TRANSMITTER

The WIKA SL-1 pressure transmitter for low pressure applications has the following technical specifications;

Pressure Ranges	: $\pm 20$ mbar ( $\pm 2$ kPa)
Type of Pressure	: Relative Pressure
Wetted Parts Material	: Stainless Steel, Silicon, Aluminum, Gold
Case Materials	: Stainless Steel
Power Supply	: 14-30 VDC
Signal Output	: 0-10 V
Accuracy	: $\leq 0.5$ %
Non-linearity	: $\leq 0.2$ %
Non-repeatability	: $\leq 0.1$ %
1-year Stability	: $\leq 0.3$ %
Time Resolution	: 1 kHz
Permissible Temperature of Medium	: -30 °C..80 °C
Permissible Temperature of Ambient	: -20 °C..80 °C
Process Connection	: G1/2"
Weight	: approx. 0.3 kg



## APPENDIX 4

### TECHNICAL SPECIFICATION OF THE DATA ACQUISITION BOARD

Resolution	: 16 bit
Sample Rate	: 1.25 MS/s single, 1.00 MS/s multi-channel
On-board Thermocouple Inputs	: 8
Analog Inputs (channels)	: 16 (differential) or 32 (single-ended)
Analog Outputs	: 4 (16 bit, 1 MHz)
Digital I/O	: 24
Counter Inputs/Timer Outputs	: 4/2
Latency	: low-latency control output capability as low as 2 $\mu$ s latency
Environment Operating Temperature	: -30 °C..70 °C
Power Supply	: 0-25 VDC
Voltage Measurement Speed	: 1 $\mu$ s per channel
Output Voltage	: $\pm 10$ V, $\pm 5$ V, $\pm 2$ V, $\pm 1$ V, $\pm 0.5$ V, $\pm 0.2$ V